UNIVERSITY OF CALIFORNIA SAN DIEGO

Transient Frequency Analysis and Distributed Synthesis for Power Networks

A dissertation submitted in partial satisfaction of the
requirements for the degree
Doctor of Philosophy

in

Engineering Sciences (Mechanical Engineering)

by

Yifu Zhang

Committee in charge:

Professor Jorge Cortés, Chair
Professor William Helton
Professor Miroslav Krstić
Professor Sonia Martínez
Professor Behrouz Touri

2019

The dissertation of Yifu Zhang is approved, and it is acceptable in quality and form for publication on microfilm and electronically:

_____

_____

_____

_____

_____

Chair

University of California San Diego

2019

EPIGRAPH

众里寻他千百度

蓦然回首

那人却在 灯火阑珊处

— 辛弃疾

TABLE OF CONTENTS

LIST OF FIGURES

LIST OF TABLES

ACKNOWLEDGEMENTS

I would like to first express my deepest gratitude to Professor Jorge Cortés, who magically and simultaneously plays the roles of a rigorous faculty advisor, a close partner, a patient listener, a knowledgeable educator, a generous supporter, and an impartial peer reviewer. Hundreds of hours of face-to-face discussions we had during the past five years constitute my academic foundations in research. His enthusiasm, optimism, and persistence alter my attitudes from numerous aspects.

I am greatly honored to have Professor William Helton, Professor Miroslav Krstić, Professor Sonia Martínez, and Professor Behrouz Touri on my doctoral committee, and I appreciate their time and effort in improving the quality of this dissertation.

For our joyful time and insightful discussions, I would thank my colleagues as well as friends at UC San Diego: Yuanjie, Yingbo, Yaoguang, Xuefeng, Vishaal, Tor, Simon, Shuxia, Shumon, Priyank, Pio, Pavan, Mike, Libin, Leobardo, Jiuyuan, Ji, Huan, Fangyao, Evan, Erfan, Eduardo, Dun, David, Dan, Chin-Yao, Bo, Beth, Ashish, Andrés, Aamodh, Aaron, and all other labmates.

During the past five years, I was fortunate to receive academic training not only in control theory from MAE, but also in mathematics, algorithm, and machine learning from MATH, CSE, and ECE. I deeply appreciate the exceptional educational environment created by the excellent professors and staffs at UC San Diego. A special thanks goes to Mr. Earl Mood for the cheerful chats we had.

I spent three wonderful months at the Mitsubishi Electric Research Laboratories as an intern, and would express my sincere appreciations to the research fellows there: Dr. Yebin Wang, Dr. Daniel Burns, Dr. Scott Bortoff, Dr. Claus Danielson, Dr. Christopher Laughman, Dr. Stefano Di Cairano, and Dr. Hongtao Qiao.

My sincere thanks goes to Professor Huijun Gao, Professor Weichao Sun, Professor Jianbin Qiu, Professor Tong Wang, Professor Okyay Kaynak, and Professor Peng Shi from the

Harbin Institute of Technology for providing a platform and igniting my initial interest in research. Thank my old but congenial friends Xuan, Xiaotian, and Songlin.

The greatest gratitude goes to my parents for their unconditional love. This dissertation is dedicated to them.

This research was generously supported by NSF award CNS-1329619, NSF award CNS-1446891, and AFOSR award FA9550-15-1-0108.

Chapter 3, in part, is a reprint of the material [ZC19a] as it appears in 'Characterizing tolerable disturbances for transient-state safety in power networks' by Y. Zhang and J. Cortés, in the IEEE Transactions on Network Science and Engineering, 2019, as well as [ZC17] where it appears as 'Transient-state feasibility set approximation of power networks against disturbances of unknown amplitude' by Y. Zhang and J. Cortés in the proceedings of the 2017 American Control Conference. The dissertation author was the primary investigator and author of these papers.

Chapter 4, in part, is a reprint of the material [ZC19c] as it appears in 'Distributed transient frequency control for power networks with stability and performance guarantees' by Y. Zhang and J. Cortés, in Automatica, 2019, as well as [ZC18a] where it appears as 'Distributed transient frequency control in power networks' by Y. Zhang and J. Cortés in the proceedings of the 2018 IEEE Conference on Decision and Control. The dissertation author was the primary investigator and author of these papers.

Chapter 5, in part, is a reprint of the material [ZC19e] submitted as 'Model predictive control for transient frequency regulation of power networks.' by Y. Zhang and J. Cortés, to the IEEE Transactions on Automatic Control, as well as [ZC18b] where it appears as 'Transient frequency control with regional cooperation for power networks' by Y. Zhang and J. Cortés in the proceedings of the 2018 IEEE Conference on Decision and Control. The dissertation author was the primary investigator and author of these papers.

Chapter 6, in part, is a reprint of the material [ZC19b] submitted as 'Distributed bilayered

control for transient frequency safety and system stability in power grids' by Y. Zhang and J. Cortés, to the EEE Transactions on Control of Network Systems, as well as [ZC19d] where it appears as 'Double-layered distributed transient frequency control with regional coordination' by Y. Zhang and J. Cortés in the proceedings of the 2019 American Control Conference. The dissertation author was the primary investigator and author of these papers.

VITA

2014	Bachelor of Engineering in Automation with honors, Harbin Institute of Technology
2015	Master of Science in Engineering Sciences (Mechanical Engineering), University of California San Diego
2019	Doctor of Philosophy in Engineering Sciences (Mechanical Engineering), University of California San Diego

PUBLICATIONS

Journal publications:

- Y. Zhang and J. Cortés. Distributed bilayered control for transient frequency safety and system stability in power grids. *IEEE Transactions on Control of Network Systems*, 2019. Submitted
- Y. Zhang and J. Cortés. Model predictive control for transient frequency regulation of power networks. *IEEE Transactions on Automatic Control*, 2019. Submitted
- Y. Zhang and J. Cortés. Distributed transient frequency control for power networks with stability and performance guarantees. *Automatica*, 105:274–285, 2019
- Y. Zhang and J. Cortés. Characterizing tolerable disturbances for transient-state safety in power networks. *IEEE Transactions on Network Science and Engineering*, 2019. To appear
- W. Sun, Y. Zhang, Y. Huang, H. Gao, and O. Kaynak. Transient-performance-guaranteed robust adaptive control and its application to precision motion control systems. *IEEE Transactions on Industrial Electronics*, 63(10):6510 – 6518, 2016
- T. Wang, Y. Zhang, J. Qiu, and H. Gao. Adaptive fuzzy backstepping control for a class of nonlinear systems with sampled and delayed measurements. *IEEE Transaction on Fuzzy Systems*, 23(2):302 – 312, 2015
- W. Sun, H. Pan, Y. Zhang, and H. Gao. Multi-objective control for uncertain nonlinear active suspension systems. *Mechatronics*, 24(4):32–40, 2014

Conference proceedings:

- Y. Zhang and J. Cortés. Double-layered distributed transient frequency control with regional coordination. In *American Control Conference*, Philadelphia, PA, July 2019. To appear
- Y. Zhang and J. Cortés. Transient frequency control with regional cooperation for power networks. In *IEEE Conf. on Decision and Control*, pages 2587–2592, Miami Beach, FL, December 2018

- Y. Zhang and J. Cortés. Distributed transient frequency control in power networks. In *IEEE Conf. on Decision and Control*, pages 4595–4600, Miami Beach, FL, December 2018
- Y. Zhang and J. Cortés. Transient-state feasibility set approximation of power networks against disturbances of unknown amplitude. In *American Control Conference*, pages 2767–2772, Seattle, WA, May 2017
- Y. Zhang and J. Cortés. Quantifying the robustness of power networks against initial failure. In *European Control Conference*, pages 2072–2077, Aalborg, Denmark, July 2016

ABSTRACT OF THE DISSERTATION

Transient Frequency Analysis and Distributed Synthesis for Power Networks

by

Yifu Zhang

Doctor of Philosophy in Engineering Sciences (Mechanical Engineering)

University of California San Diego, 2019

Professor Jorge Cortés, Chair

Electric power systems safety is a fundamental aspect of the operation and management of the grid. In order to maintain safety, the power system is operated around a nominal frequency. In fact, large frequency fluctuations can trigger generator relay-protection mechanisms and load shedding, which may further jeopardize network integrity, leading to cascading failures. Without appropriate estimations on the possible consequences resulting from contingency, operational architectures, and control safeguards in place, the likelihood of such events is not negligible, given that the high penetration of non-rotational renewable resources provides less inertia, possibly inducing higher frequency excursions. These observations motivate us in this

thesis to develop approximation and control schemes to efficiently estimate the transient-state evolution subject to disturbances and contingencies and further actively mitigate undesired transient frequency deviations.

This thesis first develops methods to efficiently compute the set of disturbances on a power network that do not tip the frequency of each bus and the power flow in each transmission line beyond their respective bounds. For a linearized power network model, we propose a sampling method to provide superset and subset approximations with a desired accuracy of the set of feasible disturbances. We also introduce an error metric to measure the approximation gap and design an algorithm that is able to reduce its value without impacting the complexity of the resulting set approximations.

As a natural follow-up to our on approximating feasible disturbances, we seek to further regulate transient frequency via novel control schemes. With regard to this, this thesis proposes three control strategies that all achieve local stabilization of power networks characterized by nonlinear swing equations and, at the same time, delimit the transient frequencies of targeted buses to a desired safe interval. To handle the coordination of large numbers of resources in an adaptive and scalable fashion, all three controllers can be implemented in an either partially or fully distributed fashion. Specifically, we synthesize the first transient frequency controller by having it satisfy a transient frequency constraint and an asymptotic stability constraint. Benefitting from its structural simplicity, the controller can be implemented in a distributed fashion by merely allowing each controlled bus physically measure the states of neighbors. To reduce the control effort, the second MPC-based controller enables control command cooperation by communication; however, the coordination is limited within a designed range, and the control algorithm is only partially distributed, potentially non-Lipschitz, and not as computationally efficient. The third controller successfully addresses all these issues via a bilayered structure and information exchange with up to 2-hop neighbors.

Chapter 1

Introduction

The electric power network has been greatly expediting the developments of numerous scientific and engineering disciplines since the 19th century, which in turns facilitate the evolution of power systems themselves. To maintain system security and integrity, the power network is required to operate within prescribed bounds around the nominal frequency of 60Hz or 50Hz. Without appropriate operational architectures and control safeguards in place, large frequency fluctuations can trigger generator relay-protection mechanisms and load shedding, which may further jeopardize network integrity, leading to cascading failures. Traditionally, the frequency deviation is regulated by shaping the generators output to preserve a balance between generation and load through a hierarchical control structure consisting of primary, secondary, and tertiary controls occurring over a continuum of time.

Tertiary control is the highest but also the slowest layer in the control hierarchy. Concerned with a global view and operating over an extensive range, it determines the generation level of generators based on the predicted load, and adjusts its commands over different time-scales, ranging from 24 hours to 10-30 mins intervals. However, due to its slow time-scale and prediction error, tertiary layer by itself cannot restore frequency to the nominal value at steady-state. This calls for the secondary layer which intervenes at a faster time-scale ranging

from 30s to 15 min. Specifically, secondary layer gathers local measurements, compares them with the prediction, and correspondingly adjusts generation determined by the tertiary layer in a more detailed fashion to finally eliminate steady-state error. Primary control, also called droop control, is regulated independently on each controlled plant to stabilize the power network, to dampen frequency deviations, and to establish power sharing. Primary control, as the lowest control layer with no need of communication, typically reacts immediately within a few seconds following disturbances.

However, the hierarchical control structure faces fundamental challenges as technological advances are driving power networks to a cleaner outlook, progressively penetrated by renewables such as wind and solar. Differing from traditional fossil fuel resources, renewables typically contribute less to stability and robustness margins. In detail, the rotating component of synchronous machines using traditional resources naturally provides inertia to the power network, whereas power electronics connecting renewable resources possess much less inertia. Therefore, in the absence of inertia dampening the reactions of the power network, disturbances and contingencies may lead to higher transient frequency fluctuations, resulting in relay protections that isolate affected generators from the rest of the network. Consequently, the loss of network integrity could further trigger larger abnormal state deviations, leading to the risk of cascading failures. This calls for a re-design of the primary control layer to adequately maintain the frequency deviations within a desired range. On the other hand, it is crucial to preserve the distributed nature of the primary layer for scalability and fast response.

Motivated by the critical issues in power network safety mentioned above, this thesis considers and attempts to answer two questions: how to identify the severity of disturbances, and, in a further step, how to mitigate severe disturbances with novel distributed control algorithms. The first part (Chapter 3) characterizes the set of tolerable disturbances that do not tip bus frequency and transmission line power flow beyond their in corresponding bounds. In this part, the control strategy is assumed to be the traditional droop control. For instance, in Fig-

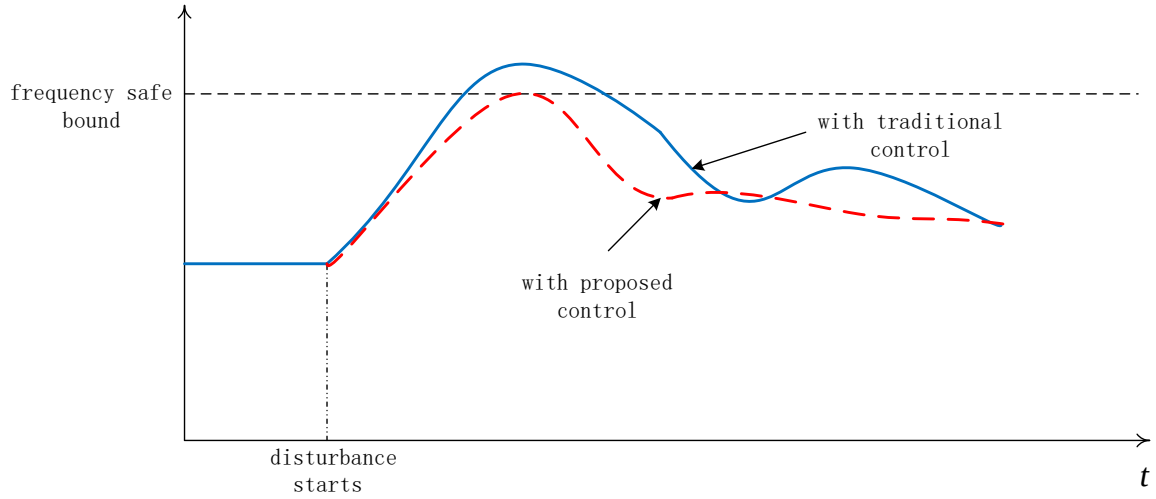

Figure 1.1: An illustration of the thesis topics on disturbance characterization and transient frequency control.

ure 1.1, the disturbance is not tolerable as it drives some frequency evolution (solid line) beyond the safe bound. The second part (Chapters 4, 5, and 6) proposes three distributed controllers that, while preserving network stability, are able to maintain transient frequency safety even under disturbances considered not tolerable with droop control. The dashed line in Figure 1.1 is a desired trajectory using the proposed controllers. These three chapters are in a progressive rather than a parallel fashion: Chapter 4 proposes the first transient frequency controller with stability guarantee. Based on it and to reduce control cost, the control algorithm in Chapter 5 enables nodal cooperation, but the coordination is only regional rather than global, and the controller is computationally intensive and potentially non-Lipschitz. Finally, the proposed controller in Chapter 6 has no such issues.

1.1 Literature review

Facing challenges and embracing opportunities, the hierarchical control structure of power systems [Ili07, GVM+11] is moving towards new designs from various sides. Concerns on en-

vironmental sustainability lead to the shift from traditional power plant using fossil fuels with bulk and steady generations to renewable distributed energy resources (DERs) with small and variable outputs [HJX08, DK08, JMLJ13, DSSPG19]. This, together with the controllable load-side devices integrated in the power network, dramatically increases the number of controllable variables and the complexity of optimizing the system [SIF16, BLR+10]. Meanwhile, with the increased numbers and types of sensors, huge amount of data are collected on the operating conditions of the power network [GM16, Dar05]. These emerging issues and opportunities, with the advancement of computation and communication, are pushing the power network control to a structure that is autonomous, scalable, safe, robust, economic, and flexible [Kro17]. Towards these directions, various control and optimization strategies have been proposed: distributed optimal power flow [DZG13, Ers14, LZT12], load-side regulation [MZL14, WA04], virtual inertia placement [MDH+18, PBD17], privacy-preserving energy management [MM09, HGKX17], and electricity market mechanism design [AMDM01, TJ13]. On the other hand, power networks fall into the general category of safety-critical systems whose failure could lead to loss of life or significant property and environment damages [Kni02]. Various analysis methodologies and protection mechanisms have been discovered, proposed and applied to guarantee safety: formal method on software engineering [BS93, NRZ+15], redundant design on flights [HG05, SLJ15], humour and sublimation on psychological defence [BDS98, Kub71], to mention a few. Specifically, this thesis focuses on transient-state safety characterization and transient frequency control.

1.1.1 Transient-state safety

There are two major methods [KPA+04, GTK14] for analyzing safety in power networks: time-domain and Lyapunov direct methods. The time-domain method [NFP+13, DN11, FCE+99] usually refers to the numerical simulation of the system behavior for some specific disturbance. Depending on the numerical solver, this method is able to consider almost any

power network model and to precisely depict the state trajectories, provided that the system parameters are accurately known. However, the time-domain method cannot answer question regarding how far the system is from (in)stability and can hardly provide guidelines for control [PERV12]. The Lyapunov direct method [Pai89, CWV94, AMA13, DB12, VAMT16] focuses on estimating the region of attraction of the system equilibrium using Lyapunov functions to ensure the stability of the power network without knowing the specific form of the disturbance (provided the initial state lies in a suitable identified region). Most of the direct methods require less simulation/computation time than time-domain methods and, more importantly, are able to provide stability margins and parameter sensitivity analysis. However, due to the difficulty of finding Lyapunov functions, especially for power systems with complex dynamics subject to time-varying disturbances, and the conservativeness required in bounding their evolution, the identified regions of attraction may in general be coarse approximations of the actual one. In this thesis we take the alternative approach of identifying the set of disturbances under which the state of the power system remains within some desired bounds during transients. The availability of these descriptions makes it possible to quantify network robustness by, for instance, defining metrics that measure the minimum disturbance that is able to force the system out of the safety region, see e.g., [ZC16, BS16]. Such notions are useful in the context of cascading failures analysis and, unlike much of the literature, see e.g., [SMZ17, YNM17], they help identify conditions for triggering initial failures that incorporate the effect of not only network connectivity, but also network dynamics.

Transient-state safety analysis is also related to the literature on the characterization of forward and backward reachability sets, see [Mit07, KB06a, Dan06] and, in the context of power systems, [CDG12] for linear dynamics, [VPA14, EGHA16, EGSS$^+$18] for nonlinear dynamics with time-varying uncertainty, and [CSD16] for constant uncertainty. Given regions of initial states and possible input signals, a state belongs to the forward reachability set if there exists an initial state and an input signal trajectory that steer the dynamical system to this particular

state. Similarly, a state belongs to the backward reachability set if the system can be driven starting from this state into the region with an input trajectory. In general, both types of sets are too difficult to compute precisely, so instead the emphasis is put on constructing accurate inner and outer approximations. An important observation is that reachability set analysis puts the emphasis on characterizing the achievable system states and ensuring that transient trajectories satisfy desired specifications *given* the set of allowable inputs or disturbances. However, there is a entirely complementary research direction worth investigating: how to characterize the set of disturbances that do not cause the system state to violate the desired specifications. Along this line, the recent paper [LAVT18] provides an inner approximation of the set of bounds on arbitrary disturbances that respect transient-state safety for the nonlinear swing dynamics but without a formal guarantee on its accuracy.

1.1.2 Distributed transient frequency control

In transient-state safety analysis, it is generally assumed that the system is closed-loop with a droop controller whose output is simply linear in frequency. Considering the numerous well-developed control frameworks [ÅströmK14] proposed in the past several decades, naturally one would like to ask the following question: given a disturbance that is able to make a power network with the droop controller unsafe during transients, it is possible to re-design the controller so that the new closed-loop system is safe during transients against the same disturbance? To answer this question, various techniques have been proposed to improve transient behavior, especially transient frequency. These include resource re-dispatch with transient stability constraints [AM06, NNK11]; thyristor-controlled series capacitor compensation to optimize transmission impedance and keep power transfer constant [GP01]; the use of power system stabilizers to damp out low frequency inter-machine oscillations [MPAH14], and placing virtual inertia in power networks to mitigate transient effects [BLH15, PBD17]. While these approaches have a qualitative effect on transient behavior, they do not offer strict guarantees as to whether the tran-

sient frequency stays within a specific region. Furthermore, the approach by [BLH15] requires a priori knowledge of the time evolution of the disturbance trajectories and an estimation of the transient overshoot. Alternative approaches rely on the idea of identifying the disturbances that may cause undesirable transient behaviors using forward and backward reachability analysis, see e.g., [Alt14, CDG12, CSD16] and our previous work [ZC17]. The lack of works that provide tools for transient frequency control motivates us here to design feedback controllers for the generators that guarantee simultaneously the stability of the power network and the desired transient frequency behavior.

Asymptotic stability can be established by identifying a control Lyapunov function and enforcing its monotonic decrease along the system dynamics. In the last two decades, researchers mainly in robotics have formally developed barrier certificates [Pra06] and latter control barrier function method [XTGA15, AXGT17] to establish provable safety control of dynamical systems. The term 'barrier' was motivated by the barrier function in the optimization literature, which works as a penalization to the cost function to avoid constraint violations [ACE+19]. Similarly, a barrier function in dynamical system plays the role of constraining state trajectorys, and prescribing control commands to gradually kick in as the trajectory approaches the boundary of a prescribed safe region. Moreover, in order to simultaneously guarantee both stability and safety, a natural idea is to seek for a controller which satisfies a stability condition as well as a barrier function condition; however, possible trade-offs have to be made [XTGA15], since such a combination may be infeasible. Interestingly, it is currently an open problem to determine if such trade-offs are necessary, or there actually exists another pair of control Lyapunov function and control barrier function that can be satisfied at the same time. In addition, besides the methodology based on barrier function, many other safety-oriented control strategies have been proposed, e.g., modified backstepping for nonovershooting control [KB06b], model reference $\mathscr{L}_1$ adaptive control with guaranteed transient performance [CH08], and adaptive sliding model control for safe output tracking [YT94], to mention but a few. However, as opposed to the bar-

rier function method, most of them more or less rely on high-gain feedback, sufficiently forcing system state to evolve only within a small region close to the equilibrium to enforce transient safety.

Considering controller cost and scalability implemented on large-scale power networks, a related body of work [VHRW08, MRRS00, JK02] looks at reducing control effort while respecting performance requirements, and investigates distributed model predictive control (MPC) for networked systems. However, the proposed distributed implementations may jeopardize network stability. Particularly, [JK02] treats each subsystem as an independent system by considering the effect of other subsystems as bounded uncertainty, which complicates obtaining stability guarantees for the whole system. In fact, [VHRW08] shows that, if each subsystem has no knowledge of other subsystems' cost functions [CJKT02], this leads to a noncooperative game, and the control input trajectory may even diverge. In addition, some MPC approaches [VHRW08, NCF$^+$14] restrict the predicted horizon to a single step in order to obtain distributed strategies, since otherwise the control signal may require global state or global system parameter information. Furthermore, a challenge in employing MPC techniques in the specific context of power networks [JLSH15, VHRW08, FIDM14] is that, as the equilibrium point heavily depends on modeling and network parameters that cannot be precisely known, it is analytically hard to establish robust stabilization given that the objective function generally requires knowledge of the equilibrium point.

1.2 Contributions

Chapter 3 focuses on characterizing tolerable disturbances for power networks transient-state safety. We consider a linearized AC power network subject to multiple disturbances, with each one modeled as amplitude multiplying a time-varying signal, injected at various buses. We distinguish between three cases: when the form of the trajectory is totally known, partially

known, or totally unknown but bounded. A disturbance is tolerable for the transient-state safety of the power network if the frequency of each bus and the power flow in each transmission line still remain in their respective bounds during a given period of time. Our main goal is to design efficient ways of computing the transient-state tolerableness set consisting of all such classes of disturbances. Our first contribution shows that all three transient-state tolerableness sets can be equivalently expressed in a unified way that contain infinitely many constraints. The second contribution develops a sampling method to approximate these sets by synthesizing inner and outer approximations. The inner approximation is computed by sampling and tightening the constraints at finite discrete-time instants. We use the network dynamics to upper and lower bound the evolution of state signals and show that satisfying the constraints at these finite instants ensures in fact that all constraints are respected at all times. The outer approximation comes from using only a finite number of the constraints appearing in the original transient-state tolerableness set. We show that, as the number of sampling points increases, the approximation sets converge to the real transient-state tolerableness set. Our third contribution consists of defining a metric to measure the approximation gap by estimating the region difference between the approximations and the real set. We characterize the sampling sequence that, for a fixed number of sampling points, results in the minimal gap of the approximations and design an algorithm to find it by efficiently adjusting the positions of the sampling points. We illustrate our results on the IEEE 39-bus power system by showing the inner and outer approximations of the three tolerableness sets.

With the transient-state safety analysis established, Chapters 4, 5, and 6 provide three controllers to regulate transient-state (especially transient frequency) so that with the assistance of the controller, transient frequency evolves within a safe region even under intolerable disturbances. As the foundation of these three chapters, Chapter 4 proposes a non-optimization-based, distributed controller, available at specific individual generator nodes, that satisfies the following requirements (i) renders the closed-loop power network asymptotically stable; (ii) for each con-

trolled generator node, if its initial frequency belongs to a desired safe frequency region, then its frequency trajectory stays in it for all subsequent time; and (iii) if, instead, its initial frequency does not belong to the safe region, then the frequency trajectory enters it in finite time, and once there, never leaves. Our technical approach to achieve this combines Lyapunov stability and set invariance theory. We first show that requirement (iii) automatically holds if (i) and (ii) hold true, and we thereby focus our attention on the latter. For each one of these requirements, we provide equivalent mathematical formulations that are amenable to control design. Regarding (i), we consider an energy function for the power system and formalize it as identifying a controller that guarantees that the time evolution of this energy function along every trajectory of the dynamics is non-decreasing. Regarding (ii), we show that this condition is equivalent to having the controller make the safe frequency interval forward invariant. To avoid discontinuities in the controller design on the boundary of the invariant set, we resort to the notion of barrier functions to have the control effort gradually kick in as the state trajectory approaches the boundary. Our final step is to use the identified constraints to synthesize a specific controller that satisfies both and is distributed. The latter is a consequence of the fact that, for each bus, the constraints only involve the state of the bus and that of neighboring states. In addition, we analyze its robustness properties against measure error and parameter uncertainty, quantify its magnitude when the initial state is uncertain, and provide an estimation on the frequency convergence rate from the unsafe to the safe region for each controlled generator. We illustrate the performance and design trade-offs of the proposed controller on the IEEE 39-bus power network.

Although it guarantees transient frequency safety and power network stability, the controller proposed in Chapter 4 is in fact myopic, without prediction capabilities. To address the issue of control cost reduction, we propose a receding-horizon MPC strategy in Chapter 5 which takes requirements (i)-(iii) into account, with consideration of control economy. Specifically, we first formulate a non-convex finite-horizon open-loop optimal control problem whose solution is the control trajectory minimizing the overall cost under stability and transient frequency

constraints. We then propose a reference trajectory technique for convexification. The centralized closed-loop control signal for each state is defined as the first-step solution of the optimal control problem. To enable distributed control, we partition the network into different regions and apply the centralized control for each region, while taking into account the dynamics of the transmission lines connecting different regions. The resulting control signal for each bus only relies on system information of the region to which the bus belongs to and its neighboring regions. However, some critical problems and potential improvements arise as we explore its analytical properties and practical applicability; first, we are not able to show the Lipschitz continuity of the controller; second, in the open-loop optimal control problem, the prediction model is discretized by first-order forward Euler method, whose discretization step has to be sufficiently small so that it approximates the real continuous-time power network dynamics. This in turns significantly constrains the prediction horizon due to the limited computational resources; third, the proposed regional implementation is only partially distributed: given a set of regions in the network, a centralized controller aggregates information and determines the control actions within each region, independently of the others.

Chapter 6 proposes a bilayer control structure that deals with these three issues while still taking the baseline requirements (i)-(iii) as well as control economy into consideration. The bottom layer solves periodically a finite-horizon convex optimization problem and globally allocates control resources to minimize the overall control effort. The optimization problem incorporates a prediction model for the system dynamics, a stability constraint, and a relaxed frequency safety constraint. The prediction model is a linearized and discretized approximation of the nonlinear continuous-time power network dynamics, carefully chosen to preserve its local nature while keeping the complexity manageable. As a consequence, in the resulting convex optimization problem, the objective function can be interpreted as the sum of local control costs, and each constraint only involves local decision variables. This enables us to apply saddle-point dynamics to recover its solution in a distributed fashion by allowing each bus (resp. line) to

exchange system information within its neighboring buses (resp. lines). On the other hand, the top layer, as a real-time feedback controller, acts as a compensator, bridging the mismatch between the actual continuous-time power network dynamics and the sampled-based information employed in the bottom layer to rigorously guarantee frequency safety. The top layer control signal regulating on a generic bus only depends on physical measurements of system information within the range of its neighboring transmission lines. We show that both two layer control signals are Lipschitz in system state. We illustrate the performance of the proposed bilayered controller architecture in the IEEE 39-bus power network.

1.3 Organization

In Chapter 2, we briefly introduce some notions, notation, and power network dynamics used throughout this thesis. In Chapter 3, we develop methods to efficiently compute the set of disturbances on a power network that do not tip the frequency of each bus and the power flow in each transmission line beyond their respective bounds. In Chapters 4, 5, and 6, we introduce three different but related distributed control strategies regulated on a subset of individual buses in a power network described by the swing equations to achieve transient frequency control while preserving asymptotic stability. Finally, Chapter 7 summarizes our contributions and provides some future research directions.

Chapter 2

Preliminaries

This section introduces basic notation and notions from graph theory, optimization, set limit, dynamical systems, set invariance, and power network dynamics. [1]

2.1 Notation

Let $\mathbb{N}$, $\mathbb{R}$, $\mathbb{R}_{>}$, and $\mathbb{R}_{\geqslant}$ denote the set of natural, real, strictly positive, and nonnegative real numbers, respectively. Variables are assumed to belong to the Euclidean space unless specified otherwise. For $a, b \in \mathbb{N}$, denote $[a,b]_{\mathbb{N}} \triangleq \{x \in \mathbb{N} \mid a \leqslant x \leqslant b\}$. Denote by $\lceil a \rceil$ as the ceiling of $a \in \mathbb{R}$. Given $\mathscr{C} \subset \mathbb{R}^n$, $\partial\mathscr{C}$ denotes its boundary. We let $\|\cdot\|_2$ denote the 2-norm on $\mathbb{R}^n$. For a point $x \in \mathbb{R}^n$ and $r \in \mathbb{R}_{>}$, denote $B_r(x) \triangleq \left\{x' \in \mathbb{R}^n \;\middle|\; \|x'-x\|_2 \leqslant r\right\}$. Denote $\mathbf{1}_n$ and $\mathbf{0}_n$ in $\mathbb{R}^n$ as the vector of all ones and zeros, respectively. For $A \in \mathbb{R}^{m\times n}$, let $[A]_i$ and $[A]_{ij}$ denote its ith row and (i,j)th element. For $A \in \mathbb{R}^n \times \mathbb{R}^n$, denote as $A \succeq 0$ and $A \succ 0$ if A is positive semidefinite and positive definite. Let $\mathbf{1}_n$ and $\mathbf{0}_n$ in $\mathbb{R}^n$ denote the vector of all ones and zeros, respectively. We denote by $A^\dagger$ its unique Moore-Penrose pseudoinverse and by range(A) its column space. A continuous function $\alpha : \mathbb{R} \to \mathbb{R}$ is of class-$\mathscr{K}$ if it is strictly increasing and $\alpha(0) = 0$ (note the slightly different convention with respect to the literature of taking the domain space to be

[1] Notations in the rest chapters are independent except for those introduced in this chapter.

$\mathbb{R}$ instead of $\mathbb{R}_{\geqslant}$). Given a differentiable function $l : \mathbb{R}^n \to \mathbb{R}$, we let ∇l denote its gradient. A function $f : \mathbb{R}_{\geqslant} \times \mathbb{R}^n \to \mathbb{R}^n,\ (t,x) \to f(t,x)$ is Lipschitz in x (uniformly in t) if for every $x_0 \in \mathbb{R}^n$, there exist $L, r > 0$ such that $\|f(t,x) - f(t,y)\|_2 \leqslant L\|x-y\|_2$ for any $x, y \in B_r(x_0)$ and any $t \geqslant 0$. For scalars $a, b \in \mathbb{R}$, let

$$[a]_b^+ = \begin{cases} a & \text{if } b > 0, \\ \max\{a, 0\} & \text{if } b \leqslant 0. \end{cases}$$

For vectors $a, b \in \mathbb{R}^n$, $[a]_b^+ \in \mathbb{R}^n$ is the vector whose ith component is $[a_i]_{b_i}^+$ for every $i \in [1,n]_{\mathbb{N}}$. Denote the sign function $\text{sgn} : \mathbb{R} \to \{0, 1\}$ as

$$\text{sgn}(a) = \begin{cases} 1 & \text{if } a \geqslant 0, \\ -1 & \text{if } a < 0. \end{cases}$$

Define the saturation function $\text{sat} : \mathbb{R} \to \mathbb{R}$ with limits $a^{\min} < a^{\max}$ as

$$\text{sat}(a; a^{\max}, a^{\min}) = \begin{cases} a^{\max} & a \geqslant a^{\max}, \\ a^{\min} & a \leqslant a^{\min}, \\ a & \text{otherwise.} \end{cases}$$

For a function : $F : \mathscr{X} \times \mathscr{Y} \to \mathbb{R},\ (x,y) \to F(x,y)$, denote by $\nabla_x F$ (resp. $\nabla_y F$) the partial derivative of F with respect to x (resp. y). Second-order derivatives follow the usual convention $\nabla_{xy} F = \frac{\partial^2 F}{\partial x \partial y}$ and $\nabla_{xx} F = \frac{\partial^2 F}{\partial x^2}$. A point $(x^*, y^*) \in \mathscr{X} \times \mathscr{Y}$ is a saddle point of F on the set $\mathscr{X} \times \mathscr{Y}$ if $F(x^*, y) \leqslant F(x^*, y^*) \leqslant F(x, y^*)$ holds for every $(x,y) \in \mathscr{X} \times \mathscr{Y}$.

2.2 Graph theory

We present basic notions in algebraic graph theory from [BCM09, Big94]. An undirected graph is a pair $\mathscr{G} = (\mathscr{I}, \mathscr{E})$, where $\mathscr{I} = \{1, \ldots, n\}$ is the vertex set and $\mathscr{E} = \{e_1, \ldots, e_m\} \subseteq \mathscr{I} \times \mathscr{I}$ is the edge set. A path is an ordered sequence of vertices such that any pair of consecutive vertices in the sequence is an edge of the graph. A graph is connected if there exists a path between any two vertices. Two nodes are neighbors if there exists an edge linking them. Denote by $\mathscr{N}(i)$ the set of neighbors of node i. For each edge $e_k \in \mathscr{E}$ with vertices i, j, the orientation procedure consists of choosing either i or j to be the positive end of e_k and the other vertex to be the negative end. The incidence matrix $D = (d_{ki}) \in \mathbb{R}^{m \times n}$ associated with $\mathscr{G}$ is then defined as

$$d_{ki} = \begin{cases} 1 & \text{if } i \text{ is the positive end of } e_k, \\ -1 & \text{if } i \text{ is the negative end of } e_k, \\ 0 & \text{otherwise.} \end{cases}$$

2.3 Set limit

We introduce basic definitions from set theory [Res98]. Given a sequence of sets $\{A_k\}_{k=1}^{\infty}$, define

$$\liminf_{k\to\infty} A_k \triangleq \bigcup_{k\geqslant 1} \bigcap_{j\geqslant k} A_j, \ \limsup_{k\to\infty} A_k \triangleq \bigcap_{k\geqslant 1} \bigcup_{j\geqslant k} A_j.$$

It holds that $\liminf_{k\to\infty} A_k \subseteq \limsup_{k\to\infty} A_k$. Furthermore, if $\liminf_{k\to\infty} A_k = \limsup_{k\to\infty} A_k = A$, then we say the limit of $\{A_k\}_{k=1}^{\infty}$ exists and is A. In shorthand notation, we write $A_k \to A$. For a set C and two set sequences $\{B_k\}_{k=1}^{\infty}$ and $\{C_k\}_{k=1}^{\infty}$, if $C \subseteq B_k \subseteq C_k$ (resp. $C_k \subseteq B_k \subseteq C$) for all $k \geqslant 1$, and $C_k \to C$, then $B_k \to C$.

2.4 Convex optimization

In this section we review basics of convexity, convex optimization with its relation to saddle points from [BV04]. A function $f : \mathscr{X} \to \mathbb{R}$ is convex if

$$f(\lambda x + (1-\lambda)y) \leqslant \lambda f(x) + (1-\lambda) f(y)$$

holds for every $x, y \in \mathscr{X}$ and $\lambda \in [0,1]$. If f is twice differentiable, then f is called strongly convex if $\nabla^2 f(x) \succeq mI$ with some $m > 0$ for every $x \in \mathscr{X}$. Specifically, a quadratic function $x^T Hx$ is strongly convex if and only if $H \succ 0$.

Consider

$$\begin{aligned} \min \quad & f(x), \\ \text{s.t.} \quad & g(x) \leqslant \mathbf{0}_m, \qquad (2.1) \\ & h(x) = \mathbf{0}_p, \qquad (2.2) \end{aligned}$$

where $f : \mathbb{R}^n \to \mathbb{R}$, $g : \mathbb{R}^n \to \mathbb{R}^m$, and $h : \mathbb{R}^n \to \mathbb{R}^p$ are continuously differentiable. The *refined Slater condition* holds for (2.1) if there exists $x \in \mathbb{R}^n$ such that $h(x) = \mathbf{0}_p$, $g(x) \leqslant \mathbf{0}_m$, and $g_j(x) < 0$ for all nonafine functions g_j, where g_j is the jth component of g. Note that the refined Slater condition reduces to feasibility when constrains are all linear equalities and inequalities. The optimization (2.1) is convex if f and g are convex and h is affine. Define the Lagrangian associated with the optimization problem as

$$\mathfrak{L}(x, \eta, \mu) = g(x) + \eta^T g(x) + \mu^T h(x), \qquad (2.3)$$

where $\eta \in \mathbb{R}^m_{\geqslant}$ and $\mu \in \mathbb{R}^p$. If the optimization is convex and satisfies the refined Slater condition, then strong duality holds, further implying that at least one primal-dual solution (x^*, η^*, μ^*)

of (2.1) exists, and the set of primal-dual solutions is exactly the set of saddle points of $\mathfrak{L}$ on the set $\mathbb{R}^n \times (\mathbb{R}^m_{\geqslant 0} \times \mathbb{R}^p)$.

2.5 Dynamical system and set invariance

We introduce here notions of forward invariance [Kha02] for dynamical system. Consider the non-autonomous system on $\mathbb{R}^n$,

$$\dot{x} = f(t,x), \quad x(0) = x_0, \tag{2.4}$$

where $f : \mathbb{R}_{\geqslant} \times \mathbb{R}^n \to \mathbb{R}^n$. We assume f is piecewise continuous in t and Lipschitz in x, so that the solution of (2.4) exists and is unique. A set $\mathscr{C} \in \mathbb{R}^n$ is *(forward) invariant* for system (2.4) if for every initial condition $x_0 \in \mathscr{C}$, the solution starting from x_0 satisfies $x(t) \in \mathscr{C}$ for all $t \geqslant 0$. The following result states a sufficient and necessary condition for a set to be forward invariant for (2.4).

Lemma 2.5.1. *(Nagumo's Theorem [BM08]): Let $l : \mathbb{R}^n \to \mathbb{R}$ be continuously differentiable and let $\mathscr{C} \triangleq \{x \mid l(x) \leqslant 0\}$. Suppose that for all $x \in \mathscr{C}$, there exists $s \in \mathbb{R}^n$ such that $l(x) + \nabla l(x)^T s < 0$. Furthermore, suppose there exists a Lipschitz function $\phi : \mathbb{R}^n \to \mathbb{R}^n$ such that $\nabla l(x)^T \phi(x) < 0$ for all $x \in \partial\mathscr{C}$. Then $\mathscr{C}$ is forward invariant if and only if $\nabla l(x)^T f(t,x) \leqslant 0$ for all $x \in \partial\mathscr{C}$.*

The assumptions in Nagumo's Theorem ensure that the set $\mathscr{C}$ is regular enough to have a well-defined interior and boundary.

2.6 Power network dynamics

Here we introduce the power network dynamical model characterized by nonlinear swing equations and its linearization.

The power network is encoded by a connected undirected graph $\mathscr{G} = (\mathscr{I}, \mathscr{E})$, where $\mathscr{I} = \{1, 2, \cdots, n\}$ is the collection of buses and $\mathscr{E} = \{e_1, \cdots, e_m\} \subseteq \mathscr{I} \times \mathscr{I}$ is the collection of transmission lines. For each node $i \in \mathscr{I}$, let $\theta_i \in \mathbb{R}$, $\omega_i \in \mathbb{R}$ and $p_i \in \mathbb{R}$ denote its voltage angle, shifted voltage frequency relative to the nominal frequency, and constant active power injection, respectively. We partition buses into $\mathscr{I}^u$ and $\mathscr{I} \setminus \mathscr{I}^u$, where every bus $i \in \mathscr{I}^u$ possesses an additional control command u_i (we explicitly allow for the possibility that $\mathscr{I}^u = \mathscr{I}$). The dynamics is described by the swing equations [MBB08, BH81] for voltage angles and frequencies,

$$\begin{aligned} \dot{\theta}_i(t) &= \omega_i(t), \ \forall i \in \mathscr{I}, \\ M_i \dot{\omega}_i(t) &= -E_i \omega_i(t) - \sum_{j \in \mathscr{N}(i)} b_{ij} \sin(\theta_i(t) - \theta_j(t)) + u_i(t) + p_i, \ \forall i \in \mathscr{I}^u, \\ M_i \dot{\omega}_i(t) &= -E_i \omega_i(t) - \sum_{j \in \mathscr{N}(i)} b_{ij} \sin(\theta_i(t) - \theta_j(t)) + p_i, \ \forall i \in \mathscr{I} \setminus \mathscr{I}^u, \end{aligned} \tag{2.5}$$

where $b_{ij} \in \mathbb{R}_>$ is the susceptance of the line connecting bus i and j, and $M_i \in \mathbb{R}_\geqslant$ and $E_i \in \mathbb{R}_\geqslant$ are the inertia and damping coefficients of bus $i \in \mathscr{I}$. For simplicity, we assume that they are all strictly positive.

For our purposes, it is convenient to rewrite the dynamics (2.5) in a more compact way. Let $\theta \triangleq [\theta_1, \cdots, \theta_n]^T \in \mathbb{R}^n$, $\omega \triangleq [\omega_1, \cdots, \omega_n]^T \in \mathbb{R}^n$ and $p \triangleq [p_1, \cdots, p_n]^T \in \mathbb{R}^n$ be the collection of voltage angles, frequencies, and power injections. Let $D \in \mathbb{R}^{m \times n}$ be the incidence matrix corresponding to an arbitrary graph orientation, and define the voltage angle difference vector

$$\lambda \triangleq D\theta \in \mathbb{R}^m. \tag{2.6}$$

Note that, if the transmission line e_k has bus i (resp. j) as its positive (resp. negative) end, then by the definition of incidence matrix, one has $\lambda_k = \theta_i - \theta_j$. Therefore, the vector λ stands for the collection of angle differences between any two adjacent buses. Denote by $Y_b \in \mathbb{R}^{m \times m}$ the diagonal matrix with $[Y_b]_{k,k} = b_{ij}$, for $k = 1, 2, \cdots, m$. We write the dynamics (2.5) in terms of λ

and ω as

$$\dot{\lambda}(t) = D\omega(t), \tag{2.7a}$$

$$M_i\dot{\omega}_i(t) = -E_i\omega_i(t) - [D^T Y_b]_i \sin\lambda(t) + u_i(t) + p_i,\ \forall i \in \mathscr{I}^u, \tag{2.7b}$$

$$M_i\dot{\omega}_i(t) = -E_i\omega_i(t) - [D^T Y_b]_i \sin\lambda(t) + p_i,\ \forall i \in \mathscr{I}\setminus\mathscr{I}^u, \tag{2.7c}$$

where $\sin\lambda(t) \in \mathbb{R}^m$ is the component-wise sine value of $\lambda(t)$. Note that the transformation (2.6) enforces $\lambda(0) \in \text{range}(D)$. We refer to an initial condition satisfying this equation as *admissible*. When convenient, for conciseness, we use $x(t) \triangleq (\lambda(t), \omega(t)) \in \mathbb{R}^{m+n}$ to denote the collection of all states, and we neglect its dependence on t if the context is clear. In a clearer way, one can re-write (2.7) into the following compact form,

$$\dot{\lambda}(t) = D\omega(t), \tag{2.8a}$$

$$M\dot{\omega}(t) = -E\omega(t) - D^T Y_b \sin\lambda(t) + p + u(t), \tag{2.8b}$$

where $u(t) \in \mathbb{A} \triangleq \left\{z \in \mathbb{R}^n \middle|\ z_w = 0 \text{ for } w \in \mathscr{I}\setminus\mathscr{I}^u\right\}$, $M \triangleq \text{diag}(M_1, M_2, \cdots, M_n) \in \mathbb{R}^{n\times n}$, and $E \triangleq \text{diag}(E_1, E_2, \cdots, E_n) \in \mathbb{R}^{n\times n}$.

Remark 2.6.1. *(Distributed dynamics):* We emphasize that the dynamics (2.8) is naturally distributed, i.e., the evolution of any given state is fully determined by the state information from its neighbors. Specifically, for each $(i,j) \in \mathscr{E}$, $\dot{\lambda}_{ij}$ is determined by ω_i and ω_j, i.e., the states of neighbors of edge (i,j); for each $i \in \mathscr{F}$; $\dot{\omega}_i$ is determined by ω_i, E_i, p_i, α_i and λ_{ij}, b_{ij} with $(i,j) \in \mathscr{E}$ that are either state, parameter, and power injections belonging to node i, or states and parameters of its neighboring edges. •

The trajectories $(\lambda(t), \omega(t))$ locally converge to a unique equilibrium point if all u_i's are set to zero. Specifically, let $L \triangleq D^T Y_b D$ and $L^\dagger$ be its pseudoinverse. Define $\omega^\infty \triangleq \frac{\sum_{i=1}^n p_i}{\sum_{i=1}^n E_i}$,

$E \triangleq \mathrm{diag}(E_1, E_2, \cdots, E_n)$, and $\tilde{p} \triangleq p - \omega^\infty E \mathbf{1}_n$. If

$$\|L^\dagger \tilde{p}\|_{\mathscr{E},\infty} < 1, \tag{2.9}$$

where $\|y\|_{\mathscr{E},\infty} \triangleq \max_{(i,j)\in\mathscr{E}} |y_i - y_j|$, then there exists

$$\lambda^\infty \in \mathscr{R} \triangleq \left\{ \lambda \;\middle|\; |\lambda_i| < \pi/2,\ \forall i \in [1,m]_{\mathbb{N}} \right\}$$

that is unique in $\mathscr{R}_{\mathrm{cl}} \triangleq \left\{ \lambda \;\middle|\; |\lambda_i| \leqslant \pi/2,\ \forall i \in [1,m]_{\mathbb{N}} \right\}$ such that

$$\tilde{p} = D^T Y_b \sin \lambda^\infty \tag{2.10}$$

$$\lambda^\infty \in \mathrm{range}(D). \tag{2.11}$$

According to [DCB13, Lemma 2 and inequality (S17)], system (2.7) with $u_i \equiv 0$ for every $i \in \mathscr{I}^u$, $(\lambda^\infty, \omega^\infty \mathbf{1}_n)$ is stable. Furthermore, $(\lambda(t), \omega(t))$ locally converges to $(\lambda^\infty, \omega^\infty \mathbf{1}_n)$ provided $\lambda(0) \in \mathrm{range}(D)$. Throughout the rest of the chapter, we assume that (2.9) holds.Interestingly, the term $\|L^\dagger \tilde{p}\|_{\mathscr{E},\infty}$ stands for the maximum angle difference between any two adjacent nodes at the steady state for the linearized dynamics of (2.7). We refer to [DCB13] for a detailed physical interpretation.

For the purpose of analyzing power network robustness against time-varying disturbances without the additional assistance from u, we set u to zero, allow p to be time-dependent, and further linearize the dynamics (2.7), leading to the following compact form [ZTLL14],

$$\begin{bmatrix} \dot{\lambda}(t) \\ M\dot{\omega}(t) \end{bmatrix} = \begin{bmatrix} \mathbf{0}_{m\times m} & D \\ -D^T Y_b & -E \end{bmatrix} \begin{bmatrix} \lambda(t) \\ \omega(t) \end{bmatrix} + \begin{bmatrix} \mathbf{0}_m \\ p(t) \end{bmatrix}. \tag{2.12}$$

It should be mentioned that there are more complicated power network models [Pai89]

that also capture the dynamics of voltage and reactive power injection and their dependencies on voltage angle, frequency, and active power injection. However, from a control perspective, we stick on the simplified models (2.8) and (2.12) to establish rigorous results on, for instance, convergence and stability.

Chapter 3

Characterizing tolerable disturbances for transient-state safety

This chapter develops methods to compute the set of disturbances on a power network that do not tip the frequency of each bus and the power flow in each transmission line beyond pre-defined bounds. For a linearized AC power network model, we consider scenarios with varying degree of knowledge about the form of the disturbance. We propose a sampling method to provide inner and outer approximations with tunable accuracy of the set of tolerable disturbances. The complexity of computing such set approximations is a function of the number of sampling points. We introduce an error metric to measure the gap between the approximations and design an algorithm that finds, for fixed number of sampling points, the sampling sequence that minimizes its value. Simulations on the IEEE 39-bus power network illustrate our results.

3.1 Problem Statement

We are interested in understanding how disturbances in the power injection affect the transient-state safety of the power network. For system (2.12) with an arbitrary initial state

$(\lambda(0), \omega(0))$ and a known nominal power injection $p^{\text{nom}}(t) \in \mathbb{R}^n$, we consider the case where an additional unknown power disturbance $p^{\text{dist}}(t) \in \mathbb{R}^n$ is injected starting at time 0, i.e.,

$$p(t) = p^{\text{nom}}(t) + p^{\text{dist}}(t), \quad \forall t \geqslant 0. \tag{3.1}$$

Such additive disturbances model the mismatch between predicted and actual power injection in power systems and might arise, for instance, from variability in the load consumption or uncertainty in power generation caused by, e,.g., renewable energy sources. As safety criteria, we consider the following:

(i) *Transient-state frequency bound:* Given $0 \leqslant t_1 < t_2$, the voltage frequency $\omega(t)$ satisfies

$$\omega^{\min} < \omega(t) < \omega^{\max}, \quad \forall t \in [t_1, t_2].$$

(ii) *Transient-state power flow bound:* Given $0 \leqslant t_1 < t_2$, the power flow $Y_b\lambda(t)$ satisfies

$$f^{\min} < Y_b\lambda(t) < f^{\max}, \quad \forall t \in [t_1, t_2].$$

Depending on how much is known about the form of the disturbance signal P_{dist}, we provide different definitions of what it means for a disturbance to be tolerable by the system, i.e., not disrupt its transient-state safety. We consider three increasingly realistic cases:

(a) *Precisely known trajectory form:* the amplitude of the disturbance is unknown but its trajectory form is precisely known,

$$p^{\text{dist}}(t) = B\text{diag}(\zeta^{\text{pre}}(t))K^{\text{pre}}, \quad \forall t \geqslant 0, \tag{3.2}$$

where $K^{\text{pre}} \in \mathbb{R}^s$ denotes the amplitude; $\zeta^{\text{pre}}(t) \in \mathbb{R}^s$ is an integrable function that stands for the trajectory form; $\text{diag}(\zeta^{\text{pre}}(t))$ is a shorthand notation for the diagonal matrix $\text{diag}(\zeta^{\text{pre}}(t)) \in$

$\mathbb{R}^{s\times s}$, and $B\in\mathbb{R}^{n\times s}$ is a constant matrix whose elements are either 0 or 1, representing the buses where the elements of $\mathrm{diag}\,(\zeta^{\mathrm{pre}}(t))\,K^{\mathrm{pre}}$ are injected. The transient-state tolerableness set is then defined as

$$\Psi^{\mathrm{pre}}\triangleq\left\{K^{\mathrm{pre}}\;\middle|\;\text{(i)-(ii) hold for (2.12) under (3.1) and (3.2)}\right\}\tag{3.3}$$

Clearly, if K^{pre} lies in Ψ^{pre}, then the disturbance $p^{\mathrm{dist}}(t)$ with amplitude K^{pre} does not violate the transient-state requirements.

(b) *Partially known trajectory form:* the amplitude is unknown and the trajectory form is partially known, in the sense that a nominal trajectory form together with an estimation error bound are available. Formally,

$$p^{\mathrm{dist}}(t)=B\mathrm{diag}\,(\zeta^{\mathrm{par}})\,K^{\mathrm{par}},\tag{3.4a}$$

$$\zeta^{\mathrm{par}}(t)=\zeta^{\mathrm{nom}}(t)+\zeta^{\mathrm{err}}(t),\tag{3.4b}$$

where $\zeta^{\mathrm{nom}}(t)\in\mathbb{R}^s$ is known and $\zeta^{\mathrm{err}}(t)\in\mathbb{R}^s$ is bounded component-wise by a known vector $\alpha\in\mathbb{R}^s$. For convenience, we define

$$\mathbf{Z}(\alpha)\triangleq\left\{\zeta\;\middle|\;|\zeta_i(t)|\leqslant\alpha_i,\ \forall i\in[1,s]_{\mathbb{N}},\ \forall t\in[t_1,t_2]\right\}$$

The transient-state tolerableness set is then defined as

$$\left\{K^{\mathrm{par}}\middle|\forall\zeta^{\mathrm{err}}\in\mathbf{Z}(\alpha),\ \text{(i)-(ii) hold for (2.12) under (3.1) and (3.4)}\right\}\tag{3.5}$$

The interpretation of this set is that, if the amplitude K^{par} belongs to Ψ^{par}, then the transient-state requirements (i)-(ii) are satisfied under the disturbance $p^{\mathrm{dist}}(t)$ no matter how the evolution of the unknown trajectory estimation error $\zeta^{\mathrm{err}}(t)$ (as long as it remains bounded by α). Notice

that if $\alpha = \mathbf{0}_s$ and $\zeta^{\text{nom}} = \zeta^{\text{pre}}$, then $\Psi^{\text{par}} = \Psi^{\text{pre}}$. We still deal with the case of precisely known trajectory form independently as its treatment sets the basis for generalization to the other two, more complicated, cases.

(c) *Unknown trajectory form:* both the amplitude and the trajectory form of the disturbance are unknown. To define the transient-state tolerableness set in this case, we consider the magnitude, rather than the amplitude, of the disturbance. Formally,

$$p^{\text{dist}}(t) = BK^{\text{unk}}(t). \tag{3.6}$$

We define the set of disturbances bounded by $R \in \mathbb{R}^s$ as

$$\mathbf{P}(R) \triangleq \left\{ K^{\text{unk}} \;\middle|\; |K_i^{\text{unk}}(t)| \leqslant R_i,\ \forall i \in [1,s]_{\mathbb{N}},\ \forall t \in [t_1,t_2] \right\}.$$

The transient-state tolerableness set is then

$$\left\{ R \geqslant \mathbf{0}_s \middle| \forall K^{\text{unk}} \in \mathbf{P}(R),\ \text{ (i)-(ii) hold for (2.12)under (3.1) and (3.6)} \right\} \tag{3.7}$$

The interpretation of this set is that, if the magnitude bound R belongs to Ψ^{unk}, then the transient-state requirements (i)-(ii) are satisfied under the disturbance $P^{\text{unk}}(t)$ no matter its evolution (as long as it magnitude is bounded by R).

Our goal is to provide formal descriptions of the transient-state tolerableness sets in each of the cases (a)-(c). Given the complexity of obtaining exact descriptions of these sets, we focus on developing inner and outer approximations of them with tunable accuracy. Our strategy to assess the impact of disturbances on system trajectories over the time interval of interest is to consider a finite set of sampling points, ensure certain bounds are satisfied by the trajectories at these points, and reason to ensure that no violations occur in between the sampling points. Figure 3.1 illustrates the main ideas behind our forthcoming discussion.

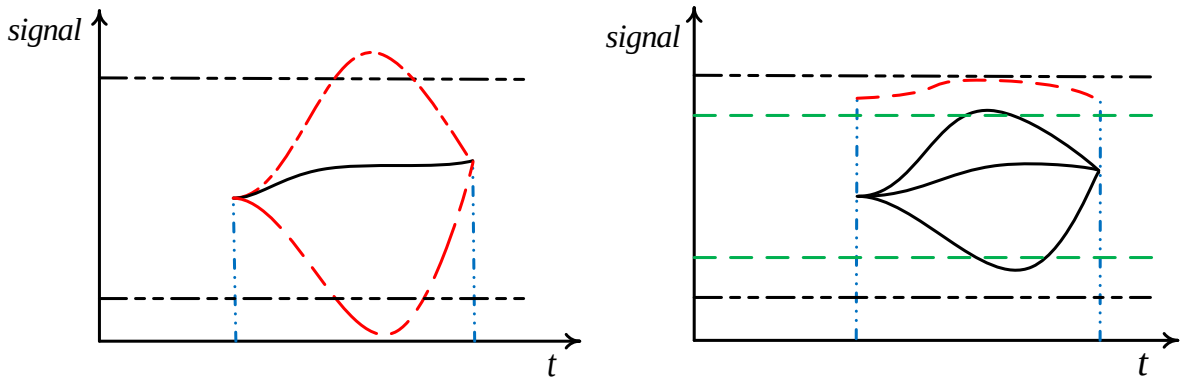

Figure 3.1: Illustration of our strategy to develop approximations of the transient-state tolerableness sets. In this example, we describe conditions under which a one-dimensional signal trajectory stays within the horizontal black dashed bounds in a time interval determined by the two sampling points. In plot (a), we only require the value of the signal to lie within the bounds at two sampling points, which leads to an outer approximation, as some trajectories (red dashed lines) may exceed the bounds within the time interval. In plot (b), we employ a similar strategy, but require the two terminal values to lie within some stricter bounds, denoted by horizontal green dashed lines, whose positions are determined by knowledge about the signal derivative inside the interval. This allows us to guarantee that the whole trajectory does not exceed the black dashed bounds at any time within the interval. This leads to an inner approximation, as there may be trajectories (e.g., the red dashed one) whose terminal values are not in the stricter green bounds but also stay within the black dashed bounds at all times.

Remark 3.1.1. *(Time interval selection):* The initial time t_1 is typically the starting time of the disturbance, $t_1 = 0$. We assume the terminal time t_2 is specified by a system operator based on desired time horizons over which the network performance must meet certain specifications. In general, the time when the system reaches steady state after the disturbance depends on the disturbance itself, the network connectivity, and the network dynamics in a complex way. The work [KPA$^+$04] shows that in transient stability studies t_2 =3 to 5s, and it may extend to 10 to 20s for very large systems with dominant inter-area swing dynamics. •

3.2 Transformation of the transient-state tolerableness sets

In this section, we show how the transient-state tolerableness sets defined in Section 3.1 can be expressed in a way that shares the same structure across all three cases. This allows for a unified treatment of all cases later.

In our treatment, we consider the case where all buses have strictly positive inertias so that the diagonal matrix M in (2.12) is invertible. Under the input (3.1), the dynamics can be written as

$$\dot{x}(t) = Ax(t) + \begin{bmatrix} \mathbf{0}_m \\ M^{-1}p(t) \end{bmatrix}, \tag{3.8}$$

where

$$x(t) = \begin{bmatrix} \lambda(t) \\ \omega(t) \end{bmatrix}, \; A = \begin{bmatrix} \mathbf{0}_{m\times m} & D \\ -M^{-1}D^T Y_b & -M^{-1}E \end{bmatrix}.$$

Solving (3.8), one has

$$x(t) = e^{At}x_0 + \int_0^t e^{A(t-\tau)} \begin{bmatrix} \mathbf{0}_m \\ M^{-1}p(\tau) \end{bmatrix} \mathrm{d}\tau, \tag{3.9}$$

where $x_0 \triangleq [\lambda^T(0)\ \omega^T(0)]^T$. Denoting

$$S(t, x_0, p^{\mathrm{nom}}) \triangleq e^{At}x_0 + \int_0^t e^{A(t-\tau)} \begin{bmatrix} \mathbf{0}_m \\ M^{-1}p^{\mathrm{nom}}(\tau) \end{bmatrix} \mathrm{d}\tau,$$

$$V(t, \zeta) \triangleq \int_0^t e^{A(t-\tau)} \begin{bmatrix} \mathbf{0}_{m\times s} \\ M^{-1}B\mathrm{diag}(\zeta(\tau)) \end{bmatrix} \mathrm{d}\tau,$$

$$x^{\max} \triangleq \begin{bmatrix} \omega^{\max} \\ Y_b^{-1} f^{\max} \end{bmatrix}, \; x^{\min} \triangleq \begin{bmatrix} \omega^{\min} \\ Y_b^{-1} f^{\min} \end{bmatrix}, \tag{3.10}$$

one has that in the case (a) of precisely known trajectory form, the state response can be re-written as $x(t) = S(t, x_0, p^{\text{nom}}) + V(t, \zeta^{\text{pre}}) K^{\text{pre}}$, and hence the transient-state tolerableness set takes the form

$$\left\{ K^{\text{pre}} \middle| x^{\min} < S(t, x_0, p^{\text{nom}}) + V(t, \zeta^{\text{pre}}) K^{\text{pre}} < x^{\max}, \; \forall t \in [t_1, t_2] \right\} \tag{3.11}$$

Based on this expression, it is easy to check whether a given amplitude K^{pre} belongs to Ψ^{pre}. However, in cases (b) and (c), one has

$$\begin{aligned} \Psi^{\text{par}} = \{ K^{\text{par}} \mid & \, x^{\min} < S(t, x_0, p^{\text{nom}}) + V(t, \zeta^{\text{nom}}) K^{\text{par}} \\ & + V(t, \zeta^{\text{err}}) K^{\text{par}} < x^{\max}, \; \forall \zeta^{\text{err}} \in \mathbf{Z}(\alpha), \; \forall t \in [t_1, t_2] \}, \\ \Psi^{\text{unk}} = \{ R \geqslant \mathbf{0}_s \mid & \, x^{\min} < S(t, x_0, p^{\text{nom}}) + V(t, \mathbf{1}_n) K^{\text{unk}}(t) \\ & < x^{\max}, \; \forall K^{\text{unk}} \in \mathbf{P}(R), \; \forall t \in [t_1, t_2] \}. \end{aligned} \tag{3.12}$$

Checking whether a disturbance amplitude belongs to either of these two sets is impractical because of the need to check for all possible values in $\mathbf{Z}(\alpha)$ or $\mathbf{P}(R)$, respectively. The following result shows that these checks can be made as simple as that for case (a).

Lemma 3.2.1. *(Transformation of the transient-state tolerableness set): The following statements hold.*

(i) $K^{\text{par}} \in \Psi^{\text{par}}$ *if and only if, for all* $t \in [t_1, t_2]$,

$$S(t, x_0, p^{nom}) + V(t, \zeta^{nom}) K^{\text{par}} + W(t) \text{diag}\,(\alpha) \, |K^{\text{par}}| < x^{\max}, \tag{3.13a}$$

$$S(t, x_0, p^{nom}) + V(t, \zeta^{nom}) K^{\text{par}} - W(t) \text{diag}\,(\alpha) \, |K^{\text{par}}| > x^{\min}, \tag{3.13b}$$

where

$$W(t) \triangleq \int_0^t |Q(t-\tau)| d\tau \in \mathbb{R}^{(m+n)\times s}, \quad Q(\bar{t}) \triangleq e^{A\bar{t}} \begin{bmatrix} \mathbf{0}_{m\times s} \\ M^{-1}B \end{bmatrix} \in \mathbb{R}^{(m+n)\times s}. \tag{3.14a}$$

(ii) $R \geqslant \mathbf{0}_s \in \Psi^{\text{unk}}$ *if and only if, for all* $t \in [t_1, t_2]$*,*

$$S(t, x_0, p^{nom}) + W(t)R < x^{\max}, \tag{3.15a}$$

$$S(t, x_0, p^{nom}) - W(t)R > x^{\min}. \tag{3.15b}$$

Proof. We only provide the proof of case *(i)*. The proof of *(ii)* follows similarly.

$\Leftarrow$) Assume K^{par} satisfies (3.13). Notice that $\forall \zeta^{\text{err}} \in \mathbf{Z}(\alpha)$, $\forall i \in [1, m+n]_{\mathbb{N}}$, it holds that

$$\begin{aligned}
[W(t)\text{diag}(\alpha)|K^{\text{par}}|]_i &= \int_0^t |[Q(t-\tau)]_i| \text{diag}(\alpha)|K^{\text{par}}| \text{d}\tau \\
&= \int_0^t \sum_{j=1}^{s} |[Q(t-\tau)]_{i,j}| \alpha_j |K_j^{\text{par}}| \text{d}\tau \\
&\geqslant \int_0^t \sum_{j=1}^{s} [Q(t-\tau)]_{i,j} \zeta_j^{\text{err}}(\tau) K_j^{\text{par}} \text{d}\tau \\
&= \int_0^t [Q(t-\tau)]_i \text{diag}(\zeta^{\text{err}}(\tau)) K^{\text{par}} \text{d}\tau \\
&= [V(t, \zeta^{\text{err}}) K^{\text{par}}]_i.
\end{aligned}$$

Therefore, one has that if (3.13) holds $\forall t \in [t_1, t_2]$, then the following inequalities hold $\forall t \in [t_1, t_2]$, $\forall \zeta^{\text{err}} \in \mathbf{Z}(\alpha)$,

$$S(t, p^{\text{nom}}) + V(t, \zeta^{\text{nom}}) K^{\text{par}} + V(t, \zeta^{\text{err}}) K^{\text{par}} < x^{\max}, \tag{3.16a}$$

$$S(t, p^{\text{nom}}) + V(t, \zeta^{\text{nom}}) K^{\text{par}} - V(t, \zeta^{\text{err}}) K^{\text{par}} > x^{\min}, \tag{3.16b}$$

and hence $K^{\text{par}} \in \Psi^{\text{par}}$.

$\Rightarrow$) On the other hand, if $K^{\rm par} \in \Psi^{\rm par}$, then (3.16) holds $\forall t \in [t_1, t_2]$, $\forall \zeta^{\rm err} \in \mathbf{Z}(\alpha)$. To prove (3.13), let us show that for all $l \in [1, m+n]_{\mathbb{N}}$, one has

$$[S(t, p^{\rm nom}) + V(t, \zeta^{\rm nom})K^{\rm par} + W(t)\mathrm{diag}\,(\alpha)\,|K^{\rm par}|]_l < x_l^{\max}, \tag{3.17a}$$

$$[S(t, p^{\rm nom}) + V(t, \zeta^{\rm nom})K^{\rm par} - W(t)\mathrm{diag}\,(\alpha)\,|K^{\rm par}|]_l > x_l^{\min}. \tag{3.17b}$$

For any $l \in [1, m+n]_{\mathbb{N}}$, we select $\hat{\zeta}^{\rm err}(t) \in \mathbf{Z}(\alpha)$ as follows: for any $\bar{t} \in [t_1, t_2]$, let

$$\hat{\zeta}_j^{\rm err}(\tau) = \alpha_l \mathrm{sgn}\{[(Q(\bar{t} - \tau)]_{l,j} K_j^{\rm par}\},\ \forall j \in [1, s]_{\mathbb{N}}. \tag{3.18}$$

One can check that $[W(\bar{t})\mathrm{diag}\,(\alpha)\,|K^{\rm par}|]_l = [V(\bar{t}, \hat{\zeta}^{\rm err})K^{\rm par}]_l$. Therefore, since the lth row of (3.16a) (resp. (3.16b)) holds at $t = \bar{t}$, one has that (3.17a) (resp. (3.17b)) holds at $t = \bar{t}$. The result follows from the arbitrariness of l and $\bar{t}$. $\square$

Given (3.11) and Lemma 3.2.1, it is clear that all the transient-state tolerableness sets $\Psi^{\rm pre}$, $\Psi^{\rm par}$ and $\Psi^{\rm unk}$ admit a common representation involving certain vector signal (different in each case) being upper and lower bounded over the time interval of interest.

Remark 3.2.2. *(Containment relations among $\Psi^{\rm pre}$, $\Psi^{\rm par}$ and $\Psi^{\rm unk}$):* The transient-state tolerableness sets for the different types of disturbances are related as follows:

(i) If $|\zeta^{\rm pre} - \zeta^{\rm nom}|$ is upper bounded by α, then $\Psi^{\rm par} \subseteq \Psi^{\rm pre}$;

(ii) If $|\zeta^{\rm pre}|$ is upper bounded by $\mathbb{R}^s \ni \beta^{\rm pre} > 0$, then for every $R \in \Psi^{\rm unk}$, it holds $\bar{R} \in \Psi^{\rm pre}$ for all $|\bar{R}| \leqslant \mathrm{diag}(\beta^{\rm pre})^{-1} R$. In particular, if $\beta^{\rm pre} \leqslant \mathbf{1}_s$, then $\Psi^{\rm unk} \subseteq \Psi^{\rm pre}$;

(iii) If $|\zeta^{\rm nom}|$ is upper bounded by $\beta^{\rm nom} \in \mathbb{R}^s$ with $\beta^{\rm nom} + \alpha > 0$, then for every $R \in \Psi^{\rm unk}$, it holds that $\bar{R} \in \Psi^{\rm par}$ for all $|\bar{R}| \leqslant (\mathrm{diag}(\beta^{\rm nom} + \alpha))^{-1} R$. In particular, if $\beta^{\rm nom} + \alpha \leqslant \mathbf{1}_s$, then $\Psi^{\rm unk} \subseteq \Psi^{\rm par}$.

These statements follow from Lemma 3.2.1 by noting that if $|\zeta|$ is upper bounded by $\beta > \mathbf{0}_s$, then $W(t)\mathrm{diag}\,(\beta) \geqslant V(t,\zeta)$, for all $t \in [t_1,t_2]$. •

Remark 3.2.3. *(Extension to linearly coupled safety criteria):* The expressions obtained above for the computation of the transient-state tolerableness sets can be extended to the case where the safety requirements involve linearly coupled states of the form

$$\bar{x}^{\min} < Cx(t) < \bar{x}^{\max},\ \forall t \in [t_1,t_2], \tag{3.19}$$

where $C \in \mathbb{R}^{c\times(m+n)}$, $\bar{x}^{\max},\ \bar{x}^{\min} \in \mathbb{R}^c$. A particular example of this scenario is the use of the center of inertia (COI) frequency [Kun94, MSV11],

$$\omega_{\mathrm{COI}}(t) \triangleq \left(\sum_{i=1}^{n} M_i\omega_i(t)\right) / \sum_{i=1}^{n} M_i,$$

which corresponds to $C = [M_1,M_2,\cdots,M_n,\mathbf{0}_m^T]/\sum_{i=1}^n M_i$. When the safety criteria is given by (3.19), the expression (3.11) to compute Ψ^{pre} should be modified by replacing $S(t,x_0,p^{\mathrm{nom}})$ and $V(t,\zeta^{\mathrm{pre}})$ by $CS(t,x_0,p^{\mathrm{nom}})$ and $CV(t,\zeta^{\mathrm{pre}})$, respectively. Similarly, the results in Lemma 3.2.1 to compute Ψ^{par} and Ψ^{unk} are stil valid by replacing $S(t,x_0,p^{\mathrm{nom}})$, $V(t,\zeta^{\mathrm{nom}})$ and $W(t)$ by $CS(t,x_0,p^{\mathrm{nom}})$, $CV(t,\zeta^{\mathrm{nom}})$ and $\int_0^t |CQ(t-\tau)|\mathrm{d}\tau$, respectively. In all cases, $x^{\min}$ (resp. $x^{\max}$) should be replaced by $\bar{x}^{\min}$ (resp. $\bar{x}^{\max}$). •

Remark 3.2.4. *(Initial state as another disturbance):* In the definitions of tolerableness sets, we assume the initial state x_0 is arbitrary but known. We can also consider the initial condition as another type of disturbance, and characterize the tolerableness sets with respect to both x_0 and K^{pre}, K^{par} or R. For instance, consider the definition of Ψ^{par} as

$$\tilde{\Psi}^{\mathrm{par}} \triangleq \Big\{ (x_0^{\mathrm{est}},K^{\mathrm{par}}) \;\Big|\; \forall\zeta^{\mathrm{err}} \in \mathbf{Z}(\alpha),\ \forall x_0 \text{ s.t. } |x_0 - x_0^{\mathrm{est}}| \leqslant x_0^{\mathrm{bnd}},$$
$$\text{(i)-(ii) hold for (2.12) under (3.1) and (3.4)} \Big\},$$

where $x_0^{\text{bnd}} \geqslant \mathbf{0}_{m+n}$ constrains the initial state uncertainty. Note that $(x_0^{\text{est}}, K^{\text{par}}) \in \tilde{\Psi}^{\text{par}}$ means that K^{par} corresponds to a tolerable disturbance for any initial state in a x_0^{bnd}-neighborhood around x_0^{est}. Similarly to Lemma 3.2.1, one can show that $(x_0^{\text{est}}, K^{\text{par}}) \in \tilde{\Psi}^{\text{par}}$ if and only if, for all $t \in [t_1, t_2]$,

$$
\begin{aligned}
&S(t, x_0^{\text{est}}, p^{\text{nom}}) + |e^{At}| x_0^{\text{bnd}} + V(t, \zeta^{\text{nom}}) K^{\text{par}} + W(t) \text{diag}(\alpha) |K^{\text{par}}| < x^{\max}, \\
&S(t, x_0^{\text{est}}, p^{\text{nom}}) - |e^{At}| x_0^{\text{bnd}} + V(t, \zeta^{\text{nom}}) K^{\text{par}} - W(t) \text{diag}(\alpha) |K^{\text{par}}| > x^{\min}.
\end{aligned}
$$

For brevity, throughout the rest of the chapter, we carry out the exposition for the simpler definition of tolerableness set where the initial condition is not an argument, but the results can be extended accordingly. •

Remark 3.2.5. *(Tolerableness sets with zero inertia buses):* The equivalent characterization of the tolerableness sets relies on the fact that M is invertible. If this is not the case, one can derive a similar equivalent transformation. For instance, if the disturbance trajectory form is precisely known, the time-domain solution for system (2.12) under (3.1) and (3.2) still takes a linear form with respect to K^{pre}, denoted by $x(t) = \hat{S}(t, x_0, p^{\text{nom}}) + \hat{V}(t, \zeta^{\text{pre}}) K^{\text{pre}}$, and hence one has

$$
\left\{ K^{\text{pre}} \middle| x^{\min} < \hat{S}(t, x_0, p^{\text{nom}}) + \hat{V}(t, \zeta^{\text{pre}}) K^{\text{pre}} < x^{\max},\ \forall t \in [t_1, t_2] \right\}
$$

Due to the non-zero inertias, $\hat{S}(t, x_0, p^{\text{nom}})$, $\hat{V}(t, \zeta^{\text{pre}})$ have more complicated expressions than $S(t, x_0, p^{\text{nom}})$, $V(t, \zeta^{\text{pre}})$), but the ensuing discussion is equally applicable. •

3.3 Inner and outer approximations of the transient-state tolerableness sets

The descriptions of the transient-state tolerableness sets obtained in Section 3.2 involve infinitely many constraints to check whether a disturbance is tolerable due to the dependence on continuous time. To address this issue, here we construct inner and outer approximations of these sets that are easier to compute and have tunable accuracy. For simplify of exposition, we first consider the case of scalar signals, and then build on this treatment to deal with the vector case.

3.3.1 Scalar-signal case

Here we deal with the case when the signal that must stay within given upper and lower bounds is scalar. Our discussion here can be interpreted as looking at one component of the actual vector signal. Let $y : \mathbb{R} \times \mathbb{R}^s \to \mathbb{R}$ be a generic scalar signal and let $y^{\min}, y^{\max} \in \mathbb{R}$ with $y^{\min} < y^{\max}$. We make the following assumption.

Assumption 3.3.1. *(Signal differentiability and upper bound):* The signal y is differentiable with respect to its first argument and its derivative is upper bounded by a time-continuous signal uniformly in K, i.e., there exists $y_d : \mathbb{R} \to \mathbb{R}_{\geqslant}$ such that

$$|\dot{y}(t,K)| \leqslant y_d(t),\ \forall t \in [t_1,t_2]. \qquad \bullet$$

Consider the set $\Sigma \triangleq \left\{K \;\middle|\; y^{\min} < y(t,K) < y^{\max},\ \forall t \in [t_1,t_2]\right\}$. Let us first define a sampling sequence

$$\tau \triangleq \{\tau_1, \tau_2, \ldots \tau_r\}, \tag{3.20}$$

where $r \geqslant 3$ and τ_i's are called sampling points ordered as $t_1 = \tau_1 < \tau_2 < \cdots < \tau_r = t_2$. Our approximations of the set Σ are based on the idea of requiring the signal to be upper and lower bounded at every sampling point, instead of at every time, and making sure that the constraints defining Σ are not violated at all the other times.

The next result makes our approximation methodology precise.

Lemma 3.3.2. *(Sufficient condition for checking constraints on continuous-time signal): Consider a sampling sequence defined in* (3.20)*. For each $q \in [1, r-1]_{\mathbb{N}}$, Under Assumption 3.3.1, define*

$$d_q^\tau \triangleq \max_{t \in [\tau_q, \tau_{q+1}]} \{y_d(t)\} \in \mathbb{R}_{\geqslant}, \tag{3.21a}$$

$$\delta_q^\tau \triangleq d_q^\tau (\tau_{q+1} - \tau_q)/2 \in \mathbb{R}_{\geqslant}. \tag{3.21b}$$

If

$$y^{\min} + \delta_q^\tau < y(\tau_q, K) \quad < y^{\max} - \delta_q^\tau, \tag{3.22a}$$

$$y^{\min} + \delta_q^\tau < y(\tau_{q+1}, K) < y^{\max} - \delta_q^\tau, \tag{3.22b}$$

for all $q \in [1, r-1]_{\mathbb{N}}$, then $y^{\min} < y(t, K) < y^{\max}$ for all $t \in [t_1, t_2]$.

Proof. We prove that the two upper bounds in (3.22) imply $y(t, K) < y^{\max}$ for all $t \in [t_1, t_2]$ (the statement for the lower bound follows similarly). For $q \in [1, r-1]_{\mathbb{N}}$, let

$$a \triangleq \frac{y(\tau_q, K) + y(\tau_{q+1}, K)}{2} + \delta_q^\tau.$$

Note that, using (3.22), one has that $a < y^{\max}$. Let us show that

$$\max_{t \in [\tau_q, \tau_{q+1}]} y(t, K) \leqslant a. \tag{3.23}$$

It is easy to see that d_q^τ is a Lipschitz constant for y constrained on $[\tau_q, \tau_{q+1}]$. First, we show that $a - y(\tau_q, K) \geqslant 0$ and $a - y(\tau_{q+1}, K) \geqslant 0$. These facts are a consequence of

$$a - y(\tau_q, K) = \frac{1}{2}\big(y(\tau_{q+1}, K) - y(\tau_q, K) + d_q^\tau(\tau_{q+1} - \tau_q)\big),$$
$$a - y(\tau_{q+1}, K) = \frac{1}{2}\big(y(\tau_q, K) - y(\tau_{q+1}, K) + d_q^\tau(\tau_{q+1} - \tau_q)\big),$$

and the fact that $|y(\tau_{q+1}, K) - y(\tau_q, K)| \leqslant d_q^\tau(\tau_{q+1} - \tau_q)$. Next, using the Lipschitz condition, one sees that, if y reaches at some time a starting from the value $y(\tau_q, K)$, it takes at least $\big(a - y(\tau_q, K)\big)/d_q^\tau > 0$ seconds from τ_q to do so. On the other hand, to come down from such a value, it would take at least $\big(a - y(\tau_{q+1}, K)\big)/d_q^\tau > 0$ seconds, so the total time would be at least $\big(2a - y(\tau_q, K) - y(\tau_{q+1}, K)\big)/d_q^\tau = \tau_{q+1} - \tau_q$. Therefore y cannot reach any value larger than a, i.e., (3.23) follows, concluding the proof. □

Lemma 3.3.2 opens the way to efficiently compute inner and outer approximations of the set Σ. The next result formally states this and shows that the two approximations can be made arbitrarily accurate.

Lemma 3.3.3. *(Inclusion relations and convergence of inner and outer sets): Let $K \in \mathbb{R}^s$, and $t \mapsto y(t, K)$ satisfy Assumption 3.3.1. For a sampling sequence τ, let*

$$\varepsilon^\tau \triangleq \max_{q \in [1, r-1]_{\mathbb{N}}} \{\tau_{q+1} - \tau_q\} \in \mathbb{R}_>$$

denote its maximum inter-time separation. With the notation of Lemma 3.3.2, define

$$\Sigma_O^\tau \triangleq \Big\{K \;\Big|\; y^{\min} \leqslant y(\tau_q, K) \leqslant y^{\max}, \quad \forall q \in [1, r]_{\mathbb{N}}\Big\},$$
$$\Sigma_I^\tau \triangleq \Big\{K \;\Big|\; y^{\min} + \delta_q^\tau < y(\tau_q, K),\ y(\tau_{q+1}, K) < y^{\max} - \delta_q^\tau, \quad \forall q \in [1, r-1]_{\mathbb{N}}\Big\}$$

Then, the following statements hold

(i) $\Sigma_I^\tau \subseteq \Sigma \subseteq \Sigma_{\mathrm{cl}} \subseteq \Sigma_O^\tau$, *and*

(ii) for a sequence of sampling sequences $\{\tau(k)\}_{k=1}^\infty$, *if* $\varepsilon^{\tau(k)} \to 0^+$ *as* $k \to \infty$, *then* $\Sigma_O^{\tau(k)} \to \Sigma_{\mathrm{cl}}$ *and* $\Sigma_I^{\tau(k)} \to \Sigma$.

Proof. We first prove (i). Since the constraints defining Σ_O^τ all appear in Σ_{cl}, we deduce $\Sigma_{\mathrm{cl}} \subseteq \Sigma_O^\tau$. By Lemma 3.3.2, it holds that $\Sigma_I^\tau \subseteq \Sigma$.

Next we prove (ii). For each sampling sequence $\tau(k)$, let

$$\delta^{\max}(k) \triangleq \varepsilon^{\tau(k)} \max_{q \in [1, r(k)-1]_{\mathbb{N}}} d_q^{\tau(k)}/2.$$

Since $d_q^{\tau(k)}$ is a Lipschitz constant for y constrained on $[\tau_q(k), \tau_{q+1}(k)]$, we have that for all $k \in \mathbb{N}$, $t \in [\tau_q(k), \tau_{q+1}(k)]$ and $q \in [1, r(k)-1]_{\mathbb{N}}$,

$$\begin{aligned} |y(t,K) - y(\tau_q(k),K)| &\leqslant d_q^{\tau(k)}(t - \tau_q(k)) \\ &\leqslant d_q^{\tau(k)}(\tau_{q+1}(k) - \tau_q(k)) \\ &= 2\delta_q^{\tau(k)} \leqslant 2\delta^{\max}(k). \end{aligned} \tag{3.25}$$

Now if $y^{\min} \leqslant y(\tau_1(k),K), \ldots, y(\tau_{r(k)}(k),K) \leqslant y^{\max}$, then by the above inequality one has $y^{\min} - 2\delta^{\max}(k) \leqslant y(t,K) \leqslant y^{\max} + 2\delta^{\max}(k)$ for any $t \in [t_1, t_2]$. Let

$$\left\{ K \middle| y^{\min} - 2\delta^{\max}(k) \leqslant y(t,K) \leqslant y^{\max} + 2\delta^{\max}(k),\ \forall t \in [t_1, t_2] \right\}$$

The above reasoning shows that $\Sigma_O \subseteq \hat{\Sigma}_O^{\tau(k)}$. Together with (i), we have $\Sigma_{\mathrm{cl}} \subseteq \Sigma_O^{\tau(k)} \subseteq \hat{\Sigma}_O^{\tau(k)}$. Next we show that

$$\hat{\Sigma}_O^{\tau(k)} \to \Sigma_{\mathrm{cl}} \text{ as } k \to \infty, \tag{3.26}$$

which, by the properties of set limits presented in the preliminaries, suffices to guarantee that

$\Sigma_O^{\tau(k)} \to \Sigma_{\mathrm{cl}}$ as $k \to \infty$.

To prove (3.26), we first show that $\limsup_{k\to\infty} \hat{\Sigma}_O^{\tau(k)} = \Sigma_{\mathrm{cl}}$ by pointing out that the two sets mutually contain each other. Since $\Sigma_{\mathrm{cl}} \subseteq \hat{\Sigma}_O^{\tau(j)}$ for every $j \in \mathbb{N}$, it holds that $\Sigma_{\mathrm{cl}} \subseteq \bigcup_{j\geqslant k} \hat{\Sigma}_O^{\tau(j)}$ for every $k \in \mathbb{N}$, which further implies that $\Sigma_{\mathrm{cl}} \subseteq \bigcap_{k\geqslant 1} \bigcup_{j\geqslant k} \hat{\Sigma}_O^{\tau(j)} = \limsup_{k\to\infty} \hat{\Sigma}_O^{\tau(k)}$. On the other hand, suppose that $K \notin \Sigma_{\mathrm{cl}}$, then by the definition of Σ_{cl}, there exists $\bar{t} \in [t_1, t_2]$ such that $y(\bar{t}, K) > y^{\max}$ or $y(\bar{t}, K) < y^{\min}$. Since by the assumptions, if $j \to \infty$, then $\varepsilon^{\tau(j)} \to 0^+$, which implies that $\delta^{\max}(j) \to 0^+$, one has that $K \notin \hat{\Sigma}_O^{\tau(j)}$ for every j large enough, i.e., $K \notin \bigcup_{j\geqslant k} \hat{\Sigma}_O^{\tau(j)}$ for k large enough. This further implies that $K \notin \bigcap_{k\geqslant 1} \bigcup_{j\geqslant k} \hat{\Sigma}_O^{\tau(j)}$, i.e., $K \notin \limsup_{k\to\infty} \hat{\Sigma}_O^{\tau(j)}$. Therefore, by contradiction, it holds that $\limsup_{k\to\infty} \hat{\Sigma}_O^{\tau(k)} \subseteq \Sigma_{\mathrm{cl}}$.

Next we show that $\liminf_{k\to\infty} \hat{\Sigma}_O^{\tau(k)} = \Sigma_{\mathrm{cl}}$. Since $\liminf_{k\to\infty} \hat{\Sigma}_O^{\tau(k)} \subseteq \limsup_{k\to\infty} \hat{\Sigma}_O^{\tau(k)}$ and we have already proven that $\limsup_{k\to\infty} \hat{\Sigma}_O^{\tau(k)} = \hat{\Sigma}_{\mathrm{cl}}$, we only need to show that $\hat{\Sigma}_{\mathrm{cl}} \subseteq \liminf_{k\to\infty} \hat{\Sigma}_O^{\tau(k)}$. This containment holds by noticing that $\hat{\Sigma}_{\mathrm{cl}} \subseteq \hat{\Sigma}_O^{\tau(j)}$ for every $j \in \mathbb{N}$, which implies that $\hat{\Sigma}_{\mathrm{cl}} \subseteq \bigcup_{k\geqslant 1} \bigcap_{j\geqslant k} \Sigma_O^{\tau(j)} = \liminf_{k\to\infty} \hat{\Sigma}_O^{\tau(k)}$.

Similarly, by letting

$$\left\{ K \middle| y^{\min} + \delta^{\max}(k) < y(t, K) < y^{\max} - \delta^{\max}(k),\ \forall t \in [t_1, t_2] \right\}$$

One has that $\hat{\Sigma}_I^{\tau(k)} \subseteq \Sigma_I^{\tau(k)} \subseteq \Sigma$ and $\hat{\Sigma}_I^{\tau(k)} \to \Sigma$ as $k \to \infty$; therefore $\Sigma_I^{\tau(k)} \to \Sigma$ as $k \to \infty$. □

As stated in Lemma 3.3.3, the inner and outer approximations can be made arbitrarily accurate as ε^τ decreases, at the cost of increasing the cardinality of the sampling sequence, which linearly raises the number of constraints in the definition of the approximations.

3.3.2 Vector-signal case

Here we build on the treatment of the generic scalar-signal case to construct inner and outer approximations of the transient-state tolerableness sets Ψ^{pre}, Ψ^{par} and Ψ^{unk}. In the pre-

cisely known case, for every $i \in [1, m+n]_{\mathbb{N}}$, if we let

$$\Psi_i^{\text{pre}} \triangleq \left\{ K^{\text{pre}} \middle| x_i^{\min} \leqslant [S(t, x_0, p^{\text{nom}})]_i + [V(t, \zeta^{\text{pre}})]_i K^{\text{pre}} \leqslant x_i^{\max},\ \forall t \in [t_1, t_2] \right\} \tag{3.27}$$

then $\Psi^{\text{pre}} = \bigcap_{i \in [1,m+n]_{\mathbb{N}}} \Psi_i^{\text{pre}}$. The inner (resp. outer) approximation of each Ψ_i^{pre} follows from Lemma 3.3.3 with respect to the signal $y(t, K^{\text{pre}}) = [S(t, x_0, p^{\text{nom}})]_i + [V(t, \zeta^{\text{pre}})]_i K^{\text{pre}}$ and bounds $y^{\max} = x_i^{\max}$ and $y^{\min} = x_i^{\min}$. Then, the inner (resp. outer) approximation of Ψ^{pre} is just the intersection of inner (resp. outer) approximations for every i. We can also approximate Ψ^{par} and Ψ^{unk} in a similar fashion.

The main difficulty then in applying the scalar-signal results lies in the fact that the signals are not necessarily known a priori, but instead are the result of the effect of the disturbances on the power network dynamics (2.12). The next result shows that, nevertheless, we can guarantee that Assumption 3.3.1 is satisfied.

Lemma 3.3.4. *(Component-wise derivative bound signal): Suppose the amplitude vector K^{pre} (resp. K^{par}) in Ψ^{pre} (resp. Ψ^{par}), and the magnitude vector R in Ψ^{unk} are bounded as follows,*

$$\|K^{\text{pre}}\|_\infty \leqslant \gamma^{\text{pre}},\ \|K^{\text{par}}\|_\infty \leqslant \gamma^{\text{par}},\ \|R\|_\infty \leqslant \gamma^{\text{unk}}. \tag{3.28}$$

For every $i \in [1, n+m]_{\mathbb{N}}$, define

$$z_i^{\text{pre}}(t) \triangleq |[S'(t, x_0, p^{nom})]_i| + \gamma^{\text{pre}} \|[V'(t, \zeta^{\text{pre}})]_i\|_1, \tag{3.29a}$$

$$z_i^{\text{par}}(t) \triangleq |[S'(t, x_0, p^{nom})]_i| + \gamma^{\text{par}} \left(\|[V'(t, \zeta^{nom})]_i\|_1 + \alpha_i \|[W'(t)_i\|_1 \right), \tag{3.29b}$$

$$z_i^{\text{unk}}(t) \triangleq |[S'(t, x_0, p^{nom})]_i| + \gamma^{\text{unk}} \|[W'(t)]_i\|_1, \tag{3.29c}$$

where $S'(t, x_0, p^{nom})$, $V'(t, \xi)$ and $W'(t)$ are the component-wise time-derivative of

$S(t,x_0,p^{nom})$, $V(t,\xi)$ and $W(t)$, and admit the following form

$$S'(t,x_0,p^{nom}) = AS(t,x_0,p^{nom}) + \begin{bmatrix} \mathbf{0}_m \\ M^{-1}p^{nom}(t) \end{bmatrix}, \tag{3.30a}$$

$$V'(t,\zeta) = AV(t,\zeta) + \begin{bmatrix} \mathbf{0}_{m\times s} \\ M^{-1}B\mathrm{diag}\,(\zeta(t)) \end{bmatrix}, \tag{3.30b}$$

$$W'(t) = |Q(t)|. \tag{3.30c}$$

Then it holds that for all $i \in [1, m+n]_{\mathbb{N}}$ and for all $t \in [t_1,t_2]$,

$$\frac{d}{dt}\left([S(t,x_0,p^{nom})]_i + [V(t,\zeta^{pre})]_i K^{pre}\right) \leqslant z_i^{\mathrm{pre}}(t), \tag{3.31a}$$

$$\frac{d}{dt}\left([S(t,x_0,p^{nom})]_i + [V(t,\zeta^{nom})]_i K^{par}(\pm)W(t)|K^{par}|\right) \leqslant z_i^{\mathrm{par}}(t), \tag{3.31b}$$

$$\frac{d}{dt}\left([S(t,x_0,p^{nom})]_i(\pm)W(t)R\right) \leqslant z_i^{\mathrm{par}}(t). \tag{3.31c}$$

Proof. One can easily verify (3.30a) and (3.30b) using the chain rule. For (3.30c), by letting $\bar{\tau} = t - \tau$, one has

$$W(t) = \int_0^t |Q(t-\tau)|\mathrm{d}\tau = \int_0^t |Q(\bar{\tau})|\mathrm{d}\bar{\tau},$$

and hence $W'(t) = |Q(t)|$ follows immediately.

Next, since

$$\begin{aligned}
\mathrm{d}\left([S(t,x_0,p^{\mathrm{nom}})]_i + [V(t,\zeta^{\mathrm{pre}})]_i K^{\mathrm{pre}}\right)/\mathrm{d}t &= [S'(t,x_0,p^{\mathrm{nom}})]_i + [V'(t,\zeta^{\mathrm{pre}})]_i K^{\mathrm{pre}} \\
&\leqslant |[S'(t,x_0,p^{\mathrm{nom}})]_i| + \|K^{\mathrm{pre}}\|_\infty \|[V'(t,\zeta^{\mathrm{pre}})]_i\|_1 \\
&\leqslant z_i^{\mathrm{pre}}(t),
\end{aligned}$$

one has (3.31a) holds. The rest follows similarly. □

Lemma 3.3.4 allows us to use the results for generic scalar signals to construct the set approximations in the case of vector signals generated by power network dynamics subject to disturbances.

Theorem 3.3.5. *(Inclusion relations and convergence of inner and outer sets for the transient-state tolerableness set): For every $i \in [1, n+m]_{\mathbb{N}}$, let $\tau^i = \{\tau^i_1, \tau^i_2, \ldots, \tau^i_{r(i)}\}$ be a sampling sequence and define for each $\lambda \in \{pre, par, unk\}$,*

$$\begin{aligned}
\varepsilon^{\tau^i} &\triangleq \max_{q \in [1, r(i)-1]_{\mathbb{N}}} \{\tau^i_{q+1} - \tau^i_q\}, \\
d^{\lambda}_{q,i} &\triangleq \max_{t \in [\tau^i_q, \tau^i_{q+1}]} \{z^{\lambda}_i(t)\},\ \forall q \in [1, r(i)-1]_{\mathbb{N}}, \\
\delta^{\lambda}_{q,i} &\triangleq d^{\lambda}_{q,i}(\tau^i_{q+1} - \tau^i_q)/2,\ \forall q \in [1, r(i)-1]_{\mathbb{N}}.
\end{aligned}$$

Further define

$$\begin{aligned}
\Psi^{pre}_{O,i} &\triangleq \left\{K^{pre} \;\middle|\; x^{min}_i \leqslant [S(\tau^i_q, x_0, p^{nom})]_i + [V(\tau^i_q, \zeta^{pre})]_i K^{pre} \leqslant x^{max}_i,\ \forall q \in [1, r(i)]_{\mathbb{N}}\right\}, \\
\Psi^{pre}_{I,i} &\triangleq \left\{K^{pre} \;\middle|\; x^{min}_i + \delta^{pre}_{q,i} < [S(t, x_0, p^{nom})]_i + [V(t, \zeta^{pre})]_i K^{pre} < x^{max}_i - \delta^{pre}_{q,i},\ \forall t \in \{\tau^i_q, \tau^{i+1}_q\},\ \forall q \in [1, r(i)-1]_{\mathbb{N}}\right\}, \\
\overline{\Psi}^{par}_{O,i} &\triangleq \left\{K^{par} \;\middle|\; [S(\tau^i_q, x_0, p^{nom})]_i + [V(\tau^i_q, \zeta^{nom})]_i K^{par} + W(\tau^i_q)|K^{par}| \leqslant x^{max}_i,\ \forall q \in [1, r(i)]_{\mathbb{N}}\right\}, \\
\underline{\Psi}^{par}_{O,i} &\triangleq \left\{K^{par} \;\middle|\; [S(\tau^i_q, x_0, p^{nom})]_i + [V(\tau^i_q, \zeta^{nom})]_i K^{par} - W(\tau^i_q)|K^{par}| \geqslant x^{min}_i,\ \forall q \in [1, r(i)]_{\mathbb{N}}\right\}, \\
\overline{\Psi}^{par}_{I,i} &\triangleq \left\{K^{par} \;\middle|\; [S(t, x_0, p^{nom})]_i + [V(t, \zeta^{nom})]_i K^{par} + W(t)|K^{par}| < x^{max}_i - \delta^{par}_{q,i},\ \forall t \in \{\tau^i_q, \tau^{i+1}_q\},\ \forall q \in [1, r(i)-1]_{\mathbb{N}}\right\}, \\
\underline{\Psi}^{par}_{I,i} &\triangleq \left\{K^{par} \;\middle|\; [S(t, x_0, p^{nom})]_i + [V(t, \zeta^{nom})]_i K^{par} - W(t)|K^{par}| > x^{min}_i + \delta^{par}_{q,i},\ \forall t \in \{\tau^i_q, \tau^{i+1}_q\},\ \forall q \in [1, r(i)-1]_{\mathbb{N}}\right\}, \\
\overline{\Psi}^{unk}_{O,i} &\triangleq \left\{R \;\middle|\; [S(\tau^i_q, x_0, p^{nom})]_i + W(\tau^i_q)R \leqslant x^{max}_i,\ \forall q \in [1, r(i)]_{\mathbb{N}}\right\}, \\
\underline{\Psi}^{unk}_{O,i} &\triangleq \left\{R \;\middle|\; [S(\tau^i_q, x_0, p^{nom})]_i - W(\tau^i_q)R \geqslant x^{min}_i,\ \forall q \in [1, r(i)]_{\mathbb{N}}\right\}, \\
\overline{\Psi}^{unk}_{I,i} &\triangleq \left\{R \;\middle|\; [S(t, x_0, p^{nom})]_i + W(t)R < x^{max}_i - \delta^{unk}_{q,i},\ \forall t \in \{\tau^i_q, \tau^{i+1}_q\},\ \forall q \in [1, r(i)-1]_{\mathbb{N}}\right\}, \\
\underline{\Psi}^{unk}_{I,i} &\triangleq \left\{R \;\middle|\; [S(t, x_0, p^{nom})]_i - W(t)R > x^{min}_i + \delta^{unk}_{q,i},\ \forall t \in \{\tau^i_q, \tau^{i+1}_q\},\ \forall q \in [1, r(i)-1]_{\mathbb{N}}\right\}. \qquad (3.32)
\end{aligned}$$

Given the sets defined in (3.32)*, let*

$$\Psi_O^{pre} \triangleq \bigcap_{i\in[1,n+m]_{\mathbb{N}}} \Psi_{O,i}^{pre}, \tag{3.33a}$$

$$\Psi_I^{pre} \triangleq \bigcap_{i\in[1,n+m]_{\mathbb{N}}} \Psi_{I,i}^{pre}, \tag{3.33b}$$

$$\Psi_O^{par} \triangleq \bigcap_{i\in[1,n+m]_{\mathbb{N}}} (\overline{\Psi}_{O,i}^{par} \cap \underline{\Psi}_{O,i}^{par}), \tag{3.33c}$$

$$\Psi_I^{par} \triangleq \bigcap_{i\in[1,n+m]_{\mathbb{N}}} (\overline{\Psi}_{I,i}^{par} \cap \underline{\Psi}_{I,i}^{par}), \tag{3.33d}$$

$$\Psi_O^{unk} \triangleq \bigcap_{i\in[1,n+m]_{\mathbb{N}}} (\overline{\Psi}_{O,i}^{unk} \cap \underline{\Psi}_{O,i}^{unk}), \tag{3.33e}$$

$$\Psi_I^{unk} \triangleq \bigcap_{i\in[1,n+m]_{\mathbb{N}}} (\overline{\Psi}_{I,i}^{unk} \cap \underline{\Psi}_{I,i}^{unk}). \tag{3.33f}$$

Then, the following statements hold for any $\lambda \in \{\text{pre}, \text{par}, \text{unk}\}$*,*

(i) $\Psi_I^\lambda \subseteq \Psi^\lambda \subseteq \Psi_{\text{cl}}^\lambda \subseteq \Psi_O^\lambda$*, and*

(ii) if $\varepsilon^{\tau^i} \to 0^+$ *for all* $i \in [1, m+n]_{\mathbb{N}}$*, then* $\Psi_O^\lambda \to \Psi_{\text{cl}}^\lambda$ *and* $\Psi_I^\lambda \to \Psi^\lambda$*.*

Proof. We only prove the case $\lambda = \text{pre}$ (the other two cases follow similarly). Notice that each Ψ_i^{pre} defined in (3.27) can be approximated individually using Lemma 3.3.3 by letting $y(t, K^{\text{pre}}) = [S(t, x_0, p^{\text{nom}})]_i + [V(t, \zeta^{\text{pre}})]_i K^{\text{pre}}$. The corresponding time-derivative bound signal is $y_d = z_i^{\text{pre}}$, which follows from Lemma 3.3.4. Therefore, it holds that for every $i \in [1, m+n]_{\mathbb{N}}$, $\Psi_{I,i}^{\text{pre}} \subseteq \Psi_i^{\text{pre}} \subseteq \Psi_{i,\text{cl}}^{\text{pre}} \subseteq \Psi_{O,i}^{\text{pre}}$, and $\Psi_{O,i}^{\text{pre}} \to \Psi_{\text{cl}}^{\text{pre}}$ and $\Psi_I^\lambda \to \Psi^{\text{pre}}$ as $\varepsilon^{\tau^i} \to 0^+$. Since finite intersections preserve containment relations and set limits, statements (i) and (ii) follow. □

Even though we assume for simplicity that the time interval $[t_1, t_2]$ is the same for each component of $x(t)$, note that this can be easily extended to scenarios where each $x_i(t)$ has its own time sampling interval $[t_1^i, t_2^i]$.

Remark 3.3.6. *(Bound on the disturbance amplitude):* Theorem 3.3.5 requires an a priori bound on the norm of K^{pre} (resp. K^{par} and R) to obtain the set Ψ_I^{pre} (resp. Ψ_I^{par} and Ψ_I^{unk}). This assumption is reasonable in the sense that the energy of the disturbance should be upper bounded. Alternatively, since Ψ_O^{pre} (resp. Ψ_O^{par} and Ψ_O^{unk}) can be computed without any knowledge of the norm bound, one can obtain an upper bound on the norm of K^{pre}, for instance, by solving $\max_{K\in\Psi_O^{\text{pre}}} \|K\|_\infty$, provided that Ψ_O^{pre} is bounded. •

Remark 3.3.7. *(Computational complexity):* Note that both $\Psi_{\text{I}}^{\lambda}$ and $\Psi_{\text{O}}^{\lambda}$ for any $\lambda \in \{\text{pre}, \text{par}, \text{unk}\}$ consist of only linear constraints, and hence are convex sets, where the number of constraints appearing in them are, depending on the case, either $2\sum_{i=1}^{m+n} r(i)$ or $4\sum_{i=1}^{m+n} r(i)$. This implies that the complexity of characterizing such sets grows linearly with respect to the number of sampling points, and, if we take the $r(i)$'s equal for each component, then it also grows linearly with $m+n$, i.e., the number of states. Furthermore, the approximations also scale well with the dimension of K because of the linear dependence of the system trajectories on this parameter.

The actual computation of the approximation sets involves the evaluation of several time-varying matrices (e.g., $S(t,x_0,p^{\text{nom}})$, $V(t,\zeta^{\text{pre}})$, $W(t)$, etc.) at each sampling time. Here, we briefly describe the procedure we employ to do this for $S(t,x_0,p^{\text{nom}})$ at $t=\tau_1^i,\tau_2^i,\cdots,\tau_r^i$ for each $i\in[1,n+m]_{\mathbb{N}}$ (other procedures are also possible). Using a first-order approximation, for sufficiently small $T>0$ and any $n\in\mathbb{N}$, we can write

$$\begin{aligned} S((n+1)T,x_0,p^{\text{nom}}) &\approx S(nT,x_0,p^{\text{nom}}) + TS'(nT,x_0,p^{\text{nom}}) \\ &= S(nT,x_0,p^{\text{nom}}) + TAS(nT,x_0,p^{\text{nom}}) + T\begin{bmatrix} \mathbf{0}_m \\ M^{-1}p^{\text{nom}}(nT) \end{bmatrix}, \end{aligned}$$

where the equality follows from substituting $S'(nT,x_0,p^{\text{nom}})$ by (3.30a). Using this equation, one can iteratively compute the value of $S(t,x_0,p^{\text{nom}})$ at $t=0,T,2T,3T,\ldots$. For T much smaller than the distance between consecutive sampling points, one can report to this approximation to

evaluate $S(t, x_0, p^{\text{nom}})$ at the sampling points. •

Remark 3.3.8. *(Robustness metric based on tolerableness set):* One can synthesize metrics that quantify the robustness to disturbances of the power network at a given steady state using the transient-state tolerableness set. The basic idea is to identify the smallest (with respect to some criteria) disturbance that leads to a violation of the safety criteria (i)-(ii). Formally, for $\lambda \in \{\text{pre}, \text{par}, \text{unk}\}$, one can define the metric, denoted by β^λ, as the optimal value of the following optimization problem,

$$\begin{aligned} \inf \quad & f(K) && \text{(3.34a)} \\ \text{s.t.} \quad & K \notin \Psi^\lambda, && \text{(3.34b)} \\ & g(K) \leqslant 0, && \text{(3.34c)} \end{aligned}$$

where $f : \mathbb{R}^s \mapsto \mathbb{R}$ is a measurement of the disturbance energy, say, $f(K) = \|K\|_2$, and (3.34c) represents some other constraints for the disturbance. Since we cannot precisely compute Ψ^λ, one can alternatively compute the optimal value, denoted β_I^λ (resp. β_O^λ), of the following optimization problem

$$\begin{aligned} \inf \quad & f(K) && \text{(3.35a)} \\ \text{s.t.} \quad & K \notin \Psi_O^\lambda (\text{resp. } \Psi_I^\lambda), && \text{(3.35b)} \\ & g(K) \leqslant 0. && \text{(3.35c)} \end{aligned}$$

By Theorem 3.3.5, one has that $\beta_I^\lambda \leqslant \beta^\lambda \leqslant \beta_O^\lambda$. If f is continuous, as $\varepsilon^{\tau^i} \to 0^+$ for all $i \in [1, m+n]_{\mathbb{N}}$, it holds that $\beta_I^\lambda \to \beta^\lambda$ and $\beta_O^\lambda \to \beta^\lambda$, i.e., we can upper and lower bound β^λ with an arbitrary degree of accuracy.

Although constraint (3.35b) is nonconvex (since it corresponds to the complement of a convex polytope), we can decompose (3.35b) into a finite union of linear constraints. We take

$\lambda =$pre as an example. Define for each $q \in [1, r(i)]$,

$$\Psi^{\text{pre}}_{O,i,q} \triangleq \left\{ K^{pre} \middle| x_i^{\min} \leqslant [S(\tau_q^i, x_0, p^{\text{nom}})]_i + [V(\tau_q^i, \zeta^{\text{pre}})]_i K^{\text{pre}} \leqslant x_i^{\max} \right\}$$

Then we deduce $\Psi^{\text{pre}}_O = \bigcap_{i\in[1,m+n]_{\mathbb{N}}} \bigcap_{q\in[1,r(i)]_{\mathbb{N}}} \Psi^{\text{pre}}_{O,i,q}$. Now denote $\beta^{\text{pre}}_{O,i,q}$ as the optimal solution of

$$\begin{aligned} \inf \quad & f(K) && \text{(3.36a)} \\ \text{s.t.} \quad & K \notin \Psi^{\lambda}_{O,i,q}, && \text{(3.36b)} \\ & g(K) \leqslant 0. && \text{(3.36c)} \end{aligned}$$

One can see that β^{pre}_O equals the smallest value among $\beta^{\text{pre}}_{O,i,q}$ over all possible i and q. Notice now (3.36b) is a linear constraint, and if f and g are convex, then (3.36) is a convex optimization problem. In the same way, we can compute β^{pre}_I. This strategy also works for $\mu \in \{\text{pre}, \text{par}\}$. •

3.4 Optimizing the sampling sequence

A relevant question regarding the inner and outer approximations developed above is how to precisely quantify how well they approximate the corresponding transient-state tolerableness set. With metrics available to provide such quantification, one can then ask the question of how to optimize the location of a fixed number of sampling points in order to provide better approximations. This aim is motivated by the fact that the complexity of characterizing the approximations grows with the number of constraints defining them. To answer these questions, we first consider the scalar-signal case and quantify the approximation gap between Σ^{τ}_I (resp. Σ^{τ}_O) and Σ (resp. Σ_{cl}). We then propose an provably correct algorithmic procedure to find the optimal sampling sequence and generalize our treatment to the vector-signal case.

3.4.1 Metric measuring the approximation gap

Here we define a metric to quantify the gap between the inner and outer approximations and the actual set. To do so, we find it useful to introduce the following set definitions with the same functional form as Σ,

$$\bar{\Sigma}_O^\tau \triangleq \left\{ K \;\middle|\; y^{\min} - 2\delta_q^\tau \leqslant y(t,K) \leqslant y^{\max} + 2\delta_q^\tau,\ \forall t \in [\tau_q, \tau_{q+1}],\ \forall q \in [1, r-1]_{\mathbb{N}} \right\}, \tag{3.37a}$$

$$\bar{\Sigma}_I^\tau \triangleq \left\{ K \;\middle|\; y^{\min} + \delta_q^\tau < y(t,K) < y^{\max} - \delta_q^\tau,\ \forall t \in [\tau_q, \tau_{q+1}],\ \forall q \in [1, r-1]_{\mathbb{N}} \right\}. \tag{3.37b}$$

Given the similarity in their definitions with Σ, these sets are easier to compare with it than the original Σ_I^τ and Σ_O^τ. In addition, note that by (3.25), it holds that $\Sigma_O^\tau \subseteq \bar{\Sigma}_O^\tau$, and since all constraints in Σ_I^τ appear in $\bar{\Sigma}_I^\tau$ as well, one has that $\bar{\Sigma}_I^\tau \subseteq \Sigma_I^\tau$. Therefore a conservative but guaranteed way to describe the approximation is to depict the gap between $\bar{\Sigma}_I^\tau$ and Σ, and between Σ_{cl} and $\bar{\Sigma}_O^\tau$.

To quantify the gap between $\bar{\Sigma}_I^\tau$ and Σ, we define the approximation metric as

$$\nu(\tau) \triangleq \max_{q \in [1, r-1]_{\mathbb{N}}} \{\delta_q^\tau\}. \tag{3.38}$$

The explanation for this choice is as follows. For a given $q \in [1, r-1]_{\mathbb{N}}$, all the K's that satisfy $y^{\min} \leqslant y(t,K) \leqslant y^{\max},\ \forall t \in [\tau_q, \tau_{q+1}]$ while do not satisfy $y^{\min} + \delta_q^\tau \leqslant y(t,K) \leqslant y^{\max} - \delta_q^\tau,\ \forall t \in [\tau_q, \tau_{q+1}]$ are given by $cns(\delta_q^\tau)$ defined as,

$$cns(\delta_q^\tau) \triangleq \Upsilon_1 \backslash \Upsilon_2 = \left(\Upsilon_3 \bigcap \Upsilon_4\right) \bigcup \left(\Upsilon_5 \bigcap \Upsilon_6\right), \tag{3.39}$$

where

$$\Upsilon_1 \triangleq \left\{ K \;\middle|\; y^{\min} < y(t,K) < y^{\max}, \quad \forall t \in [\tau_q, \tau_{q+1}] \right\},$$

$$\Upsilon_2 \triangleq \left\{ K \;\middle|\; y^{\min} + \delta_q^\tau < y(t,K) < y^{\max} - \delta_q^\tau, \quad \forall t \in [\tau_q, \tau_{q+1}] \right\},$$
$$\Upsilon_3 \triangleq \left\{ K \;\middle|\; y^{\max} - \delta_q^\tau \leqslant y(t,K) < y^{\max}, \quad \forall t \in [\tau_q, \tau_{q+1}] \right\},$$
$$\Upsilon_4 \triangleq \left\{ K \;\middle|\; y^{\min} < y(t,K), \quad \forall t \in [\tau_q, \tau_{q+1}] \right\},$$
$$\Upsilon_5 \triangleq \left\{ K \;\middle|\; y^{\min} < y(t,K) \leqslant y^{\min} + \delta_q^\tau, \quad \forall t \in [\tau_q, \tau_{q+1}] \right\},$$
$$\Upsilon_6 \triangleq \left\{ K \;\middle|\; y(t,K) < y^{\max}, \quad \forall t \in [\tau_q, \tau_{q+1}] \right\}.$$

The region $cns(\delta_q^\tau)$ becomes smaller as δ_q^τ decreases, and is empty if δ_q^τ is 0. Hence a proxy to measure the size of $cns(\delta_q^\tau)$ is simply δ_q^τ. Furthermore, by noting that $\nu(\tau)$ characterizes the largest size of all $cns(\delta_q^\tau)$'s and that $\Sigma \backslash \bar{\Sigma}_I^\tau$ is a subset of $\bigcup_{q \in [1,r-1]_{\mathbb{N}}} cns(\delta_q^\tau)$, we conclude $\nu(\tau)$ measures the gap between $\bar{\Sigma}_I^\tau$ and Σ. Given the symmetry with the definition of $\bar{\Sigma}_O^\tau$, note that one can also use the metric to measure the gap between $\bar{\Sigma}_O^\tau$ and Σ_{cl}.

Our next result characterizes the minimization of ν. Formally, consider

$$\min_{\tau} \quad \nu(\tau) \tag{3.40a}$$
$$\text{s.t.} \quad t_1 = \tau_1 < \tau_2 < \cdots < \tau_r = t_2. \tag{3.40b}$$

This problem possesses a unique global minimizer, which can be equivalently characterized by a set of equations.

Proposition 3.4.1. *(Characterization of global optimum of metric): The optimization problem* (3.40) *has a unique global minimizer, which is uniquely determined by,*

$$\delta_i^\tau = \delta_{i+1}^\tau, \ \forall i \in [1, r-2]_{\mathbb{N}}, \tag{3.41a}$$
$$\tau_1 = t_1, \ \tau_r = t_2. \tag{3.41b}$$

Proof. Note that the result holds if the following three statements are true:

(i) There exists at least one global minimizer for (3.40)

(ii) Any global minimizer of (3.40) satisfies condition (3.41).

(iii) There exists a unique solution for (3.41).

To see this, by (i) and (ii), a solution for (3.41) exists. By (iii), since the solution for (3.41) is unique, it has to be the only global minimizer. Our strategy is then to prove (i)-(iii) separately.

To prove (i), consider the optimization problem (3.40) but with non-strict inequality constraints. Since ν is continuous and the constraints define a compact feasibility set, by the extreme value theorem [PM97], there exists at least one global minimizer $\bar{\tau}^*$. If at least one of these minimizers satisfies the constraint (3.40b), then it is also a global minimizer of (3.40). If it does not, then it is easy to find a sampling sequence $\hat{\tau}^*$ that satisfies the constraint and has at most the same metric value. In fact, without loss of generality, assume that $\bar{\tau}^*_{q-1} < \bar{\tau}^*_q = \bar{\tau}^*_{q+1} = \cdots = \bar{\tau}^*_{q+k} < \bar{\tau}^*_{q+1}$ for some $q \in [1, r-1]_{\mathbb{N}}$ and $k \in \mathbb{N}$. Let $\hat{\tau}^*_j = \bar{\tau}^*_j$ for every $j \in [1,r]_{\mathbb{N}}/[q, q+k-1]_{\mathbb{N}}$ and $\hat{\tau}^*_j = \bar{\tau}^*_{q-1} + (\bar{\tau}^*_q - \bar{\tau}^*_{q-1})(j-q+1)/(k+1)$ for every $j \in [q, q+k-1]_{\mathbb{N}}$. By this way one can easily check that $\nu(\hat{\tau}^*) \leqslant \nu(\bar{\tau}^*)$ holds.

We prove statement (ii) by contradiction. Suppose (3.40) admits a global minimizer τ that does not satisfy condition (3.41) and let us construct another sequence $\bar{\tau}$ with $\nu(\bar{\tau}) < \nu(\tau)$. We first consider the case where consecutive subintervals achieve the same maximum value, i.e., for some $k \in \mathbb{N} \cup \{0\}$, it holds that $\delta^\tau_j < \delta^\tau_q = \delta^\tau_{q+1} = \cdots = \delta^\tau_{q+k} = \nu(\tau)$ for every $j \in [1, r-1]_{\mathbb{N}} \backslash [q, q+k]_{\mathbb{N}}$. Since condition (3.41) does not hold, either $\tau_q \neq t_1$ or $\tau_{q+k} \neq t_2$. Without loss of generality, assume the first case. Now construct $\bar{\tau}$ by letting $\bar{\tau}_j = \tau_j$ for every $j \in [1,r]_{\mathbb{N}} \backslash [q, q+k]_{\mathbb{N}}$ and $\bar{\tau}_j = \tau_j + \mathrm{d}x_j$ for every $j \in [q, q+k]_{\mathbb{N}}$, where $\mathrm{d}x_j$ is determined as follows: since every δ^τ_j is a strictly monotonically decreasing and continuous function of τ_j, one can always find $\mathrm{d}x_j > 0$ small enough for every $j \in [q, q+k]_{\mathbb{N}}$ such that $\delta^{\bar{\tau}}_{q-1} < \delta^{\bar{\tau}}_j < \delta^\tau_q = \delta^\tau_{q+1} = \cdots = \delta^\tau_{q+k}$ holds for every $j \in [q, q+k]_{\mathbb{N}}$, which implies that $\nu(\bar{\tau}) < \nu(\tau)$. In the most general case where there are several groups of consecutive subintervals achieving the same maximum

value, and all groups share no common sampling point, one can construct $\bar{\tau}$ by tuning the points using the idea above for each individual group, resulting in $\nu(\bar{\tau}) < \nu(\tau)$.

To prove statement (iii), assume there exist two different sampling sequences τ^a and τ^b that both satisfy condition (3.41). We first consider the case when $\delta_i^{\tau^a} \neq \delta_i^{\tau^b}$ for every $i \in [1, r-1]_{\mathbb{N}}$, and, without loss of generality, assume that $\delta_i^{\tau^a} < \delta_i^{\tau^b}$. Notice that if $\tau_2^b \leqslant \tau_2^a$, then

$$\delta_1^{\tau^b} \triangleq (\tau_2^b - t_1)/2 \max_{t\in[t_1,\tau_2^b]} \{y_d(t)\} \leqslant (\tau_2^a - t_1)/2 \max_{t\in[t_1,\tau_2^a]} \{y_d(t)\} = \delta_1^{\tau^a},$$

violating the assumption, and hence $\tau_2^b > \tau_2^a$. Similarly, it holds that $\tau_3^b > \tau_3^a$. Along this one has that $\tau_{r-1}^b > \tau_{r-1}^a$. The contradiction occurs as one can easily see that $\delta_{r-1}^{\tau^b} \leqslant (t_2 - \tau_2^a)/2 \max_{t\in[t_1,\tau_2^a]}\{y_d(t)\} = \delta_{r-1}^{\tau^a}$. Next, we consider the case when $\delta_i^{\tau^a} = \delta_i^{\tau^b}$ for every $i \in [1, r-1]_{\mathbb{N}}$. Since δ_1^{τ} is a strictly monotonically increasing function of τ_2, to have $\delta_1^{\tau_b} = \delta_1^{\tau_b}$, it must hold that $\tau_2^a = \tau_2^b$. Similarly, $\tau_i^a = \tau_i^b$ for every $i \in [1, r]_{\mathbb{N}}$, i.e., τ^a and τ^b are the same sequence. Therefore, equation (3.41) admits only one solution. □

Given Proposition 3.4.1, we denote the unique minimizer of (3.40) by τ^*, and the optimal value by $\nu(\tau^*)$.

3.4.2 Algorithm to reduce the approximation gap

Here, we introduce a strategy that, for a fixed number r of sampling points, finds the sampling sequence that minimizes v. Our design is based on Proposition 3.4.1. Notice that we can equivalently obtain τ^* by solving the transcendental equations (3.41). Based on this equivalence relation, we propose Algorithm 1 to provide a sampling sequence $\hat{\tau}$ whose metric value $\nu(\hat{\tau})$ can be made arbitrarily close to $\nu(\tau^*)$. The algorithm proceeds by approximating $\nu(\tau^*)$ through the bisection method, i.e., starts from an initial interval that contains $\nu(\tau^*)$, and iteratively obtains intervals containing $\nu(\tau^*)$ whose length is half the length of the one generated in the previous step. This process terminates when the approximation is optimal within a prescribed tolerance

error.

Algorithm 1: Obtain near-optimal sampling sequence

Data: Derivative bound signal y_d, tolerance error value $\nu^{\text{err}} > 0$, t_1 and t_2
Result: Near-optimal value η^N and near-optimal sequence $\hat{\tau}$

Initialization: $\tau_i^{\text{even}} = t_1 + (i-1)(t_2-t_1)/(r-1)\ \forall i \in [1,r]_{\mathbb{N}}$, $a^0 = 0,\ b^0 = \nu(\tau^{\text{even}}),\ \eta^0 = (a^0+b^0)/2,\ k = 0,\ flag$=true
while *flag* **do**
  $\tau_1^k = t_1,\ \tau_r^k = t_2$
  for $i = 2 : r-1$ **do**
    Set τ_i^k such that $\delta_{i-1}^{\tau^k} = \eta^k$
  end
  if $b^k - a^k \leqslant \nu^{error}/2$ **then**
    $N = k$, $flag$=false
  end
  Compute $\delta_{r-1}^{\tau^k}$
  if $\delta_{r-1}^{\tau^k} - \eta^k > 0$ **then**
    $a^{k+1} = \eta^k,\ b^{k+1} = b^k$
  else
    $a^{k+1} = a^k,\ b^{k+1} = \eta^k$
  end
  $\eta^{k+1} = (a^{k+1} + b^{k+1})/2,\ k = k+1$
end
$\hat{\tau}_1 = t_1,\ \hat{\tau}_r = t_2$
for $i = 2 : r-1$ **do**
  Set $\hat{\tau}_i$ such that $\delta_{i-1}^{\hat{\tau}} = \eta^N + \nu^{\text{err}}/2$
end

The following result formally characterizes the convergence properties of Algorithm 1.

Proposition 3.4.2. *(Algorithm 1 finds optimal sampling sequence): Given a tolerance error* $\nu^{err} > 0$*, there exists a unique N such that the sampling sequence* $\tau^k,\ k \in [1,N]_{\mathbb{N}}$ *and outputs* η^N*,* $\hat{\tau}$ *from Algorithm 1 satisfy*

(i) $|\eta^k - \nu(\tau^*)| \leqslant \nu(\tau^{even})2^{-k}$ *for every* $k \in [1,N]_{\mathbb{N}}$*;*

(ii) $|\eta^N - \nu(\tau^*)| \leqslant \nu^{err}/2$*, with* $N < \log_2 \nu(\tau^0) - \log_2 \nu^{err} + 2$*;*

(iii) $\nu(\hat{\tau}) \leqslant \nu(\tau^*) + \nu^{err}$.

Proof. With the notation of Algorithm 1, we first show that for the sampling sequence τ^k , if $\delta_{r-1}^{\tau^k} > \eta^k$, then $\eta^k < \nu(\tau^*)$. One can see that since $\eta^k = \delta_1^{\tau^k} = \delta_2^{\tau^k}, \cdots, = \delta_{r-2}^{\tau^k}$, if $\eta^k \geqslant \nu(\tau^*)$, then using the same argument as in the proof of Proposition 3.4.1(ii), it holds that $\tau_i^k \geqslant \tau_i^*$ for any $i \in [2, r-1]_{\mathbb{N}}$, leading to $\delta_{r-1}^{\tau^k} \leqslant \delta_{r-1}^{\tau^*} = \nu(\tau^*) \leqslant \eta^k$, which contradicts the assumption. Similarly, one can prove that if $\delta_{r-1}^{\tau^k} \leqslant \eta^k$, then $\eta^k \geqslant \nu(\tau^*)$. Along with these observations, one can easily see that via step 11 to step 16, plus the initialization condition, it holds that $\nu(\tau^*) \in [a^k, b^k]$ for every $k \in [1, N]_{\mathbb{N}}$, and $b^{k+1} - a^{k+1} = (b^k - a^k)/2$. Finally, statement (i) holds by noticing that $|\eta^k - \nu(\tau^*)| \leqslant b^k - a^k = (b^0 - a^0)/2^k = \nu(\tau^0)/2^k$. This implies that $\nu(\tau^k)$ exponentially converges to the optimal value $\nu(\tau^*)$.

The first part of statement (ii) is simply due to the termination condition in step 7 in Algorithm 1. Since $k = N$ is the first satisfying $b^k - a^k \leqslant \nu^{\text{error}}/2$, it holds that $\nu^{\text{error}}/2 < b^{N-1} - a^{N-1} = \nu(\tau^0)/2^{N-1}$, and hence the rest of statement (ii) follows immediately.

To prove statement (iii), notice $\delta_i^{\hat{\tau}} = \eta^N + \nu^{\text{err}}/2 \geqslant \nu(\tau^*) = \delta_j^{\tau^*}$ for any $i, j \in [1, r-1]_{\mathbb{N}}$, where the inequality follows from (ii). Therefore, $\delta_i^{\hat{\tau}} \geqslant \delta_i^{\tau^*}$ for every $i \in [1, r-1]_{\mathbb{N}}$, which implies that $\hat{\tau}_i \geqslant \tau_i^*$ for every $i \in [1, r-1]_{\mathbb{N}}$, and hence $\delta_{r-1}^{\hat{\tau}} \leqslant \delta_{r-1}^{\tau^*} = \nu(\tau^*)$. Now, one has

$$\begin{aligned}\nu(\hat{\tau}) &= \max\{\eta^N + \nu_{\text{err}}/2, \delta_{r-1}^{\hat{\tau}}\} \\ &\leqslant \max\{\eta^N + \nu_{\text{err}}/2, \nu(\tau^*)\} = \eta^N + \nu_{\text{err}}/2 \leqslant \nu(\tau^*) + \nu^{\text{err}},\end{aligned}$$

where the last inequality follows from (ii). □

Notice that steps 5 and 20 of Algorithm 1 require the solution of a transcendental equation in one variable. Even though an exact solution is not available, we discuss in the following remark a bisection method to approximate it with an arbitrary degree of accuracy.

Remark 3.4.3. *(Solving transcendental equation in one variable):* Here we describe a strategy to approximate the solution in steps 5 and 20 of Algorithm 1. For conciseness, we describe it in general as Algorithm 2: one can apply it to solve step 5 (resp. step 20) by simply letting $\tau = \tau^k$

(resp. $\tau = \hat{\tau}$) and $\eta = \eta^k$ (resp. $\eta = \eta^N$). Algorithm 2 uses bisection method too, where we tighten the length of the interval containing the solution of $\delta_{i-1}^{\tau} = \eta$ iteratively.

Algorithm 2: Solve transcendental equation in one variable

Data: Derivative bound signal y_d, τ_{i-1} and t_2
Result: τ_i that satisfies $\delta_{i-1}^{\tau} = \eta$
Initialization: $c(0) = \tau_{i-1}$, $d(0) = t_2$, and $\tau_i(0) = (c(0) + d(0))/2$
while *true* **do**
  if $(\tau_i(l) - \tau_{i-1}) \max_{t \in [\tau_{i-1}, \tau_i(l)]} \{y_d(t)\} > \eta$ **then**
    $c^{l+1} = c^l$, $d^{l+1} = \tau_i(l)$
  else
    $c^{l+1} = \tau_i(l)$, $d^{l+1} = d^l$
  end
  $\tau_i(l) = (c^{k+1} + d^{k+1})/2$ and $l = l + 1$
end

Similar to the way we prove Proposition 3.4.2, one can easily check that $|\tau_i(l) - \tau_i| \leqslant (t_2 - \tau_{i-1})2^{-l}$ for every $l \in \mathbb{N}$. Due to the fact that $\tau_i(l)$ converges to τ_i exponentially fast, in practice, we terminate Algorithm 2 when l is large enough and take $\tau_i(l)$ as our approximation of τ_i. •

Figure 3.2 shows an execution of Algorithm 1. Note that the sampling sequence obtained by the optimization algorithm is optimal for a class of disturbances (rather than for a *specific* disturbance), as defined by the cases (a), (b), and (c) in Section 3.1.

Remark 3.4.4. *(Generalized metric for vector-signal):* Similar to the way we define ν in (3.38), for any $\mu \in \{\text{pre, par, unk}\}$, we define

$$\begin{aligned} \pi_i^{\mu} &\triangleq \max_{q \in [1, r(i)]_{\mathbb{N}}} \{\delta_{q,i}^{\mu}\}, \\ \pi^{\mu} &\triangleq \max_{i \in [1, m+n]_{\mathbb{N}}} \{\pi_i^{\mu} / (x_i^{\max} - x_i^{\min})\}, \end{aligned} \tag{3.42}$$

and use π^{μ} as the metric measuring the approximation gap between Ψ_I^{μ} (resp. Ψ_O^{μ}) and Ψ^{μ} (resp. Ψ_{cl}^{μ}), where the coefficient $1/(x_i^{\max} - x_i^{\min})$ scales π_i^{μ} relative to its bounds. One can

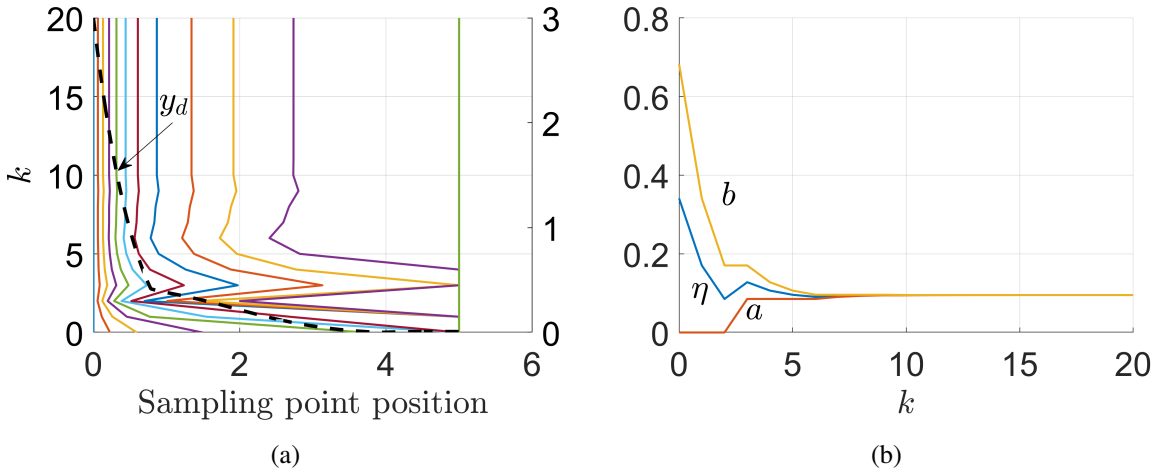

(a) (b)

Figure 3.2: Execution of Algorithm 1. Here $y : \mathbb{R} \to \mathbb{R}$, $t \mapsto e^{-2t} + \sin t e^{-t} K$, with $|K| \leqslant 1$. One can easily check that $y_d : \mathbb{R} \to \mathbb{R}_{\geqslant}$, $t \to 2|e^{-2t}| + |\cos t e^{-t} - \sin t e^{-t}|$ satisfies $|\dot{y}(t)| \leqslant y_d(t)$ for any $t \geqslant 0$. The interval of interest is determined by $t_1 = 0$, $t_2 = 5$. We run the algorithm for $r = 12$ sampling points and set $v^{\text{err}} = 2^{-19} v(\tau^{\text{even}})$. (a) shows y_d and the trajectories of the 12 sampling points at each iteration. Since y_d is monotonically decreasing, as k increases, τ^k tends to be dense around $t = 0$s and sparse around $t = 5$s. (b) shows the convergence of a^k, b^k and η^k.

reduce π^μ by applying Algorithm 1 component-wise to optimize the sampling sequence τ^i for each $i \in [1, m+n]_{\mathbb{N}}$. •

3.5 Simulations

Here we illustrate our results on the IEEE 39-bus New England power network displayed in Figure 3.3. This network has 46 transmission lines and 10 generators serving a load of approximately 6GW. We run our simulations in MATLAB on a desktop with a 3.5GHz Intel Core i7-4770k quad-core CPU and 8GB of RAM. For system (2.12), the susceptance b_{ij} and the rotational inertia M_i for generator nodes are taken from the Power System Toolbox [CCR09]. We assign all non-generator buses an uniform small inertia $M_i = 0.1$. Let the damping parameter (or droop coefficient) to be $D_i = 1$ for all buses. The nominal power injection $p^{\text{nom}}(t)$ is chosen to be a constant P_0 obtained from the same toolbox. The initial state $(\lambda(0), \omega(0))$ is chosen to be the equilibrium with respect to the input $P(t) = P_0$. The frequency bounds are

$F^{\max} = -F^{\min} = 10$ unit $\times \mathbf{1}_{46}$, the power flow bounds are $\omega^{\max} = -\omega^{\min} = 0.5$ Hz $\times \mathbf{1}_{39}$, and the time period considered for transient-safety is $[t_1, t_2] = [0, 3]$. If there is no disturbance injection, then the state $(\lambda(t), \omega(t))$ stays at equilibrium, which trivially satisfies the transient-safety requirements.

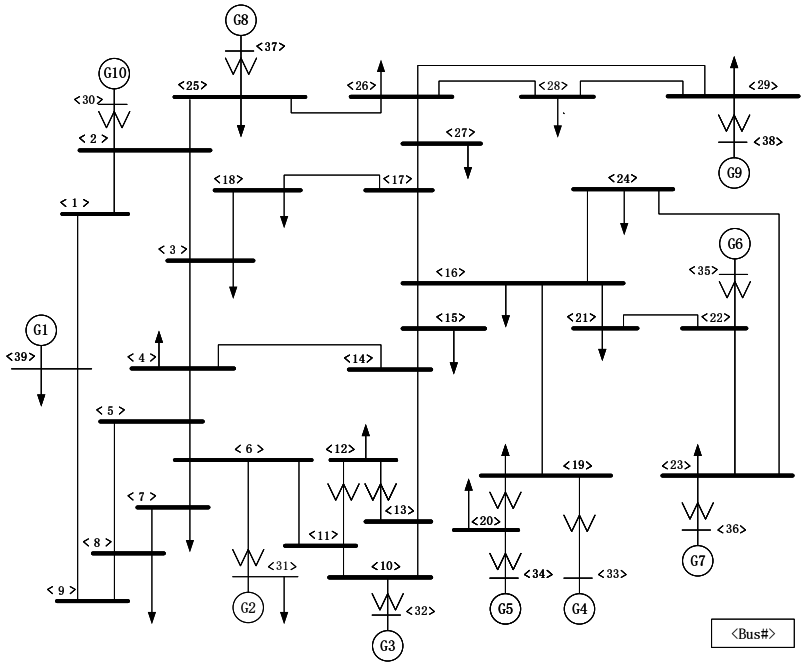

Figure 3.3: IEEE 39-bus power network.

We start by showing the efficiency of the approximation gap reduction obtained by Algorithm 1. We consider the case when a precisely known disturbance occurs at the 16th and the 24th buses, with the trajectory form of a step signal. Formally, this corresponds to the model (3.2) with $B \in \mathbb{R}^{39\times 2}$, where $B_{ij} = 1$ only when (i, j) equals $(16, 1)$ and $(24, 2)$; $\text{diag}\,(\zeta^{\text{pre}}(t)) = \text{diag}([1(t)\ 1(t)])$, and $K^{\text{pre}} = [K_1^{\text{pre}}\ K_2^{\text{pre}}]$ for which the bound $\gamma^{\text{pre}} = 4.7$ is known. We compute the approximations Ψ_I^{pre} and Ψ_O^{pre} using the expressions (3.33) in Theorem 3.3.5. We use the same sampling sequence for each component $i \in [1, m+n]_{\mathbb{N}}$ and consider two cases: an even sampling sequence of period $0.02s$ and the sequence that results from optimizing it by applying Algorithm 1. Figure 3.4(a) and (b) show the approximation sets Ψ_O^{pre} and Ψ_I^{pre} obtained

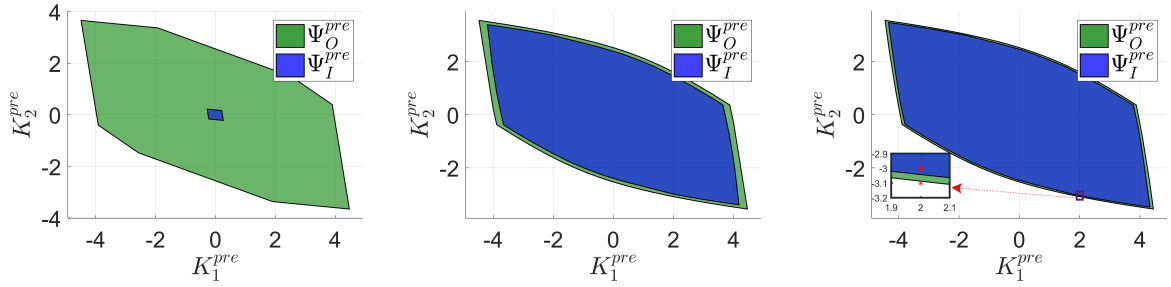

Figure 3.4: Inner and outer approximations of the transient-state tolerableness set for the precisely known case with different sampling sequences. Plot (a) uses even sampling with 151 points. Plots (b) and (c) use optimized sampling sequences with 151 and 301 points, respectively. The first two plots show that Algorithm 1 reduces the gap between the inner and outer approximations for a fixed number of sampling points. The last two plots illustrate the convergence of the approximations as the number of sampling points increases.

in each case, with a marked improvement in the case of the optimized sequence. Figure 3.4(c) shows the result obtained with an optimized sequence using Algorithm 1 on an even sampling sequence of period 0.01s. The gap between the two approximation sets is smaller than in Figure 3.4(b), which is in agreement with the convergence result in Theorem 3.3.5(ii).

Figure 3.5 illustrates how the trajectory form impacts the shape and size of the tolerableness set. Figure 3.5(a) shows the inner and outer approximations when the step function in the first component of the disturbance trajectory is delayed by one second, i.e., $\zeta^{\text{pre}}(t) = [1(t-1)\ 1(t)]^T$. Figure 3.5(b) shows the same sets when the trajectory form is the sinusoid $\zeta^{\text{pre}}(t) = [\sin(\pi t)\ \sin(\pi t)]^T$. Comparing with Figure 3.4(c), one observes that the tolerableness set can take remarkably different forms depending on the type of disturbance (even though all the three trajectory forms are bounded by 1).

Next, we illustrate the containment relations among the approximations and the exact tolerableness set stated in Theorem 3.3.5(i). To do this, we select two nearby disturbance amplitudes, $K_I^{\text{pre}} = [2\ -3]^T \in \Psi_I^{\text{pre}}$ and $K_O^{\text{pre}} = [2\ -3.1]^T \notin \Psi_O^{\text{pre}}$. The plots in the top row in Figure 3.6 show the state trajectories of (2.12) corresponding to each disturbance. In the case of K_I^{pre}, the frequency responses (resp. flow responses) of all buses (resp. transmission lines) stay within the

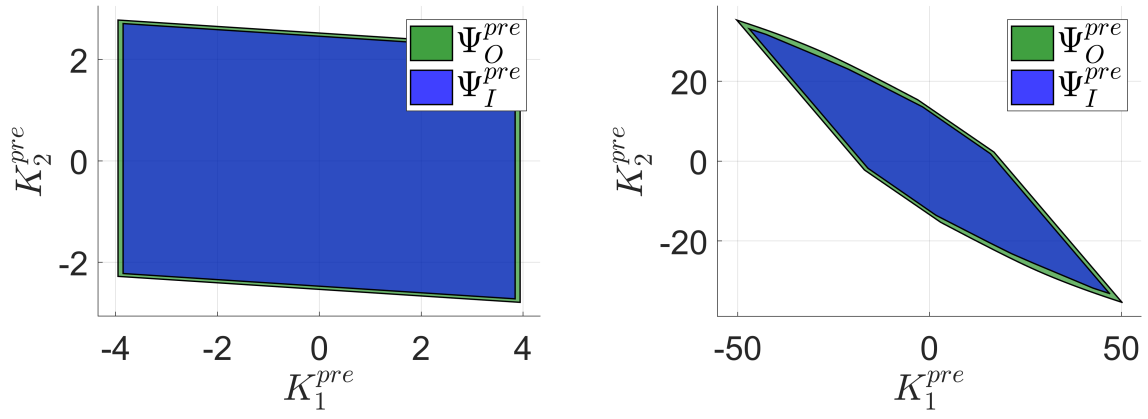

(a) (b)

Figure 3.5: Inner and outer approximations of transient-state tolerableness set for the precisely known case with different trajectory forms. In plot (a), the trajectory form is $\zeta^{\text{pre}}(t) = [1(t - 1s)\ 1(t)]^T$ and in plot (b) $\zeta^{\text{pre}}(t) = [\sin(\pi t)\ \sin(\pi t)]^T$, respectively.

$\pm$0.5Hz (resp. $\pm$10unit) bound, and hence $K_I^{\text{pre}} \in \Psi^{\text{pre}}$ according to (3.3), which is consistent with the inclusion $\Psi_I^{\text{pre}} \subseteq \Psi^{\text{pre}}$. In the case of K_O^{pre}, one frequency response goes beyond the -0.5Hz bound, reaching to approximately -0.506Hz, violating the frequency safety requirement slightly, and hence $K_O^{\text{pre}} \notin \Psi_{\text{cl}}^{\text{pre}}$, which is consistent with the inclusion $\Psi_{\text{cl}}^{\text{pre}} \subseteq \Psi_O^{\text{pre}}$. The plots in the bottom row in Figure 3.6 show the state responses generated by the nonlinear swing equations [MBB08] instead of the linear model (2.12). Although the containment relationships are not guaranteed in the nonlinear case, one can see that they still hold in this particular example.

Figure 3.7 illustrates the computation of the inner and outer approximation sets in the cases when the disturbance trajectory form is partially known and unknown. In the first case, for the model (3.4), we have the nominal trajectory form $\zeta^{\text{nom}}(t) = 0.9 \cdot [1(t)\ 1(t)]^T$ and the uncertainty bound $\alpha = 0.1 \cdot \mathbf{1}_2$ on ζ^{err}. Since $|\zeta^{\text{pre}}(t) - \zeta^{\text{nom}}(t)| \leqslant \alpha$ and $|\zeta^{\text{nom}}(t)| + \alpha \leqslant 1$ for every $t \in [t_1, t_2]$, we deduce from Remark 3.2.2 that $\Psi^{\text{unk}} \subset \Psi^{\text{par}} \subset \Psi^{\text{pre}}$. The comparison of Figures 3.4 and 3.7 validates these containment relations.

Table 3.1 gathers the computational time for the inner and outer approximations in Figures 3.4, 3.5 and 3.7. The additional 2 seconds for Figure 3.4(b) with respect to Figure 3.4(a) are

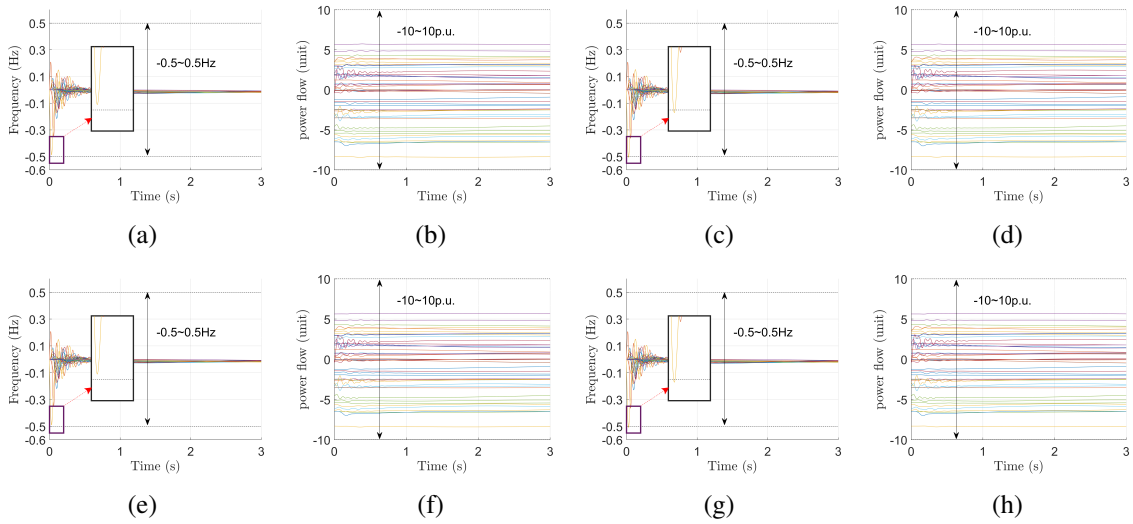

Figure 3.6: Frequency and power flow trajectories with different disturbance amplitudes. The problem data is the same as in Figure 3.4. Plots (a) and (b) show the trajectories with a disturbance amplitude $K_I^{\text{pre}} = [2 \ -3]^T$ (which, from Figure 3.4(c), is contained in the inner approximation set Ψ_I^{pre}), while plots (c) to (d) show the trajectories for $K_O^{\text{pre}} = [2 \ -3.1]^T$ (which is not contained in the outer approximation set Ψ_O^{pre}). In both cases, the power flow trajectories stay within the ± 10 unit bound. However, all the frequency trajectories stay within the ± 0.5 Hz bound when the disturbance amplitude is K_I^{pre}, while for the K_O^{pre}case, one frequency trajectory hits up to approximately -0.506Hz, exceeding the -0.5Hz bound. Plots (e) to (h) in the bottom row display the corresponding state trajectories generated with the nonlinear swing equations instead of the linear dynamics (2.12) for plots (a) to (d).

due to the take taken by the optimization of the sampling sequence. This latter time increases as more sampling points are considered, cf. Figure 3.4(c). We also see a slight computational time difference among Figure 3.4(c), Figure 3.5(a), and Figure 3.5(c), corresponding to different disturbance trajectory forms. Finally, for a fixed number of sampling points, the computational time does not vary dramatically for precisely known, partially known, and totally unknown disturbances. Computational times are also reported in [ZC17] for a simulation on the IEEE 118-bus network with 91 disturbances.

Finally, we illustrate the robustness metric definition based on tolerableness sets introduced in by Remark 3.3.8. We consider 39 different scenarios: in the ith scenario, we inject a power disturbance with trajectory form $1(t)$ only at node i. For each $i \in \{1, \cdots, 39\}$, β_O^{pre} (resp.

Table 3.1: Times for the computation of for various tolerableness sets.

Sets	Time(s)	Sets	Time(s)
Figure 3.4(a)	12.41	Figure 3.5(a)	18.62
Figure 3.4(b)	14.39	Figure 3.5(b)	16.52
Figure 3.4(c)	20.38	Figure 3.7(a) and (b)	20.26 and 20.39

β_I^{pre}) stands for the upper (resp. lower) approximation of the maximum allowable disturbance magnitude injected at node i so that the whole network maintains transient-state safety. One can see from Figure 3.8 that nodes $1, 9, 12$ and 38 are the most vulnerable. The first three cases have similar causes – either low inertia, making the transient frequency easily affected by disturbances or low dissipation capabilities due to a small number of neighboring nodes, resulting in a relatively long time required to dissipate the disturbances. The 38th node case is primarily due to the fact that the only transmission line connecting the node with the rest of the network is almost saturated before the disturbance injection.

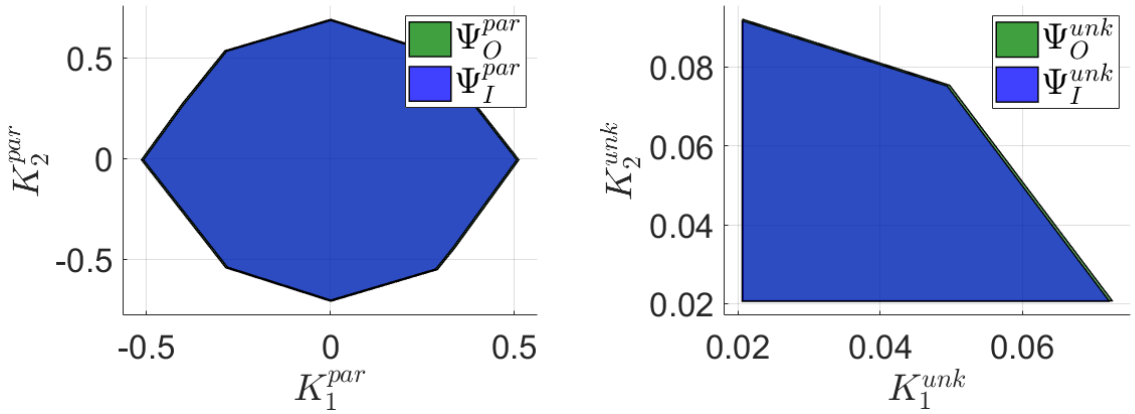

(a) (b)

Figure 3.7: Inner and outer approximations of the transient-state tolerableness set with partially known and totally unknown trajectory forms. Plot (a) shows the tolerableness set with nominal trajectory form $\zeta^{\text{nom}}(t) = 0.9 \cdot [1(t)\ 1(t)]^T$ and uncertainty $\alpha = 0.1 \cdot \mathbf{1}_2$. Plot (b) shows the set with totally unknown trajectory. Together with Figure 3.4(c) one has that $\Psi^{\text{unk}} \subseteq \Psi^{\text{par}} \subseteq \Psi^{\text{pre}}$, as stated in Remark 3.2.2.

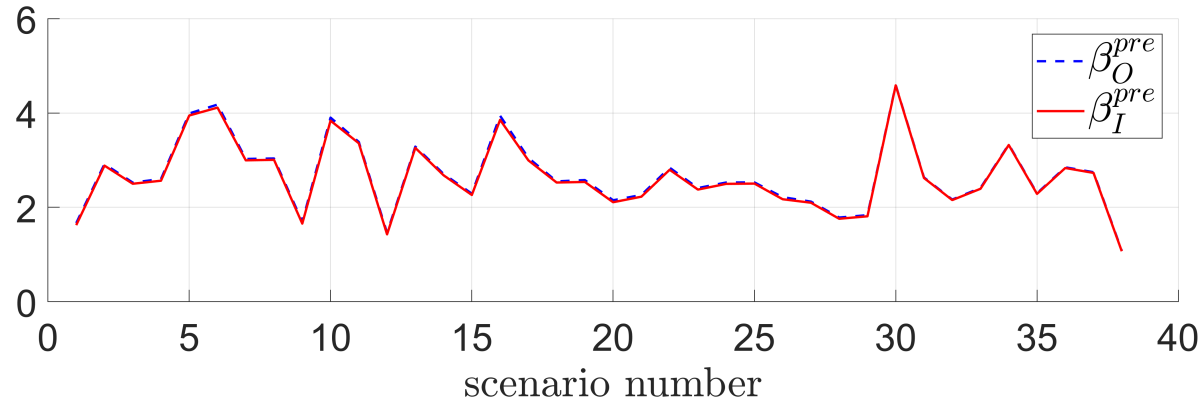

Figure 3.8: Robustness characterization of the IEEE39 bus network based on tolerableness sets. In each scenario, we inject a disturbance at the corresponding node and compute the approximations of the robustness metric defined in Remark 3.3.8. This metric measures the maximum allowable disturbance that does not violate transient safety. Both approximations use 301 sampling points optimized through Algorithm 1.

Acknowledgements

This chapter, in part, is a reprint of the material [ZC19a] as it appears in 'Characterizing tolerable disturbances for transient-state safety in power networks' by Y. Zhang and J. Cortés, in the IEEE Transactions on Network Science and Engineering, 2019, as well as [ZC17] where it appears as 'Transient-state feasibility set approximation of power networks against disturbances of unknown amplitude' by Y. Zhang and J. Cortés in the proceedings of the 2017 American Control Conference. The dissertation author was the primary investigator and author of these papers. This work was partially supported by NSF award CNS-1329619 and AFOSR Award FA9550-15-1-0108.

Chapter 4

Distributed transient frequency control with stability and performance guarantees

Note that our transient-state analysis in Chapter 3 is based on open-loop power network dynamics in the sense that the extra control signal is set to zero. Therefore, it is of interest to design control strategy so that the closed-loop system is safe even with disturbance able to jeopardize transient-state safety for the open-loop system. Especially, here we focus on transient frequency control.

This chapter proposes a distributed strategy regulated on a subset of individual buses in a power network described by the swing equations to achieve transient frequency control while preserving asymptotic stability. Building on Lyapunov stability and set invariance theory, we formulate the stability and the transient frequency requirements as two separate constraints for the control input. Our design synthesizes a controller that satisfies both constraints simultaneously. The controller is distributed and Lipschitz, guaranteeing the existence and uniqueness of the trajectories of the closed-loop system. We further bound its magnitude and demonstrate its robustness against measurement inaccuracies. Simulations on the IEEE 39-bus power network illustrate our results.

4.1 Problem statement

For the nonlinear power network characterized by (2.7), our goal is to design a state-feedback controller for each bus $i \in \mathscr{I}^{\omega} \subseteq \mathscr{I}$ that guarantees that the frequency transient behavior stays within desired safety bounds while preserving the stability properties that the system (2.7) enjoys when no external input u_i is present. Due to the structural limitation of the controller proposed in this chapter, we assume that $\mathscr{I}^{\omega} = \mathscr{I}^{u}$, i.e. control resources at nodes without transient frequency requirement cannot be utilized. We will later relax this assumption in the next two chapters. We state these requirements explicitly next.

Stability and convergence requirement: Since the system (2.7) without u_i is locally stable, we require that the same system with the proposed controller u_i is also locally stable. Furthermore, for every admissible initial condition, the two systems should converge to the same equilibrium $(\lambda^{\infty}, \omega^{\infty}\mathbf{1}_n)$, meaning that u_i only affects the transient behavior.

Frequency invariance requirement: For each $i \in \mathscr{I}^{u}$, let $\underline{\omega}_i \in \mathbb{R}$ and $\bar{\omega}_i \in \mathbb{R}$ be lower and upper safe frequency bounds, where $\underline{\omega}_i < \bar{\omega}_i$. We require that the frequency $\omega_i(t)$ stays inside the safe region $[\underline{\omega}_i, \bar{\omega}_i]$ for any $t > 0$, provided that the initial frequency $\omega_i(0)$ lies inside $[\underline{\omega}_i, \bar{\omega}_i]$. This forward invariance requirement corresponds to underfrequency/overfrequency avoidance.

Attractivity requirement: If, for some $i \in \mathscr{I}^{u}$, the initial frequency $\omega_i(0) \notin [\underline{\omega}_i, \bar{\omega}_i]$, then after a finite time, ω_i enters the safe region and never leaves afterwards. This requirement corresponds to underfrequency/overfrequency recovery.

In addition to these requirements, we also seek the designed controller to be Lipschitz as a function of the state. This guarantees the existence and uniqueness of solutions for the closed-loop system and, at the same time, provides robustness for practical implementation against errors in state measurements.

Remark 4.1.1. *(Selection of buses with transient frequency specification):* The set $\mathscr{I}^{u}$ consists of buses belonging to either of the following two types: a) buses with specified over/underfrequency

requirement [PKT06] and b) buses whose transient frequency behavior is key in evaluating system performance, or are used as indexes for load shedding schemes [MCS11]. We assume each individual bus in $\mathscr{I}^u$ is equipped with an external input directly tuning its transient behavior. We show later that this is necessary condition to obtain frequency invariance guarantees. •

Note that the attractivity requirement is automatically satisfied once the controller meets the first two requirements, provided that $\omega^\infty \in (\underline{\omega}_i, \bar{\omega}_i)$. However, in general it is still of interest to provide estimates for how fast the frequency reaches the safe region. Our objective is to design a controller that satisfies the above three requirements simultaneously and is distributed, in the sense that each bus can implement it using its own information and that of its neighboring buses and transmission lines.

4.2 Constraints on controller design

In this section, we identify constraints on the controller design that provide sufficient conditions to ensure, on the one hand, the stability and convergence requirement and, on the other hand, the frequency invariance requirement.

4.2.1 Constraint ensuring stability and convergence

We establish a stability constraint by identifying an energy function and restricting the input so that its evolution along every trajectory of the closed-loop dynamics is monotonically non-increasing. We select the energy function [VNM+18]

$$V(\lambda, \omega) \triangleq \frac{1}{2}\sum_{i=1}^{n} M_i(\omega_i - \omega^\infty)^2 + \sum_{j=1}^{m} [Y_b]_{j,j} a(\lambda_j), \tag{4.1}$$

where $a(\lambda_j) \triangleq \cos\lambda_j^\infty - \cos\lambda_j - \lambda_j \sin\lambda_j^\infty + \lambda_j^\infty \sin\lambda_j^\infty$. The next result uses the LaSalle Invariance Principle to show this property.

Lemma 4.2.1. *(Sufficient condition for local stability and convergence): Consider the system* (2.7)*. Under condition* (2.9)*, further suppose that, for every* $i \in \mathscr{I}^u$, $u_i : \mathbb{R}^{m+n} \times \mathbb{R}^n \to \mathbb{R}$, $(x,y) \mapsto u_i(x,y)$ *is Lipschitz in* x*. Let*

$$\bar{r} \triangleq \min_{\lambda \in \partial \mathscr{R}_{\mathrm{cl}}} V(\lambda, \omega^\infty \mathbf{1}_n) \tag{4.2}$$

and define

$$\mathscr{T}(r) \triangleq \left\{ (\lambda, \omega) \;\middle|\; \lambda \in \mathscr{R}_{\mathrm{cl}},\, V(\lambda,\omega) \leqslant r \right\} \tag{4.3}$$

with $r \in \mathbb{R}_>$*. If for every* $i \in \mathscr{I}^u$, $x \in \mathbb{R}^{m+n}$*, and* $p \in \mathbb{R}^n$*,*

$$(\omega_i - \omega^\infty) u_i(x,p) \leqslant 0 \quad \text{if } \omega_i \neq \omega^\infty, \tag{4.4a}$$

$$u_i(x,p) = 0 \quad \text{if } \omega_i = \omega^\infty, \tag{4.4b}$$

then the following results hold provided $\lambda(0) \in \mathrm{range}(D)$ *and* $(\lambda(0), \omega(0)) \in \mathscr{T}(r)$ *for some* $0 < r < \bar{r}$*:*

(i) The solution of the closed-loop system exists and is unique for any $t \geqslant 0$*;*

(ii) $\lambda(t) \in \mathrm{range}(D)$ *and* $(\lambda(t), \omega(t)) \in \mathscr{T}(r)$ *for any* $t \geqslant 0$*;*

(iii) $(\lambda^\infty, \omega^\infty \mathbf{1}_n)$ *is stable, and* $(\lambda(t), \omega(t)) \to (\lambda^\infty, \omega^\infty \mathbf{1}_n)$ *as* $t \to \infty$*.*

Proof. To prove *(i)*, as $(x,y) \mapsto u_i(x,y)$ is Lipschitz in x, there exists a unique local solution over $[0, \delta]$ for some $\delta > 0$, according to [Kha02, Theorem 3.1]. Let $[0, T)$ be the maximal interval of existence. We then show that $\mathscr{T}(r)$ is non-empty and compact, and that $(\lambda(t), \omega(t))$ lies entirely in $\mathscr{T}(r)$ for any $t \in [0, T)$. These two facts together, by [Kha02, Theorem 3.3], imply the existence and uniqueness of the solution for every $t \geqslant 0$. To show the non-emptiness of $\mathscr{T}(r)$, note that in (4.1) if $|\lambda_i| \leqslant \pi/2$ and $|\lambda_i^\infty| < \pi/2$, then $a(\lambda_i) \geqslant 0$, which implies that

$V(\lambda,\omega) \geqslant 0$ for every $\lambda \in \mathscr{R}_{\text{cl}}$ and every $\omega \in \mathbb{R}^n$; hence $\bar{r} \geqslant 0$. Then $(\lambda^\infty, \omega^\infty \mathbf{1}_n) \in \mathscr{T}(r)$ as $V(\lambda^\infty, \omega^\infty \mathbf{1}_n) = 0$.

To show the compactness of $\mathscr{T}(r)$, note that the set is clearly closed. Since the polytope $\mathscr{R}_{\text{cl}}$ is bounded, the variable λ is bounded too. Therefore, $a(\lambda_i)$ is bounded for every $i \in [1,m]_{\mathbb{N}}$. Since $V(\lambda,\omega) \leqslant r$, we deduce that $\sum_{i=1}^n M_i(\omega_i - \omega^\infty)^2$ is bounded, implying that ω is bounded. Hence, $\mathscr{T}$ is bounded.

Regarding statement *(ii)*, note that $\lambda(t) \in \text{range}(D)$ holds for every $t \geqslant 0$ since both $\lambda(0)$ and $\dot{\lambda}(t)$ lie in range(D). To establish the invariance of $\mathscr{T}(r)$, we examine the evolution of the function V along the dynamics (2.7),

$$\begin{aligned}
\dot{V}(\lambda,\omega) &= \sum_{i=1}^n (\omega_i - \omega^\infty)\left(-E_i\omega_i - [D^T Y_b]_i \sin\lambda + p_i\right) \\
&\quad + \sum_{i\in\mathscr{I}^u} (\omega_i - \omega^\infty) u_i(x,p) + \sum_{j=1}^m [Y_b]_{j,j}(\sin\lambda_j - \sin\lambda_j^\infty)[D]_j\omega \\
&= -\sum_{i=1}^n E_i(\omega_i - \omega^\infty)^2 + \sum_{i\in\mathscr{I}^u} (\omega_i - \omega^\infty) u_i(x,p) \\
&\leqslant -\sum_{i=1}^m E_i(\omega_i - \omega^\infty)^2 \leqslant 0,
\end{aligned}$$

where

$$\begin{aligned}
&\sum_{i=1}^n (\omega_i - \omega^\infty)\left(-[D^T Y_b]_i \sin\lambda + p_i - \omega^\infty E_i\right) + \sum_{j=1}^m [Y_b]_{j,j}(\sin\lambda_j - \sin\lambda_j^\infty)[D]_j\omega \\
&= \sum_{i=1}^n (\omega_i - \omega^\infty)\left(-[D^T Y_b]_i \sin\lambda + p_i - \omega^\infty E_i\right) + \sum_{j=1}^m (\sin\lambda_j - \sin\lambda_j^\infty)[Y_b D]_j(\omega - \omega^\infty \mathbf{1}_n) \\
&= \sum_{i=1}^n (\omega_i - \omega^\infty)\left(p_i - \omega^\infty E_i\right) - \sum_{j=1}^m (\sin\lambda_j^\infty)[Y_b D]_j(\omega - \omega^\infty \mathbf{1}_n) \\
&= \sum_{i=1}^n (\omega_i - \omega^\infty)\left(p_i - \omega^\infty E_i - D^T Y_b \sin\lambda_i^\infty\right) = (\omega - \omega^\infty \mathbf{1}_n)^T(\tilde{p} - D^T Y_b \sin\lambda^\infty) = 0.
\end{aligned}$$

This monotonicity of V implies that the constraint $V(\lambda,\omega) \leqslant r$ defining $\mathscr{T}(r)$ can never be

violated. Now if there exists a time $t_1 > 0$ such that $(\lambda(t_1), \omega(t_1)) \notin \mathscr{T}(r)$, then it must be the case where $\lambda(t_1) \notin \mathscr{R}$. By the continuity of the trajectory, there must exist another time t_2 before t_1 such that $\lambda(t_2) \in \partial\mathscr{R}_{\text{cl}}$, in which case $V(\lambda(t_2), \omega(t_2)) \geqslant V(\lambda(t_2), \omega^{\infty}\mathbf{1}_n) \geqslant \bar{r} > r$, which is a contradiction. Hence $\mathscr{T}(r)$ is invariant.

To prove *(iii)*, notice that, for any $(\lambda, \omega) \in \mathscr{T}(r)$, $\dot{V}(\lambda, \omega) \leqslant 0$; second, $V(\lambda^{\infty}, \omega^{\infty}\mathbf{1}_n) = 0$; third, $V(\lambda, \omega) > 0$, for every $(\lambda, \omega) \in \mathscr{T}(r)$ with $(\lambda, \omega) \neq (\lambda^{\infty}, \omega^{\infty}\mathbf{1}_n)$. By [Kha02, Theorem 4.1], $(\lambda^{\infty}, \omega^{\infty}\mathbf{1}_n)$ is stable. Finally, to establish convergence, let

$$\Omega \triangleq \mathscr{T}(r) \cap \left\{ (\lambda, \omega) \;\middle|\; \lambda \in \text{range}(D) \right\}. \tag{4.5}$$

Note that $(\lambda(0), \omega(0)) \in \Omega$. Clearly, the set Ω is compact and invariant with respect to the dynamics (2.7a)-(2.7c) with controller satisfying (4.4). Noticing that $\dot{V}(\lambda, \omega) = 0$ implies $\omega = \omega^{\infty}\mathbf{1}_n$, let $S \triangleq \left\{ (\lambda, \omega) \;\middle|\; \omega = \omega^{\infty}\mathbf{1}_n \right\} \bigcap \Omega$. It is easy to see that no solution can identically stay in S other than the trivial solution $(\lambda(t), \omega(t)) \equiv (\lambda^{\infty}, \omega^{\infty}\mathbf{1}_n)$. The conclusion then follows from the LaSalle Invariance Principle [Kha02, Theorem 4.4]. □ □

Remark 4.2.2. *(Computation of the region of attraction):* The set $\mathscr{T}(\bar{r})$ is an estimate of the region of attraction but its explicit computation requires the solution of a non-convex optimization problem to determine the value of $\bar{r}$. We can equivalently compute $\bar{r}$ by solving $2m$ convex problems. For each $j \in [1, m]_{\mathbb{N}}$, let

$$\bar{c}_j \triangleq \min_{\substack{\lambda_j = \pi/2 \\ |\lambda_i| \leqslant \pi/2, \forall i \neq j}} V(\lambda, \omega^{\infty}\mathbf{1}_n), \quad \underline{c}_j \triangleq \min_{\substack{\lambda_j = -\pi/2 \\ |\lambda_i| \leqslant \pi/2, \forall i \neq j}} V(\lambda, \omega^{\infty}\mathbf{1}_n).$$

Note that these problems are convex, as the Hessian of $V(\tilde{\lambda}, \omega^{\infty}\mathbf{1}_n)$ with respect to $\tilde{\lambda}$, $\nabla^2 V = \text{diag}([Y_b]_{1,1}\cos(\lambda_1), \cdots, [Y_b]_{m,m}\cos(\lambda_m))$, is positive definite on $\mathscr{R}_{\text{cl}}$, and the feasible set is a closed convex subset of $\mathscr{R}_{\text{cl}}$. One can easily see that $\bar{r} = \min_{j \in [1,m]_{\mathbb{N}}} \{\bar{c}_j, \underline{c}_j\}$. •

4.2.2 Constraint ensuring frequency invariance

We next focus our attention on the frequency invariance requirement. We start by defining the invariant sets we are interested in,

$$\bar{\mathscr{C}}_i \triangleq \left\{x \;\middle|\; \omega_i - \bar{\omega}_i \leqslant 0\right\}, \quad \underline{\mathscr{C}}_i \triangleq \left\{x \;\middle|\; \underline{\omega}_i - \omega_i \leqslant 0\right\}. \tag{4.6}$$

The characterization stated in the next result directly follows from Nagumo's Theorem.

Lemma 4.2.3. *(Sufficient and necessary condition for frequency invariance): Assume that the solution of* (2.7) *exists and is unique for every admissible initial condition. Then, for any $i \in \mathscr{I}^u$, the sets $\bar{\mathscr{C}}_i$ and $\underline{\mathscr{C}}_i$ are invariant if and only if for every $x \in \mathbb{R}^{m+n}$ and $p \in \mathbb{R}^n$,*

$$u_i(x,p) - q_i(x,p) \leqslant 0 \quad \textit{if } \omega_i = \bar{\omega}_i, \tag{4.7a}$$

$$-u_i(x,p) + q_i(x,p) \leqslant 0 \quad \textit{if } \omega_i = \underline{\omega}_i, \tag{4.7b}$$

where $q_i(x,p) \triangleq E_i\omega_i + [D^T Y_b]_i \sin\lambda - p_i$.

Proof. For simplicity, we only deal with the case of $\bar{\mathscr{C}}_i$ (the other case follows similarly). For each $i \in \mathscr{I}^u$, let $\bar{l}_i, \underline{l}_i : \mathbb{R}^n \to \mathbb{R}$ be defined by $\bar{l}_i(x) \triangleq \omega_i - \bar{\omega}_i$ and $\underline{l}_i(x) \triangleq -\omega_i + \underline{\omega}_i$. Notice that, by letting $s = -\mathbf{1}_{m+n}$ and $\phi(x) \equiv -\mathbf{1}_{m+n}$, one has that $\bar{l}_i(x) + \nabla\bar{l}_i(x)^T s < 0$ for every $x \in \bar{\mathscr{C}}_i$ and $\nabla\bar{l}_i(x)^T\phi(x) < 0$ for every $x \in \partial\bar{\mathscr{C}}_i$, and hence the assumptions in Nagumo's Theorem hold. Denote by $f(t,x)$ the right-hand side of the dynamics (2.7). Then $\bar{\mathscr{C}}_i$ is invariant if and only if $\nabla\bar{l}_i(x)^T f(t,x) \leqslant 0$ when $\omega_i(t) = \bar{\omega}_i$, which is equivalent to (4.7a). □

From Lemma 4.2.3, one sees that if some bus $j \in \mathscr{I}^u$ does not possess an external control input (i.e., $u_j \equiv 0$), then one can not guarantee the invariance of $\bar{\mathscr{C}}_j$ and $\underline{\mathscr{C}}_j$, since without an active control signal, condition (4.7) can easily be violated. The characterization of Lemma 4.2.3 points to the value of the input at the boundary of $\bar{\mathscr{C}}_i$ and $\underline{\mathscr{C}}_i$. However, having a controller that

is only nonvanishing at such points is undesirable, as the actuator effort would be discontinuous, affecting the system evolution. A more sensible policy is to have the controller become active as the system state gets closer to the boundary of these sets, and do so in a gradual way. This is captured by the following result.

Lemma 4.2.4. *(Sufficient condition for frequency invariance): Assume that the solution of* (2.7) *exists and is unique for every admissible initial condition. For each $i \in \mathscr{I}^u$, let $\bar{\omega}_i^{\text{th}}$, $\underline{\omega}_i^{\text{th}} \in \mathbb{R}$ be such that $\underline{\omega}_i < \underline{\omega}_i^{\text{th}} < \bar{\omega}_i^{\text{th}} < \bar{\omega}_i$ and let $\bar{\alpha}_i$ and $\underline{\alpha}_i$ be functions of class-$\mathscr{K}$. If for every $x \in \mathbb{R}^{m+n}$ and $p \in \mathbb{R}^n$,*

$$(\omega_i - \bar{\omega}_i^{\text{th}})(u_i(x,p) - q_i(x,p)) \leqslant -\bar{\alpha}_i(\omega_i - \bar{\omega}_i), \quad \text{if } \bar{\omega}_i^{\text{th}} < \omega_i \leqslant \bar{\omega}_i, \tag{4.8a}$$

and

$$(\underline{\omega}_i^{\text{th}} - \omega_i)(-u_i(x,p) + q_i(x,p)) \leqslant -\underline{\alpha}_i(\underline{\omega}_i - \omega_i), \quad \text{if } \underline{\omega}_i \leqslant \omega_i < \underline{\omega}_i^{\text{th}}, \tag{4.8b}$$

then $\bar{\mathscr{C}}_i$ and $\underline{\mathscr{C}}_i$ are invariant.

The proof of Lemma 4.2.4 follows by noting that, when $\omega_i = \bar{\omega}_i$ (resp. $\omega_i = \underline{\omega}_i$), condition (4.8a) (resp. (4.8b)) becomes (4.7a) (resp. (4.7b)). The introduction of class-$\mathscr{K}$ functions enables the design of controllers that gradually kick in as the margin for satisfying the requirement for frequency invariance gets increasingly small. In fact, using (2.7), we can equivalently write (4.8a) as

$$M\dot{\omega}_i \leqslant -\bar{\alpha}_i(\omega_i - \bar{\omega}_i)/(\omega_i - \bar{\omega}_i^{\text{th}}), \quad \text{if } \bar{\omega}_i^{\text{th}} < \omega_i \leqslant \bar{\omega}_i. \tag{4.9}$$

Notice that, as ω_i grows from the threshold $\bar{\omega}_i^{\text{th}}$ to the safe bound $\bar{\omega}_i$, the value of $-\bar{\alpha}_i(\omega_i - \bar{\omega}_i)/(\omega_i - \bar{\omega}_i^{\text{th}})$ monotonically decreases to 0. Thus, the constraint on $\dot{\omega}_i$ becomes tighter (while allowing $\dot{\omega}_i$ to still be positive) as ω_i approaches $\bar{\omega}_i$, and when ω_i hits $\bar{\omega}_i$, prescribes $\dot{\omega}_i$ to be

nonpositive to ensure invariance.

It is interesting to point out the trade-offs present in the choice of class-$\mathscr{K}$ functions. A function with a large derivative, for instance, corresponds to a controller design that allows the derivative above to be significant near the boundary, at the risk of increasing the sensitivity to changes in the state. We re-examine this point later after introducing our specific controller design.

4.3 Distributed controller synthesis

In this section we introduce a distributed controller design that meets the stability and convergence condition (4.4) as well as the frequency invariance condition (4.8). Our next result formally introduces this controller and characterizes its continuity property.

Proposition 4.3.1. *(Distributed frequency controller): For each $i \in \mathscr{I}^u$, let $\bar{\alpha}_i$ and $\underline{\alpha}_i$ be Lipschitz functions of class-$\mathscr{K}$. Then,*

$$u_i(x,p) = \begin{cases} \min\{0, \frac{-\bar{\alpha}_i(\omega_i - \bar{\omega}_i)}{\omega_i - \bar{\omega}_i^{\text{th}}} + q_i(x,p)\} & \omega_i > \bar{\omega}_i^{\text{th}}, \\ 0 & \underline{\omega}_i^{\text{th}} \leqslant \omega_i \leqslant \bar{\omega}_i^{\text{th}}, \\ \max\{0, \frac{\underline{\alpha}_i(\underline{\omega}_i - \omega_i)}{\underline{\omega}_i^{\text{th}} - \omega_i} + q_i(x,p)\} & \omega_i < \underline{\omega}_i^{\text{th}}, \end{cases} \tag{4.10}$$

is Lipschitz in its first argument.

Proof. Let $i \in \mathscr{I}^u$. We show that for any $x \in \mathbb{R}^{m+n}$, there exist $L, r \in \mathbb{R}_>$ such that $|u_i(y,p) - u_i(z,p)| \leqslant L\|y - z\|$ for any $y, z \in B_r(x)$. Notice that this condition holds true for x belonging to $\mathbb{H} \triangleq \left\{ x \in \mathbb{R}^{m+n} \;\middle|\; \omega_i \neq \bar{\omega}_i^{\text{th}},\ \omega_i \neq \underline{\omega}_i^{\text{th}} \right\}$, in that $x \mapsto \frac{-\bar{\alpha}_i(\omega_i - \bar{\omega}_i))}{(\omega_i - \bar{\omega}_i^{\text{th}})} + q_i(x,p)$ (resp. $x \mapsto \frac{\underline{\alpha}_i(\underline{\omega}_i - \omega_i)}{\underline{\omega}_i^{\text{th}} - \omega_i} + q_i(x,p)$) is Lipschitz for any x in $\mathbb{H}$, and the min (resp. max)) operator preserves Lipschitz continuity. Hence we only need to establish Lipschitzness for $x \notin \mathbb{H}$. For simplicity we only reason for the case when x satisfies $\omega_i = \bar{\omega}_i^{\text{th}}$. Denote $r_0 \triangleq \min\{\frac{1}{2}(\bar{\omega}_i - \bar{\omega}_i^{\text{th}}),\ \frac{1}{2}(\bar{\omega}_i^{\text{th}} - \underline{\omega}_i^{\text{th}})\} \in \mathbb{R}_>$.

One can see that for any $x' \in B_{r_0}(x)$, it holds that $\underline{\omega}_i^{\text{th}} \leqslant \omega_i$. Next we show that there always exists $r \leqslant r_0$ such that

$$\frac{-\bar{\alpha}_i(\omega_i - \bar{\omega}_i)}{(\omega_i - \bar{\omega}_i^{\text{th}})} + q_i(x', p) > 0, \tag{4.11}$$

for all $x' \in B_r(x) \cap \left\{x' \;\middle|\; \omega_i > \bar{\omega}_i^{\text{th}}\right\}$. Notice that for any $x' \in B_r(x)$, $\omega_i - \bar{\omega}_i \leqslant \bar{\omega}_i^{\text{th}} + r - \bar{\omega}_i \leqslant \omega_i^{\text{th}} + (\bar{\omega}_i - \bar{\omega}_i^{\text{th}})/2 - \bar{\omega}_i = -(\bar{\omega}_i - \bar{\omega}_i^{\text{th}})/2 < 0$, and $q_i(x', p) = \omega_i + [D^T]_i\lambda - p_i \geqslant -(n+1)\|x'\|_2 - |p_i|$. Therefore, it holds that

$$\frac{-\bar{\alpha}_i(\omega_i - \bar{\omega}_i)}{(\omega_i - \bar{\omega}_i^{\text{th}})} + q_i(x', p) \geqslant \frac{-\bar{\alpha}_i(\omega_i - \bar{\omega}_i)}{2r} - (n+1)\|x'\|_2 - |p_i|.$$

It is easy to see that for any $x' \in B_r(x) \cap \left\{x' \;\middle|\; \omega_i > \bar{\omega}_i^{\text{th}}\right\}$, the first term can be arbitrarily large by reducing r, while the other two terms are bounded; therefore, there exits $r > 0$ small enough such that (4.11) holds. By (4.10), this implies that $u_i(x', p) = 0$ for any $x' \in B_r(x)$, and hence u_i is Lipschitz in x. □ □

Remark 4.3.2. *(Distributed character and practical implementation):* The controller (4.10) is distributed since each controlled bus $i \in \mathscr{I}^u$, u_i only utilizes ω_i, p_i, and information of buses it is connected to in the power network in order to compute $[D^T Y_b]_i\lambda$. This term corresponds to the aggregate power flow injected at node i from its neighboring nodes. In turn, this means that, instead of measuring λ_j and its corresponding susceptance for every i's neighboring node j, in practice, each node can simply measure the signed power flows in each neighboring transmission lines of node i and sum it up, which is equivalent to $[D^T Y_b]_i\lambda$ as well. •

The next result shows that the proposed distributed controller achieves the objectives identified in Section 3.1 regarding stability, convergence, and frequency invariance.

Theorem 4.3.3. *(Transient frequency control with stability guarantees): Under condition* (2.9)*, let* $\omega^\infty \in (\underline{\omega}_i^{\text{th}}, \bar{\omega}_i^{\text{th}})$ *and consider the closed-loop system* (2.7) *with controller* (4.10)*. If* $\lambda(0) \in$

range(D) *and* $(\lambda(0),\omega(0)) \in \mathscr{T}(r)$ *for some* $0 < r < \bar{r}$*, then*

(i) The solution exists and is unique for every $t \geqslant 0$*;*

(ii) $\lambda(t) \in$ range(D) *and* $(\lambda(t),\omega(t)) \in \mathscr{T}(r)$ *for any* $t \geqslant 0$*;*

(iii) $(\lambda^\infty, \omega^\infty \mathbf{1}_n)$ *is stable, and* $(\lambda(t),\omega(t)) \to (\lambda^\infty, \omega^\infty \mathbf{1}_n)$ *as* $t \to \infty$*;*

(iv) The controllers become inactive in finite time, i.e., there exists a time $t_0 > 0$ *such that* $u_i(x(t),p) = 0$ *for all* $t \geqslant t_0$ *and all* $i \in \mathscr{I}^u$*.*

(v) For any $i \in \mathscr{I}^u$*, if* $\omega_i(0) \in [\underline{\omega}_i, \bar{\omega}_i]$*, then* $\omega_i(t) \in [\underline{\omega}_i, \bar{\omega}_i]$ *for all* $t > 0$*;*

(vi) For any $i \in \mathscr{I}^u$*, if* $\omega_i(0) \notin [\underline{\omega}_i, \bar{\omega}_i]$*, then* $\omega_i(t)$ *monotonically approaches* $[\underline{\omega}_i, \bar{\omega}_i]$*. Furthermore, there exists a finite time* $t_1 > 0$ *such that* $\omega_i(t) \in [\underline{\omega}_i, \bar{\omega}_i]$ *for all* $t \geqslant t_1$*.*

In addition, if (i) holds for $(\lambda(0),\omega(0)) \notin \mathscr{T}$*, then (v) and the monotonic convergence in (vi) still hold, but with no guarantee on the existence of a finite* t_1*.*

Proof. It is easy to see that (4.10) guarantees $u_i(x,p) \leqslant 0$ if $\omega_i > \bar{\omega}_i^{\text{th}}$, $u_i(x,p) = 0$ if $\omega_i \in (\underline{\omega}_i^{\text{th}}, \bar{\omega}_i^{\text{th}})$, and $u_i(x,p) \geqslant 0$ if $\omega_i < \underline{\omega}_i^{\text{th}}$. Therefore, (4.4) holds as $\omega^\infty \in (\underline{\omega}_i^{\text{th}}, \bar{\omega}_i^{\text{th}})$. Hence *(i)-(iii)* directly follow from Lemma 4.2.1 (Proposition 4.3.1 justifies the Lipschitzness of the controller).

To prove *(iv)*, we use the convergence established in *(iii)*. For $\varepsilon = \min_{i\in\mathscr{I}^u}\{\bar{\omega}_i^{\text{th}} - \omega^\infty, \omega^\infty - \underline{\omega}_i^{\text{th}}\}$, there exists $t_0 \in \mathbb{R}_>$ such that $\|(\lambda(t),\omega(t)) - (\lambda^\infty, \omega^\infty \mathbf{1}_n)\|_2 < \varepsilon$, for $t \geqslant t_0$. Therefore, for any $i \in \mathscr{I}^u$, $|\omega_i(t) - \omega^\infty| \leqslant \|(\lambda(t),\omega(t)) - (\lambda^\infty, \omega^\infty \mathbf{1}_n)\|_2 \leqslant \min\{\bar{\omega}_i^{\text{th}} - \omega^\infty, \omega^\infty - \underline{\omega}_i^{\text{th}}\}$, for $t \geqslant t_0$, which implies $\underline{\omega}_i^{\text{th}} \leqslant \omega_i(t) \leqslant \bar{\omega}_i^{\text{th}}$, for $t \geqslant t_0$. The result follows now from the definition (4.10) of the controller. Regarding *(v)*, the controller (4.10) satisfies (4.8a) if $\bar{\omega}_i^{\text{th}} < \omega_i \leqslant \bar{\omega}_i$, and satisfies (4.8b) if $\underline{\omega}_i \leqslant \omega_i < \underline{\omega}_i^{\text{th}}$; hence by Lemma 4.2.4 both $\bar{\mathscr{C}}_i$ and $\underline{\mathscr{C}}_i$ are invariant. Proving monotonicity in *(vi)* is equivalent to showing that $\dot{\omega}_i(t) \leqslant 0$ when $\omega_i(t) > \bar{\omega}_i$ and $\dot{\omega}_i(t) \geqslant 0$ when $\omega_i(t) < \underline{\omega}_i$. For simplicity we only prove the first case. Note that

$u_i(x,p) \leqslant \frac{-\bar{\alpha}_i(\omega_i-\bar{\omega}_i)}{(\omega_i-\bar{\omega}_i^{\text{th}})} + q_i(x,p)$. Plugging this into (2.7b) and using $\omega_i > \bar{\omega}_i$, one has

$$M_i\dot{\omega}_i \leqslant \frac{-\bar{\alpha}_i(\omega_i-\bar{\omega}_i)}{(\omega_i-\bar{\omega}_i^{\text{th}})} \leqslant 0, \tag{4.12}$$

establishing monotonicity (notice that the inequality holds even if the initial condition does not belong to $\mathscr{T}(r)$). Finally, since $\omega^\infty \in (\underline{\omega}_i^{\text{th}}, \bar{\omega}_i^{\text{th}})$ and $\omega_i(t) \to \omega^\infty$ for every $i \in \mathscr{I}$, there exists t_1 such that $\omega_i(t_1) \in [\underline{\omega}_i^{\text{th}}, \bar{\omega}_i^{\text{th}}]$, which, by *(v)*, further implies that $\omega(t) \in [\underline{\omega}_i^{\text{th}}, \bar{\omega}_i^{\text{th}}]$ for every $t \geqslant t_1$. □

Remark 4.3.4. *(Performance trade-offs via selection of class-$\mathscr{K}$ functions):* As pointed out in Section 4.2.2, the choice of class-$\mathscr{K}$ functions affects the system behavior. To illustrate this, consider the linear choice $\bar{\alpha}_i = \underline{\alpha}_i : \mathbb{R} \to \mathbb{R},\ s \mapsto \Gamma_i s$, where $\Gamma_i > 0$ is a design parameter. A smaller Γ_i leads to more stringent requirements on the derivative of the frequency. This is because $u_i(x,p)$ can be non-zero only when either of the following happen,

$$\begin{aligned}
&\frac{-\bar{\alpha}_i(\omega_i-\bar{\omega}_i)}{(\omega_i-\bar{\omega}_i^{\text{th}})} + q_i(x,p) < 0 \text{ and } \omega_i > \bar{\omega}_i^{\text{th}},\\
&\frac{\underline{\alpha}_i(\underline{\omega}_i-\omega_i)}{\underline{\omega}_i^{\text{th}}-\omega_i} + q_i(x,p) > 0 \text{ and } \omega_i < \underline{\omega}_i^{\text{th}}.
\end{aligned}$$

In this first case, the term $\frac{-\bar{\alpha}_i(\omega_i-\bar{\omega}_i)}{(\omega_i-\bar{\omega}_i^{\text{th}})} = \frac{\Gamma_i(\bar{\omega}_i-\omega_i)}{\omega_i-\bar{\omega}_i^{\text{th}}} > 0$ becomes smaller as Γ_i decreases, making its addition with $q_i(x,p)$ more likely to be less than 0, and resulting in an earlier activation of u_i. The second case follows similarly.

A small Γ_i may also lead to high control magnitude because it prescribes a smaller bound on the frequency derivative, which in turn may require a larger control effort. However, choosing a large Γ_i may cause the controller to be highly sensitive to ω_i. This is because the absolute value of the partial derivative of $\frac{-\bar{\alpha}_i(\underline{\omega}_i-\omega_i)}{(\omega_i-\bar{\omega}_i^{\text{th}})}$ (resp. $\frac{\underline{\alpha}_i(\underline{\omega}_i-\omega_i)}{\underline{\omega}_i^{\text{th}}-\omega_i}$) with respect to ω_i grows proportionally with Γ_i; consequently, when $u_i(x,p)$ is non-zero, its sensitivity against ω_i increases as Γ_i grows,

resulting in low tolerance against slight changes in ω_i. In the limit, as $\Gamma_i \to \infty$, this yields

$$u_i^{\infty}(x,p) = \begin{cases} \min\{0, q_i(x,p)\} & \omega_i = \bar{\omega}_i, \\ 0 & \underline{\omega}_i < \omega_i < \bar{\omega}_i, \\ \max\{0, q_i(x,p)\} & \omega_i = \underline{\omega}_i, \end{cases} \tag{4.13}$$

which in general is discontinuous. We illustrate in simulation the dependence of the controller on the choice of linear class-$\mathscr{K}$ functions in Section 6.4. •

Remark 4.3.5. *(Incorporating transient frequency control and economic dispatch):* The power injections p_i's from the generator side are typically determined via economic dispatch, which specifies setpoints for individual generator buses to balance the power consumptions given from the load side while minimizing economic cost at steady state. Although we do not consider it here, it is possible to combine economic dispatch with the transient frequency controller discussed here. Intuitively, this is because our proposed controller affects the system transient behavior without changing the steady-state equilibrium. However, such combination must be done carefully, because the economic dispatch mechanism may enable the dependence of the power injection from the generators on the system state, whereas here we assume that it is constant. In the former case, this would require analyzing the asymptotic stability of the resulting closed-loop system. •

4.4 Closed-loop performance analysis

In this section, we characterize additional properties of the closed-loop system under the proposed distributed controller beyond stability and frequency invariance. We characterize the attractivity rate of trajectories for initial conditions outside the safe frequency region, the boundedness of the control effort prescribed by the controller along the system trajectories, and

its robustness against measurement and parameter uncertainty.

4.4.1 Estimation of the attractivity rate

Here we provide an estimate of the convergence rate to the safe region (cf. Theorem 4.3.3(vi)) when the frequency of a node is initially outside it. The next result identifies a specific trajectory bounding the frequency evolution.

Lemma 4.4.1. *(Upper bound on frequency evolution): With the notation of Theorem 4.3.3, assume that for some $i \in \mathscr{I}^u$, $\omega_i(0) > \bar{\omega}_i$. Let $z_i(t)$ be the unique solution of*

$$M_i \dot{z}_i(t) = \frac{-\bar{\alpha}_i(z_i(t) - \bar{\omega}_i)}{z_i(t) - \bar{\omega}_i^{\text{th}}},\ z_i(0) = \omega_i(0). \tag{4.14}$$

Then it holds that $\omega_i(t) \leqslant z_i(t)$, for any $t \geqslant 0$. Furthermore, $z_i(t)$ converges to $\bar{\omega}_i$ monotonically without reaching it in finite time.

Proof. It is easy to check that if $z_i(0) > \bar{\omega}_i$, then there exists a unique solution of (4.14) for every $t \geqslant 0$. Since (4.12) holds for every $i \in \mathscr{I}^u$, by the Comparison Lemma [Kha02, Lemma 3.4], one has that $\omega_i(t) \leqslant z_i(t)$ for any $t \geqslant 0$. On the other hand, one can easily prove via Lemma 2.5.1 that the set $\left\{z_i \middle| \bar{\omega}_i - z_i \leqslant 0\right\}$ is invariant, which, together with the fact that $z_i(0) > \bar{\omega}_i$, implies $z_i(t) \geqslant \bar{\omega}_i$ for every $t \geqslant 0$. By the dynamics (4.14), we deduce $\dot{z}_i(t) \leqslant 0$ for every $t \geqslant 0$ and the monotonicity follows. Finally, since $z_i(t)$ is monotone decreasing and lower-bounded, $z_i(t)$ is convergent, with limit $\bar{\omega}_i$ (since $\dot{z}_i(t) < 0$ if $z_i(t) \neq \bar{\omega}_i$). Finally, since the uniqueness of trajectories is guaranteed by the Lipschitzness of the dynamics (4.14) and $\bar{\omega}_i$ is an equilibrium, it follows that $z_i(t) > \bar{\omega}_i$ for any $t \geqslant 0$. □

A similar statement holds for the case when the initial frequency is lower than the lower safe bound, but we omit it for brevity. When $\bar{\alpha}_i$ is linear, the next result provides an explicit expression for the bounding trajectory.

Corollary 4.4.2. *(Estimation of frequency convergence rate with linear class-$\mathscr{K}$ function): With the notation of Lemma 4.4.1, if $\bar{\alpha}_i(s) = \bar{\Gamma}_i s$ with $\bar{\Gamma}_i > 0$, then $z_i(t)$ is uniquely determined by*

$$z_i(t) + (\bar{\omega}_i - \bar{\omega}_i^{\text{th}}) \ln\left(\frac{z_i(t) - \bar{\omega}_i}{\omega_i(0) - \bar{\omega}_i}\right) = -\bar{\Gamma}_i t/M_i + \omega_i(0). \tag{4.15}$$

Furthermore, it holds that for any $t \geqslant 0$,

$$z_i(t) \leqslant \bar{\omega}_i + (\omega_i(0) - \bar{\omega}_i) \exp\Big(\frac{-\bar{\Gamma}_i t/M_i + \omega_i(0) - \bar{\omega}_i}{\bar{\omega}_i - \bar{\omega}_i^{\text{th}}}\Big).$$

Proof. In the case where $\bar{\alpha}_i(s) = \bar{\Gamma}_i s$, by separation of variables, one has that (4.14) is equivalent to

$$\frac{z_i - \bar{\omega}_i^{\text{th}}}{z_i - \bar{\omega}_i} \mathrm{d}z_i = -\bar{\Gamma}_i \mathrm{d}t/M_i,\ z_i(0) = \omega_i(0).$$

Equation (4.15) follows by integrating the above differential equation. Since by Lemma 4.4.1 $z_i(t) \geqslant \bar{\omega}_i$ for every $t \geqslant 0$, it holds

$$\bar{\omega}_i + (\bar{\omega}_i - \bar{\omega}_i^{\text{th}}) \ln\left(\frac{z_i(t) - \bar{\omega}_i}{\omega_i(0) - \bar{\omega}_i}\right) \leqslant -\bar{\Gamma}_i t/M_i + \omega_i(0),$$

concluding the proof. □

Remark 4.4.3. *(Estimation of safe-frequency entry time):* Corollary 4.4.2 establishes the exponential convergence rate of the frequency evolution to the safe region, but it does not provide an estimate of the finite time of entry t_1 stated in Theorem 4.3.3(vi). This is because the upper-bound signal z_i never hits $\bar{\omega}_i$ in finite time. This drawback is caused by the fact that the existence of t_1 is justified by (cf. proof of Theorem 4.3.3(vi)) the combination of frequency invariance and convergence of the closed-loop system, where we do not utilize the latter in obtaining the upper-bound signal. To fix this, one may replace $\bar{\omega}_i$ by $\bar{\omega}_i - \varepsilon_i$ in (4.10) with $\varepsilon_i \in \mathbb{R}_>$, and deter-

mine t_1 by solving $z(t_1) = \bar{\omega}_i$ along the dynamics (4.14). Note that, although this procedure does not jeopardize any statement in Theorem 4.3.3, it actually puts a stricter frequency invariance requirement on the controller. •

4.4.2 Bounds on controller magnitude

Here, we provide bounds on the amplitude of the proposed controller (4.10) along the system trajectories for a given constant power injection profile p. Our approach to do this is to constrain the allowable initial conditions by employing the energy function V as a measure of how far an initial state can be from the equilibrium point. The next result bounds the control input as a function of r in (4.1), with $0 < r < \bar{r}$.

Lemma 4.4.4. *(Lower bound on control effort): For $i \in \mathscr{I}^u$, let $g_i(\lambda, \omega) \triangleq \frac{-\bar{\alpha}_i(\omega_i - \bar{\omega}_i)}{\omega_i - \bar{\omega}_i^{\text{th}}} + q_i(x,p)$ and $d_i \triangleq 1/2M_i(\bar{\omega}_i^{\text{th}} - \omega^{\infty})^2$. Let (λ^*, ω^*) be the optimal solution of*

$$
\begin{aligned}
(\mathbf{Q}) \qquad & \min_{(\lambda,\omega)} \quad g_i(\lambda,\omega) \\
& s.t. \qquad (\lambda,\omega) \in \mathscr{T}(r), && \text{(4.16a)} \\
& \qquad\quad \lambda \in \text{range}(D), && \text{(4.16b)} \\
& \qquad\quad \omega_i > \bar{\omega}_i^{\text{th}}, && \text{(4.16c)}
\end{aligned}
$$

and define

$$
u_i^{\min}(r) \triangleq \begin{cases} 0 & \text{if } 0 \leqslant r \leqslant d_i, \\ \min\{0, g_i(\lambda^*, \omega^*)\} & \text{if } d_i < r < \bar{r}. \end{cases} \tag{4.17}
$$

Then, for any $(\lambda(0), \omega(0)) \in \mathscr{T}(r)$ with $\lambda(0) \in \text{range}(D)$,

$$
u_i(x(t), p) \geqslant u_i^{\min}(r), \tag{4.18}
$$

for any $t \geqslant 0$, and there exists initial states such that equality holds at some $t \geqslant 0$.

Proof. Note that by Theorem 4.3.3 with $0 < r < \bar{r}$, one has $(\lambda(t), \omega(t)) \in \mathscr{T}(r)$ and $\lambda(t) \in \text{range}(D)$ for every $t > 0$, provided they hold at $t = 0$. Therefore, to show (4.18) for every $t \geqslant 0$, it suffices to show it holds for $t = 0$. If $0 \leqslant r \leqslant d_i$, then $1/2M_i(\omega_i(0) - \omega^\infty)^2 \leqslant V(\omega(0), \lambda(0)) \leqslant d_i = 1/2(M_i(\bar{\omega}_i^{\text{th}} - \omega^\infty)^2$, which implies $\omega_i(0) \leqslant \bar{\omega}_i^{\text{th}}$; therefore, $u_i(x(0), p) \geqslant 0$ follows by (4.10). Also, $u_i(x(0), p)$ can be 0 in the case when, say, $x(0) = (\lambda^\infty, \omega^\infty)$. In the other case, if $d_i < r < \bar{c}$, then $u_i(x(0), p)$ is lower bounded by the optimal value of

$$
\begin{aligned}
(\hat{\mathbf{Q}}) \qquad & \min_{(\lambda,\omega)} \quad u_i(x, p) \\
& \text{s.t.} \qquad \text{(4.16a) and (4.16b).}
\end{aligned} \tag{4.19}
$$

Denote this optimal value by $v_i(r)$. Also, the value of $u_i(x(0), p)$ can be exactly $v_i(r)$, e.g., in the case when $x(0)$ is the optimal solution of $(\hat{Q})$. Note that $v_i(r) \leqslant 0$ as $(\lambda^\infty, \omega^\infty)$ satisfies (4.19) and $u_i((\lambda^\infty, \omega^\infty), p) = 0$. Since it holds that a) $u_i(x, p) \geqslant 0$ for any $\omega_i \leqslant \bar{\omega}_i^{\text{th}}$, and b) $u_i(x, p) \leqslant 0$ for any $\omega_i \geqslant \bar{\omega}_i^{\text{th}}$, one can, without changing the optimal value, replace $u_i(x, p)$ by $\min\{0, g_i(\lambda, \omega)\}$ in $(\hat{Q})$, and meanwhile add an additional constraint (4.16c). With a simple reasoning effort, one can show that for this new optimization problem, the optimal value is exactly $\min\{0, g_i(\lambda^*, \omega^*)\}$.

□

Note that the control amplitude lower bound $u_i^{\min}(r)$ depends nonlinearly on the power injection p. This is because, although the objective function in the optimization problem (Q), linearly depends on p, the optimal value does depend nonlinearly on p through the constraint (4.16a). This is due to the fact that the equilibrium $(\lambda^\infty, \omega^\infty \mathbf{1}_n)$ depends on p through the transcendental equation (2.10).

A similar result can be stated regarding an upper bound of the controller magnitude, but we omit it for brevity. The problem (Q) is non-convex due to the non-convexity of the objective function. We next show that its optimal value equals that of another optimization problem with

convex objective function and non-convex feasible set. Define the function $h_i : \mathbb{R}^{m+n} \times \mathbb{R} \to \mathbb{R},\ (z,\omega) \to h_i(z,\omega)$ exactly the same as g_i but replacing $\sin\lambda_i$ by z_i in the definition of q_i. In this way, $h_i(\sin\lambda,\omega) = g_i(\lambda,\omega)$. Let $\mathscr{D}_i^+ \triangleq \{j \big| [D^T Y_b]_{ij} > 0\}$ and $\mathscr{D}_i^- \triangleq \{j \big| [D^T Y_b]_{ij} < 0\}$. Consider the optimization

$$
\begin{aligned}
(\mathbf{R}) \qquad & \min_{(z,\lambda,\omega)} \quad h_i(z,\omega) \\
& \text{s.t.} \quad \sin\lambda_j \leqslant z_j,\ \forall j \in \mathscr{D}_i^+, && \text{(4.20a)} \\
& \qquad\ \ \sin\lambda_j \geqslant z_j,\ \forall j \in \mathscr{D}_i^-, && \text{(4.20b)} \\
& \qquad\ \ \text{(4.16a) to (4.16c).} && \text{(4.20c)}
\end{aligned}
$$

We claim that the optimal value of this problem is the same as that of (Q). The claim holds if every optimal solution of (R), denoted by $(z^\sharp,\lambda^\sharp,\omega^\sharp)$, satisfies (4.20a) and (4.20b) with equality signs. This has to be the case since, for instance, if $\sin\lambda_k^\sharp < z_k^\sharp$ for some $k \in \mathscr{D}_i^+$, then $(z^\sharp,\lambda^\sharp,\omega^\sharp)$ can no more be an optimal solution, since $(\hat{z}^\sharp,\lambda^\sharp,\omega^\sharp)$, where $\hat{z}^\sharp$ differs from $z^\sharp$ only in its kth component, $\hat{z}_k^\sharp = \sin\lambda_k^\sharp$, has $h_i(\hat{z}^\sharp,\omega^\sharp) < h_i(z^\sharp,\omega^\sharp)$, violating optimality.

Our next step is to convexify (R). Here we assume that $\omega_i \mapsto \frac{-\bar{\alpha}_i(\omega_i-\bar{\omega}_i)}{\omega_i-\bar{\omega}_i^{\text{th}}}$ is convex in ω_i in the region $\omega_i > \bar{\omega}_i^{\text{th}}$, which suffices to guarantee the convexity of $(z,\omega) \mapsto h_i(z,\omega)$ in (z,ω) under constraint (4.20) (this convexity assumption holds if, for instance, $\bar{\alpha}_i$ is a linear function). To handle the non-convexity of the constraints (4.20a) and (4.20b), in the following two results, we separately provide inner and outer approximations, leading to upper and lower approximations of the optimal value of (R), and equivalently (Q).

Lemma 4.4.5. *(Upper bound of optimal value): Define* $\mathscr{H}^+ \triangleq \{(a,b) \big|\ |a| < \pi/2,\ \sin a \leqslant b \text{ if } a \in [-\pi/2,0),\ \text{and } a \leqslant b \text{ if } a \in [0,\pi/2]\}$, *and* $\mathscr{H}^- \triangleq \{(a,b) \big|\ |a| < \pi/2,\ a \geqslant b \text{ if } a \in [-\pi/2,0),$

and $\sin a \geqslant b$ *if* $a \in [0, \pi/2]\}$. *Consider the convex optimization problem*

$$
\begin{aligned}
(\bar{\mathbf{R}}) \qquad & \min_{(z,\lambda,\omega)} \quad h_i(z,\omega) \\
& \textit{s.t.} \qquad (\lambda_j, z_j) \in \mathscr{H}^+, \ \forall j \in \mathscr{D}_i^+, && \text{(4.21a)} \\
& \qquad\quad (\lambda_j, z_j) \in \mathscr{H}^-, \ \forall j \in \mathscr{D}_i^-, && \text{(4.21b)} \\
& \qquad\quad \text{(4.16a) } \textit{to} \text{ (4.16c)}, && \text{(4.21c)}
\end{aligned}
$$

and denote its optimal solution by $(z^o, \lambda^o, \omega^o)$. *Then it holds that* $h_i(z^o, \omega^o) \geqslant g_i(\lambda^o, \omega^o) \geqslant g_i(\lambda^*, \omega^*)$.

Proof. The second inequality holds since (λ^o, ω^o) satisfies (4.16a) to (4.16c), making it a feasible point for (Q). To show the first inequality, one can easily check that for any $j \in \mathscr{D}_i^+$, if $(\lambda_j, z_j) \in \mathscr{H}^+$, then $\sin \lambda_j \leqslant z_j$ (cf. Figure 4.1(a)). Therefore, (4.21a) is stricter than (4.20a). Similarly, (4.21b) is stricter than (4.20b). Therefore, $[D^T Y_b]_{ij} z_j^o \geqslant [D^T Y_b]_{ij} \sin \lambda_j^o$ holds for any $j \in [1,m]_{\mathbb{N}}$, completing the proof since $h_i(z^o, \omega^o) \geqslant h_i(\sin \lambda^o, \omega^o) = g_i(\lambda^o, \omega^o)$. □ □

Lemma 4.4.6. *(Lower bound of optimal value): Define* $\mathscr{M}_0^+ \triangleq \{(a,b) \big| \ -\pi/2 < a \leqslant 0, \ \sin a \leqslant b\}$, $\mathscr{M}_1^+ \triangleq \{(a,b) \big| \ 0 \leqslant a \leqslant \pi/2, \ 2a/\pi \leqslant b\}$, $\mathscr{M}_0^- \triangleq \{(a,b) \big| \ -\pi/2 < a \leqslant 0, \ 2a/\pi \geqslant b\}$, *and* $\mathscr{M}_1^- \triangleq \{(a,b) \big| \ 0 \leqslant a \leqslant \pi/2, \ \sin a \leqslant b\}$. *Consider the convex optimization problem for* $\mu \triangleq \{\mu_j\}_{j \in \mathscr{D}_i^+ \bigcup \mathscr{D}_i^-}$, *with* $\mu_j \in \{0,1\}$,

$$
\begin{aligned}
(\underline{\mathbf{R}}^{\mu}) \qquad & \min_{(z,\lambda,\omega)} \quad h_i(z,\omega) \\
& \textit{s.t.} \qquad (\lambda_j, z_j) \in \mathscr{M}_{\mu_j}^+, \ \forall j \in \mathscr{D}_i^+, && \text{(4.22a)} \\
& \qquad\quad (\lambda_j, z_j) \in \mathscr{M}_{\mu_j}^-, \ \forall j \in \mathscr{D}_i^-, && \text{(4.22b)} \\
& \qquad\quad \text{(4.16a) } \textit{to} \text{ (4.16c)}, && \text{(4.22c)}
\end{aligned}
$$

and denote its optimal solution by $(\underline{z}^{\mu}, \underline{\lambda}^{\mu}, \underline{\omega}^{\mu})$. *Let* $\mu^* \triangleq \arg\min_{\mu} h_i(\underline{z}^{\mu}, \underline{\omega}^{\mu})$, *then* $h_i(\underline{z}^{\mu^*}, \underline{\omega}^{\mu^*}) \leqslant$

$g_i(\lambda^*, \omega^*)$.

Proof. Define

$$
\begin{aligned}
(\underline{\mathbf{R}}) \qquad & \min_{(z,\lambda,\omega)} \quad h_i(z,\omega) \\
& \text{s.t.} \quad (\lambda_j, z_j) \in \mathscr{M}_0^+ \cup \mathscr{M}_1^+, \ \forall j \in \mathscr{D}_i^+, && \text{(4.23a)} \\
& \qquad\quad (\lambda_j, z_j) \in \mathscr{M}_0^- \cup \mathscr{M}_1^-, \ \forall j \in \mathscr{D}_i^-, && \text{(4.23b)} \\
& \qquad\quad \text{(4.16a) to (4.16c).} && \text{(4.23c)}
\end{aligned}
$$

One can easily see that (4.20a)-(4.20b) is stricter than (4.23a)-(4.23b) (cf. Figure 4.1(b)). Hence the optimal value of $(\underline{R})$ lower bounds $g_i(\lambda^*, \omega^*)$. Notice that (4.22a)-(4.22b) simply splits (4.23a)-(4.23b) into convex regions, and hence $(\underline{z}^{\mu^*}, \underline{\lambda}^{\mu^*}, \underline{\omega}^{\mu^*})$ is also the optimal solution of $(\underline{R}^{\mu})$. □

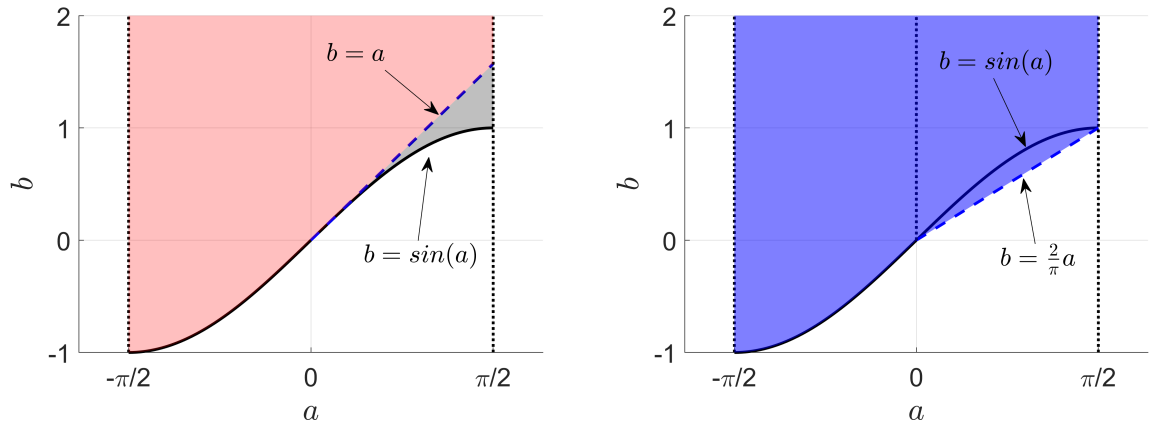

Figure 4.1: Tightening and relaxation of a sinusoidal non-convex constraint. In plot (a), within $|a| < \pi/2$, by ignoring the gray region delimited by $b = a$, $b = \sin(a)$ and $a = \pi/2$, the non-convex set characterized by $\sin(a) \leqslant b$ appearing in (4.20a) contains the red convex subset $\mathscr{H}^+$. On the other hand, in plot (b), this non-convex set is contained in the blue region. Each of the blue regions separated by the dotted line at $a = 0$ are convex.

Together, Lemmas 4.4.5 and 4.4.6 provide us with efficient ways of approximating the value of the bound on the control effort $u_i^{\min}(r)$.

4.4.3 Robustness to measurement and parameter uncertainty

Here we study the controller performance under measurement and parameter uncertainty. This is motivated by scenarios where the state or the power injection may not be precisely measured, or scenarios where some system parameters, like the damping coefficient, are only approximately known. Formally, we let $\hat{x} = (\hat{\lambda}, \hat{\omega})$, $\hat{p}$, and $\hat{E}$ be the measured or estimated state, power injection, and damping parameters, respectively. For every $i \in \mathscr{I}^u$, we introduce the error variables

$$\varepsilon_i^\omega \triangleq \hat{\omega}_i - \omega_i, \quad \varepsilon_i^\lambda \triangleq [D^T Y_b]_i \hat{\lambda} - [D^T Y_b]_i \lambda, \quad \varepsilon_i^p \triangleq \hat{p}_i - p_i, \quad \varepsilon_i^E \triangleq \hat{E}_i - E_i.$$

We make the following assumption regarding the error.

Assumption 4.4.7. *(Bounded uncertainties): For each $i \in \mathscr{I}^u$,*

(i) the uncertainties are piece-wise continuous and can be bounded by $|\varepsilon_i^\omega(t)| \leqslant \bar{\varepsilon}_i^\omega$, $|\varepsilon_i^\lambda(t)| \leqslant \bar{\varepsilon}_i^\lambda$, $|\varepsilon_i^p(t)| \leqslant \bar{\varepsilon}_i^p$, and $|\varepsilon_i^E(t)| \leqslant \bar{\varepsilon}_i^E$ for all $t \geqslant 0$;

(ii) $\omega^\infty \in (\underline{\omega}_i^{\text{th}} + \bar{\varepsilon}_i^\omega, \bar{\omega}_i^{\text{th}} - \bar{\varepsilon}_i^\omega)$;

(iii) $\bar{\varepsilon}_i^\omega < \min\{\bar{\omega}_i - \bar{\omega}_i^{\text{th}}, \underline{\omega}_i^{\text{th}} - \underline{\omega}_i\}$.

Condition *(i)* provides uniform bounds on the uncertainties; *(ii)* ensures that, even with uncertainty, the control input is identically 0 around the equilibrium; *(iii)* guarantees that the control input is always non-singular.

For convenience, we use $\hat{u}_i(\hat{x}, \hat{p}(t))$ to refer to the controller with the same functional expression as (4.10) but implemented with approximate parameter values and evaluated at the inaccurate state $\hat{x}$ and power injection $\hat{p}(t)$. Notice that $\hat{p}(t)$ can be time-varying. The next result shows that $\hat{u}_i$ still stabilizes the power network and enforces the satisfaction of a relaxed frequency invariance condition. For simplicity, we restrict our attention to linear class-$\mathscr{K}$ functions in the controller design.

Proposition 4.4.8. *(Robust stability and frequency invariance under uncertainty): Under condition* (2.9) *and Assumption 4.4.7, consider the evolution of the system* (2.7) *with the controller $\hat{u}_i$ for each $i \in \mathscr{I}^u$. Then the following results hold provided $\lambda(0) \in \text{range}(D)$ and $(\lambda(0), \omega(0)) \in \mathscr{T}(r)$ for some $0 < r < \bar{r}$:*

(i) The solution exists and is unique for every $t \geqslant 0$.

(ii) $\lambda(t) \in \text{range}(D)$ and $(\lambda(t), \omega(t)) \in \mathscr{T}(r)$ for any $t \geqslant 0$;

(iii) $(\lambda^\infty,\ \omega^\infty \mathbf{1}_n)$ is stable, and $(\lambda(t),\ \omega(t))$ converges to $(\lambda^\infty,\ \omega^\infty \mathbf{1}_n)$;

(iv) There exists a finite time t_2 such that $\hat{u}_i(\hat{x}(t), \hat{p}(t)) = 0$ for every $t \geqslant t_2$ and every $i \in \mathscr{I}^u$.

(v) Suppose $\bar{\alpha}_i(s) = \underline{\alpha}_i(s) = \Gamma_i s$ for every $i \in \mathscr{I}^u$. Then, if there exists $\Delta > 0$ such that satisfy

$$\frac{-\Gamma_i(\bar{\varepsilon}_i^\omega + \Delta)}{\bar{\omega}_i - \bar{\omega}_i^{\text{th}} + \Delta + \bar{\varepsilon}_i^\omega} + \bar{\varepsilon}_i^E(\Delta + \bar{\omega}_i) + \hat{E}_i \bar{\varepsilon}_i^\omega + \bar{\varepsilon}_i^\lambda + \bar{\varepsilon}_i^p \leqslant 0, \tag{4.24a}$$

$$\frac{-\Gamma_i(\bar{\varepsilon}_i^\omega + \Delta)}{\underline{\omega}_i^{\text{th}} - \underline{\omega}_i + \Delta + \bar{\varepsilon}_i^\omega} + \bar{\varepsilon}_i^E(\Delta - \underline{\omega}_i) + \hat{E}_i \bar{\varepsilon}_i^\omega + \bar{\varepsilon}_i^\lambda + \bar{\varepsilon}_i^p \leqslant 0, \tag{4.24b}$$

then $\omega_i(t) \in [\underline{\omega}_i - \Delta, \bar{\omega}_i + \Delta]$ for all $t > 0$, provided $\omega_i(0) \in [\underline{\omega}_i - \Delta, \bar{\omega}_i + \Delta]$, and, if $\omega_i(0) \notin [\underline{\omega}_i - \Delta, \bar{\omega}_i + \Delta]$, then there exists a finite time t_3 such that $\omega_i(t) \in [\underline{\omega}_i - \Delta, \bar{\omega}_i + \Delta]$ for all $t \geqslant t_3$.

Proof. The proofs of *(i)-(iii)* follow similar arguments as the proofs of Theorem *(i)-(iii)*. For stability, one can show that $\frac{d}{dt}V(\omega(t), \lambda(t)) = -\tilde{\omega}^T(t) E \tilde{\omega}(t) + \sum_{i \in \mathscr{I}^u} \tilde{\omega}_i(t) \hat{u}_i(\hat{x}(t), \hat{p}(t))$. By Assumption 4.4.7 and the definition of $\hat{u}_i$, it holds that $\sum_{i \in \mathscr{I}^u} \tilde{\omega}_i(t) \hat{u}_i(\hat{x}(t), \hat{p}(t)) \leqslant 0$, implying $\frac{d}{dt}V(\lambda(t), \omega(t)) \leqslant 0$. The convergence follows by LaSalle Invariance Principle and noticing that $\hat{u}_i(\hat{x}, \hat{p}(t))$ is identically 0 so long as $\omega_i \in [\underline{\omega}_i^{\text{th}} + \bar{\varepsilon}_i^\omega, \bar{\omega}_i^{\text{th}} - \bar{\varepsilon}_i^\omega]$, which, together with the convergence, implies that $\hat{u}_i(\hat{x}(t), \hat{p}(t))$ is 0 after a finite time. For *(v)*, to prove the invariance of

$[\underline{\omega}_i - \Delta, \bar{\omega}_i + \Delta]$, by Lemma 4.2.3, we only need to show that

$$\hat{u}_i(\hat{x}, \hat{p}(t)) - q_i(x,t) \leqslant 0, \text{ if } \omega_i = \bar{\omega}_i + \Delta, \tag{4.25a}$$

$$-\hat{u}_i(\hat{x}, \hat{p}(t)) + q_i(x,t) \leqslant 0, \text{ if } \omega_i = \underline{\omega}_i - \Delta. \tag{4.25b}$$

For simplicity, we only show that (4.24a) implies (4.25a) (the fact that (4.24b) implies (4.25b) follows similarly). Notice that if $\omega_i = \bar{\omega}_i + \Delta$, then $\hat{u}_i(\hat{x}, \hat{p}(t)) - q_i(x,t)$ equals

$$\frac{-\Gamma_i(\Delta + \varepsilon_i^{\omega})}{\bar{\omega}_i - \bar{\omega}_i^{\text{th}} + \Delta + \varepsilon_i^{\omega}} + \varepsilon_i^E(\bar{\omega}_i + \Delta) + \hat{E}_i \varepsilon_i^{\omega} + \varepsilon_i^{\lambda} + \varepsilon_i^p, \tag{4.26}$$

which, by Assumption 4.4.7, is smaller than or equal to the left-hand side of (4.24a) by letting the uncertainties take their individual bounds; hence (4.25a) holds. Finally, the existence of t_3 follows a similar proof in Theorem *(vi)*. □

One should look at (4.24) as a condition that, independently of the specific realization of the uncertainty, guarantees that the invariance of the frequency interval is ensured.

4.5 Simulations

We illustrate the performance of our control design in the IEEE 39-bus power network displayed in Figure 3.3. Parameter set-ups of the power network are in line with those in Section 3.5, and we use Power System Toolbox [CCR09] to assign the initial power injection $p_i(0)$ for every bus (although the analytical results hold for constant power injections, in simulation we have also tested the more general time-varying case). We assign all non-generator buses a uniform small inertia $M_i = 0.1$. The damping parameter is $E_i = 1$ for all buses. The initial state $(\lambda(0), \omega(0))$ is chosen to be the unique equilibrium with respect to the initial power injection. We implement the distributed controller in (4.10) in the generators with indices $\mathscr{I}^u = \{30, 31, 32\}$ to tune their transient frequency behavior. The controller parameters are

as follows: for every $i \in \mathscr{I}^u$, we let $\bar{\alpha}_i(s) = \underline{\alpha}_i(s) = \Gamma_i s$, with $\Gamma_i = 2$, $\bar{\omega}_i = -\underline{\omega}_i = 0.2$Hz and $\bar{\omega}_i^{\text{th}} = -\underline{\omega}_i^{\text{th}} = 0.1$Hz. The nominal frequency is 60Hz, and hence the safe frequency region is [59.8Hz, 60.2Hz].

We first show how the proposed controller maintains the targeted generator frequencies within the safe region provided that these frequencies are initially in it. For our first scenario, we consider a generator loss and recovery process. Specifically, we set the power injection of node 38 to zero (i.e., generator G9) during the time interval [10,40]s. As shown in Figure 4.2, without the transient controller (4.10), the frequency of node 30 first gradually goes down, exceeding the safe bound 59.8Hz a few times, even tending to converge to a frequency below it. As node 38 recovers its power supply at 40s, the frequency comes back to 60Hz. In comparison, with the transient controller, the frequency trajectory never goes beyond 59.8Hz during the transient.

For our second scenario, we perturb all non-generator nodes by a sinusoidal power injection whose magnitude is proportional to the corresponding node's initial power injection. Specifically, for every $i \in \{1, 2, \cdots, 29\}$,

$$p_i(t) = \begin{cases} p_i(0) & \text{if } t \geqslant 30, \\ \left(1 + 0.3\sin(\frac{\pi t}{30})\right) p_i(0) & \text{otherwise.} \end{cases}$$

For $i \in \{30, 31, \cdots, 39\}$, $p_i(t)$ remains constant all the time. Figure 4.3(a) shows the frequency responses of generators 30, 31, and 32 without the transient controller. One can see that all trajectories exceed the 59.8Hz lower frequency bound. For comparison, Figure 4.3(b) shows the trajectories with the transient controller (4.10), where all remain within the safe frequency region. Figure 4.3(c) displays the corresponding input trajectories, which converge to 0 in finite time, as stated in Theorem 4.3.3*(iv)*. We also illustrate the robustness of the controller against uncertainty. We have each controller employ $\hat{E}_i = 2$ and $\hat{p}_i(t) = 1.1 p_i(t)$, corresponding to 100% and 10% deviations on droop coefficients and power injections, respectively. Figure 4.3(d)

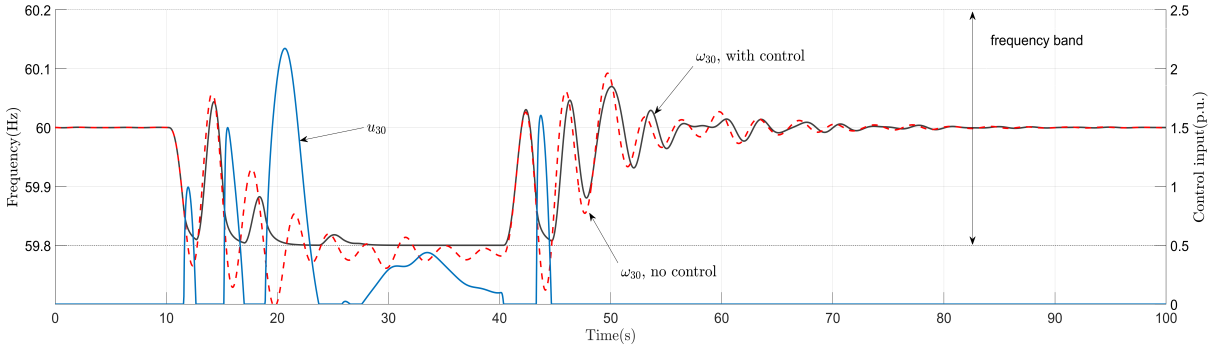

Figure 4.2: Frequency and control input trajectories at node 30 corresponding to the power supply loss of generator G9 during [10,40]s. The frequency trajectory without transient controller goes beyond the safe bounds during the contingency, while this is avoided with the proposed controller. Notice that the latter only takes effect when the frequency is close to the safe bound.

illustrates the frequency trajectories of the 3 controlled generators. Since condition (4.24) is satisfied with $\Delta = 0.1$Hz, Proposition 4.4.8 ensures that the invariant frequency interval is now $[59.7\text{Hz}, 60.3\text{Hz}]$.

Next, we illustrate the effect of unmodeled actuator dynamics in the performance of our controller. Instead of the ideal assumption adopted in our analysis that the control command u is applied to the physical system without delay, we run simulations on the same setup of Figure 4.3(b), that incorporate the actuator response time by having the actuator of each controlled node be modeled as a first-order linear system with response time $5s$, see e.g. [WLL$^+$18]. Figure 4.4(a) shows the outcome of the simulation. One can see that, since the controller does not take the actuator dynamics into account, the guarantee on frequency invariance is not maintained. Still, the frequency trajectories are better than the open-loop trajectories displayed in Figure 3.6(a). On the other hand, if we use $\underline{\omega}_i = -0.06$Hz and $\underline{\omega}_i^{\text{thr}} = -0.03$Hz for each $i \in \mathscr{U}$ (that is to say, we narrow down the safe frequency bound) for the controller (4.10), then the frequency trajectories stay above 59.8Hz in this scenario, as shown in Figure 4.4(b).

Next, we examine the effect of the choice of class-$\mathscr{K}$ function on the behavior of the transient frequency. We focus our attention on bus 30 and simulate the network behavior for

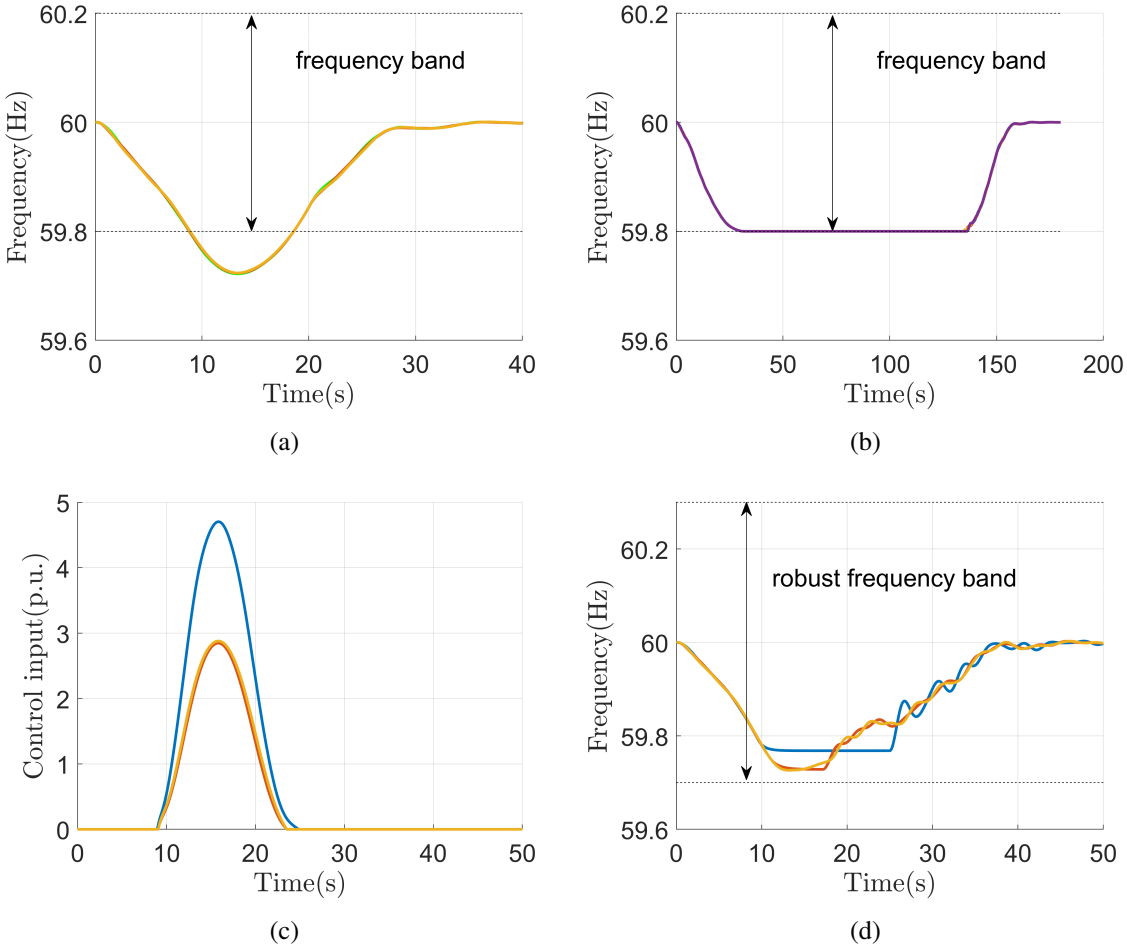

Figure 4.3: Frequency and control input trajectories with and without transient controller. Plot (a) shows the frequency trajectories of the generators 30, 31, and 32 without the transient controller (4.10), with all of them going beyond the lower safe frequency bound. With the transient controller, plot (b) shows that all frequency trajectories stay within the safe bound. Plot (c) shows the corresponding trajectories of the control inputs. Plot (d) shows the controller performance under parameter uncertainty and errors in the power injection approximation.

a linear function with $\Gamma_{30} = 0.1, 2, 10$, and $+\infty$ (the latter corresponding to the discontinuous controller in (4.13)). Figure 4.5 shows the corresponding frequency and control input trajectories for the first 30 seconds at node 30. From Figure 4.5(a), one can see that the frequency trajectory with $\Gamma_{30} = 0.1$ tends to stay away from the lower safe bound (overprotection), compared with the trajectories with $\Gamma_{30} = 2, 10$, and $+\infty$, and this results in a larger control input, cf. Figure 4.5(b). As Γ_{30} increases, the control input is triggered later. On the other hand, choosing a large Γ_{30}

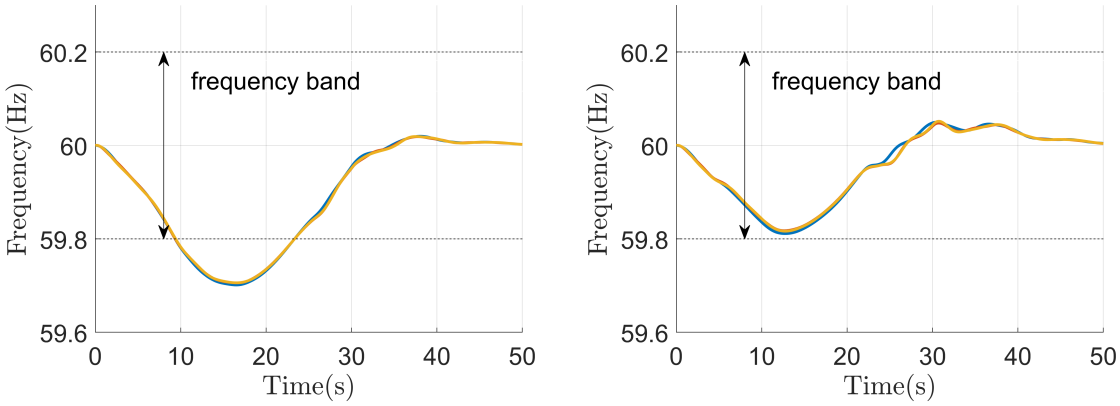

Figure 4.4: Frequency trajectories under non-ideal actuator dynamics. Plot (a) shows the frequency trajectories of generators 30, 31, and 32 with the control command (4.10) as the setpoint of a first-order actuator. Plot (b) shows the same but with the control command (4.10) implemented with tighter safe frequency bounds.

lead to higher sensitivity, as observed in Figure 4.5(b), where the input trajectory with large Γ_{30} grows faster at the time when the control input first becomes non-zero. In fact, the controller with $\Gamma_{30} = 10$ exhibits a sharp change around $t = 9s$, similar to the discontinuous controller (4.13). The discontinuity of the latter is more evident under state measurements errors. In Figure 4.6, we run the same simulation but with $\hat{\omega}_{30}(t) = \omega_{30}(t) + 0.001\sin(200\pi t)$ as the measured frequency. One can observe the high-frequency fluctuation in the control input trajectory around 9.4s for $\Gamma_{30} = +\infty$, whereas this does not happen for $\Gamma_{30} = 2$ due to its Lipschitz continuity character. These simulations validate the observations of Remark 4.3.4.

Next, we simulate the case where some of the generator frequencies are initially outside the safe region to show how the transient controller brings the frequencies back to it. We use the same setup as in Figure 4.3, but we only turn on the distributed controller after $t = 12s$. Figure 4.7(a) shows the frequency trajectories of generators 30, 31, and 32. As the controller is disabled for the first 12s, all 3 frequency trajectories are lower than 59.8hz at $t = 12$s. After $t = 12$s, all of them return to the safe region in a monotonic way, and once they are in the region, they never leave, in accordance with Theorem 4.3.3*(vi)*. Figure 4.7(b) shows the corresponding

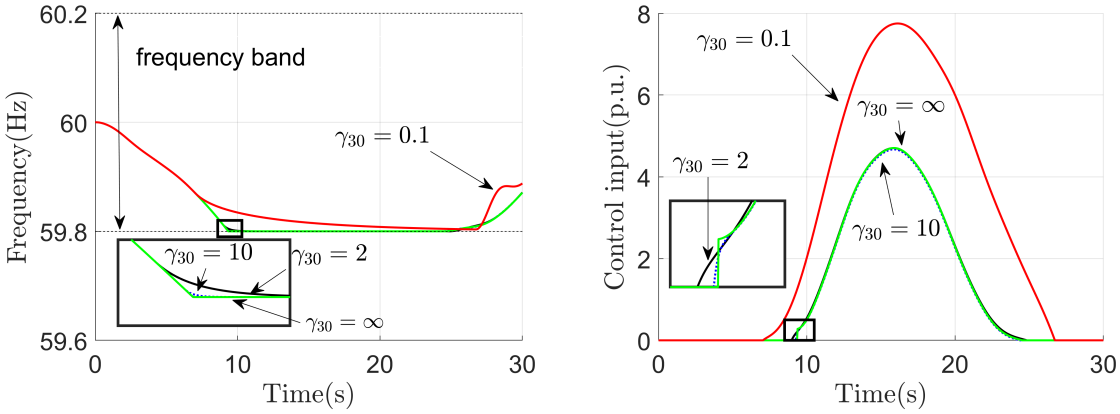

(a) (b)

Figure 4.5: Frequency and control input trajectories at node 30 with linear class-$\mathscr{K}$ function with slope $\Gamma_{30} = 0.1, 2, 10$ and $+\infty$, respectively. We observe from plot (a) that the frequency trajectory with small Γ_{30} tends to stay away from the safe frequency bound, at the cost of having a large control input, as shown in plot (b). A large Γ_{30} causes the controller to be sensitive to ω_{30}, making the input change rapidly around 9s.

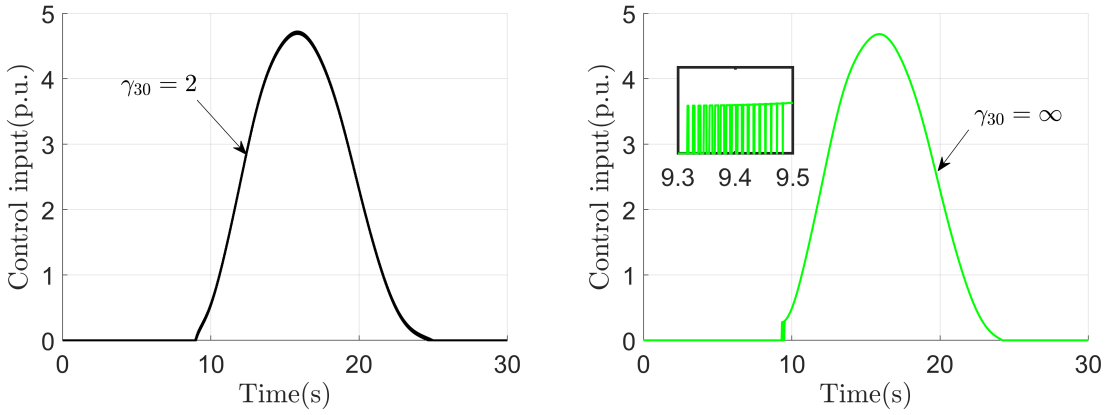

(a) (b)

Figure 4.6: Control input trajectories at node 30 with linear class-$\mathscr{K}$ function with slope $\Gamma_{30} = 2$ and $+\infty$, respectively, under state measurement errors in ω_{30}. The controller with $\gamma_{30} = 2$ is Lipschitz continuous (cf. plot (a)), whereas the controller with $\gamma_{30} = +\infty$ (cf. plot (b)) is discontinuous.

control input trajectories.

Finally, we illustrate the bounds on control amplitude of Section 4.4.2. Let $r = 0.5$ and $i = 30$. By Lemma 4.4.4, the control input is lower bounded by $u_i^{\min}(\gamma)$, which requires

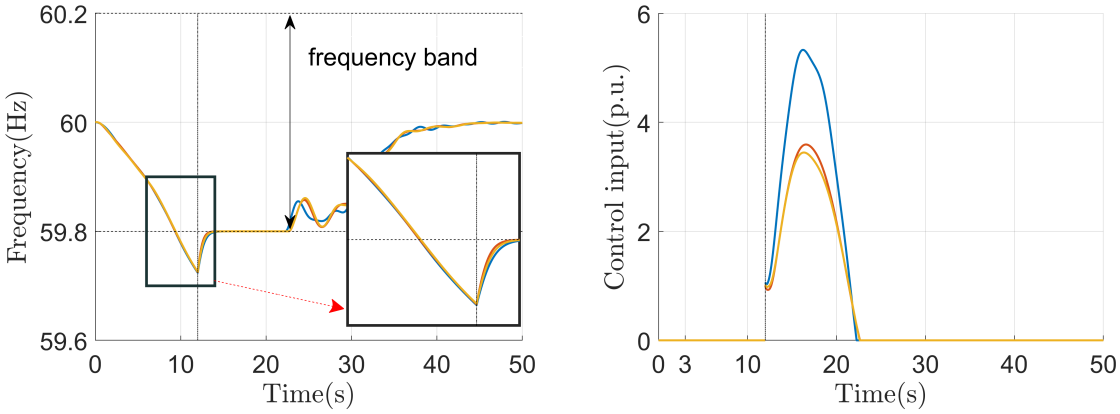

Figure 4.7: Frequency and control input trajectories with transient controller available after $t = 12$s. Plot (a) shows the frequency trajectories of generators 30, 31, and 32. Due to the disturbance, and without the transient controller, all 3 frequency trajectories exceed the 59.8Hz safe bound at $t = 12$s. As the transient controller kicks in, the unsafe trajectories come back to the safe region and never leave afterwards. Plot (b) shows the control input trajectories.

$g_i(\lambda^*, \omega^*)$. The numerical computation of the upper $g_i(\lambda^o, \omega^o)$ (cf. Lemma 4.4.5) and lower $h_i(\underline{z}^{\mu^*}, \underline{\omega}^{\mu^*})$ (cf. Lemma 4.4.6) bounds both yield -5.8686. Figure. 4.8(a) shows 100 input trajectories with initial states randomly selected around (λ^o, ω^o), all lower bounded by -5.8686.

Acknowledgements

Chapter 4, in part, is a reprint of the material [ZC19c] as it appears in 'Distributed transient frequency control for power networks with stability and performance guarantees' by Y. Zhang and J. Cortés, in Automatica, 2019, as well as [ZC18a] where it appears as 'Distributed transient frequency control in power networks' by Y. Zhang and J. Cortés in the proceedings of the 2018 IEEE Conference on Decision and Control. The dissertation author was the primary investigator and author of these papers. This research was supported by NSF award CNS-1446891 and AFOSR Award FA9550-15-1-0108.

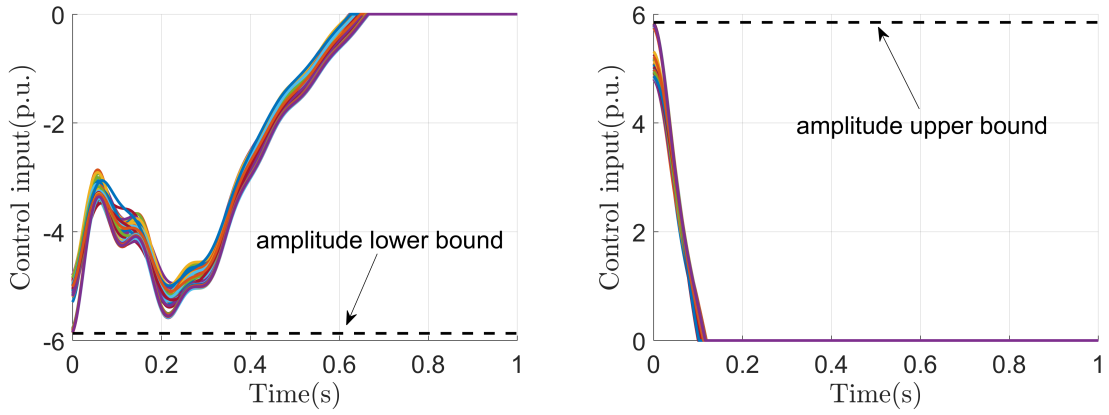

Figure 4.8: Control input trajectories at node 30 corresponding to 100 different initial states. In plot (a), with all initial states randomly selected around the worst-case scenario, all 100 trajectories are lower bounded by -5.8686 (denoted by the dashed line), as guaranteed by Lemma 4.4.4. A similar result is illustrated in plot (b), where another 100 trajectories with random initial states are upper bounded by 5.8494.

Chapter 5

Model predictive control for transient frequency regulation

As the controller designed in Chapter 4 only takes frequency safety and network stability into account, this chapter further introduces a control strategy that enables control cooperation on multiple nodes to reduce their overall control efforts. The control command is generated by iteratively solving an open-loop control cost minimization problem with stability and transient frequency constraints. To deal with the non-convexity of the stability constraint, we propose a convexification strategy that uses a reference trajectory based on the system's current state. We also detail how to employ network partitions to implement the proposed control strategy in a distributed way, where each region only requires system information from neighboring regions to execute its controller.

5.1 Problem statement

We consider the same power network dynamics (2.8) used in Chapter 4. Besides the three basic requirements on *stability and convergence*, *frequency invariance*, and *attractivity*

mentioned in Section 4.1, we aim to design state-feedback controllers u_i for each bus $i \in \mathscr{I}^u$ that also satisfies the following requirement,

Coordination requirement: Each controller u_i, $i \in \mathscr{I}^u$, should cooperate with others to lower the overall control effort, as measured by some given cost function. Moreover, here we allow $\mathscr{I}^\omega$ to be a subset of $\mathscr{I}^u$, that is to say, a node with an available control command can also participate in transient frequency regulation on other nodes, even if the node itself has no such a requirement.

Our design strategy is to first set up an open-loop optimization problem with control cost as objective function, and with frequency and stability requirements as constraints. Then, we design a centralized controller by solving this optimization problem in a receding horizon fashion. Finally, the distributed controller comes from partitioning the network into several regions, and treating each region as an independent network.

5.2 Open-loop optimal control

We start by formulating an optimization problem whose goal is to minimize a cost function measuring control input effort subject to the system dynamics, safe frequency invariance, and asymptotic stability constraints. As this problem turns out to be non-convex and non-smooth, we propose a convexification strategy by generating a set of linear constraints. Later, we build on this to design centralized and distributed controllers.

5.2.1 Open-loop finite-horizon optimal control

We introduce a robust asymptotic stability condition with respect to the open-loop equilibrium point and estimate the region of attraction.

Lemma 5.2.1. *(Robust asymptotic stability condition): For system* (2.8)*, suppose that the solution exists and is unique. For every $i \in \mathscr{I}^u$, let $\bar{\omega}_i^{thr} > 0$ and $\underline{\omega}_i^{thr} < 0$ be threshold values*

satisfying $\underline{\omega}_i^{thr} < \omega^\infty < \bar{\omega}_i^{thr}$. *If for every* $t \in \mathbb{R}_{\geqslant}$,

$$\omega_i(t)u_i(x(t),p) \leqslant 0, \text{ if } \omega_i(t) \notin (\underline{\omega}_i^{thr}, \bar{\omega}_i^{thr}), \tag{5.1a}$$

$$u_i(x(t),p) = 0, \text{ if } \omega_i(t) \in (\underline{\omega}_i^{thr}, \bar{\omega}_i^{thr}), \tag{5.1b}$$

then under condition (2.9), $(\lambda^\infty, \omega^\infty \mathbf{1}_n)$ *is locally asymptotically stable. Furthermore, with* V, $\bar{r}$, *and* $\mathscr{T}$ *defined in* (4.1), (4.2),*and* (4.3), *for every* $(\lambda(0),\omega(0)) \in \mathscr{T}(r)$ *with* $0 < r < \bar{r}$, *it holds that* $(\lambda(t),\omega(t)) \in \mathscr{T}(r)$ *for every* $t \geqslant 0$ *and* $(\lambda(t),\omega(t)) \to (\lambda^\infty, \omega^\infty \mathbf{1}_n)$.

Proof. Note that (5.1) implies (4.4), and the proof follows by Lemma 4.2.1. □

Notice that the dependence of the robust asymptotic stability condition (5.1) on the equilibrium point $(\lambda^\infty, \omega^\infty \mathbf{1}_n)$ is limited to an approximate knowledge of ω^∞. This reflects a practical consideration under which the controller should still ensure asymptotic stability: although ideally ω^∞ is 0 when load and supply are balanced (i.e., $\sum_{i=1}^n p_i^* = 0$), due to imperfect estimation on the load side and transmission losses, ω^∞ tends to slightly deviate from 0.

We here formally introduce the finite-horizon optimal control problem. For every $t \in \mathbb{R}_{\geqslant}$, we consider a piece-wise continuous signal $p_t^{fcst} : [t, t+\tilde{t}] \to \mathbb{R}^n$ forecasting its value for the first $\tilde{t}$ seconds starting from t. When convenient, we invoke the following assumption in our technical analysis.

Assumption 5.2.2. *(Forecast reveals true value at current time): For any* $t \in \mathbb{R}_{\geqslant}$, $p_t^{fcst}(t) = p$.

The open-loop finite-horizon optimal control problem is defined by

$$(Q_{cont}) \qquad \min_{\lambda,\omega,u,\beta,\gamma} \quad \sum_{i\in\mathscr{J}^u} \int_{\tau_0}^{\tau_0+\tilde{t}} c_i u_i^2(\tau) + d_i \beta_i^2(\tau) \mathrm{d}\tau + \sum_{i\in\mathscr{J}^\omega} \int_{\tau_0}^{\tau_0+\tilde{t}} e_i \gamma_i^2(\tau) \mathrm{d}\tau$$

$$\text{s.t.} \qquad \dot{\lambda}(\tau) = D\omega(\tau), \tag{5.2a}$$

$$M\dot{\omega}(\tau) = -E\omega(\tau) - D^T Y_b \lambda(\tau) + p_t^{fcst}(\tau) + u(\tau), \tag{5.2b}$$

$$\lambda(\tau_0) = \sin\lambda_0,\ \omega(\tau_0) = \omega_0, \tag{5.2c}$$

$$u(\tau) \in \mathbb{U}, \quad \forall \tau \in [\tau_0, \tau_0 + \tilde{t}], \tag{5.2d}$$

$$u_i^{\min} - \xi_i \beta_i(\tau) \leqslant u_i(\tau) \leqslant u_i^{\max} + \xi_i \beta_i(\tau), \quad \forall i \in \mathscr{I}^u,\ \forall \tau \in [\tau_0, \tau_0 + \tilde{t}], \tag{5.2e}$$

$$\beta_i(\tau) \geqslant 0, \forall i \in \mathscr{I}^u,\ \forall \tau \in [\tau_0, \tau_0 + \tilde{t}], \tag{5.2f}$$

$$\begin{aligned} &\underline{\omega}_i - \lambda_i(\omega_0, \xi_i)(\gamma_i(\tau) - \delta) \leqslant \omega_i(\tau) \\ &\qquad \leqslant \bar{\omega}_i + \lambda_i(\omega_0, \xi_i)(\gamma_i(\tau) - \delta), \quad \forall i \in \mathscr{I}^\omega,\ \forall \tau \in [\tau_0, \tau_0 + \tilde{t}], \end{aligned} \tag{5.2g}$$

$$\gamma_i(\tau) \geqslant 0, \quad \forall i \in \mathscr{I}^\omega,\ \forall \tau \in [\tau_0, \tau_0 + \tilde{t}], \tag{5.2h}$$

$$(\omega, u) \in \Phi_{cont}, \tag{5.2i}$$

where constraints (5.2a)-(5.2c) represent system dynamics and initial state. Notice that we linearize the dynamics in (5.2b), which contributes to the convexification of the open-loop optimization with a slight loss of optimality (in Section 5.3, we show that employing this linearization for controller design does not jeopardize the asymptotic stability or safe frequency invariance requirements in the closed-loop system); constraint (5.2d) reflects the available control signal indexes; constraints (5.2e) and (5.2f) delimit the control magnitude bounds, in which $\xi \in \{0, 1\}$ indicates the magnitude constraint type, i.e., if $\xi_i = 1$ for $i \in \mathscr{I}^u$, then the constraint is soft as $u_i(\tau)$ could exceed $u_i^{\max} \in \mathbb{R}$ or $u_i^{\min} \in \mathbb{R}$, but penalized by $\beta_i(\tau)$ in the objective function, and if $\xi_i = 0$ then it is a hard constraint; constraints (5.2g) and (5.2h) refer to the safe frequency invariance requirement, in which

$$\lambda_i(\omega_0, \xi_i) = \begin{cases} 0 & \text{if } \omega_{i,0} \in [\underline{\omega}_i, \bar{\omega}_i] \text{ and } \xi_i = 1, \\ 1 & \text{otherwise.} \end{cases} \tag{5.3}$$

Intuitively, these two constraints require that ω_i stays in $[\underline{\omega}_i, \bar{\omega}_i]$ provided that it is initially inside and the magnitude constraint on the controller is soft, and penalize through γ_i if not. The

parameterδ_i with $0 < \delta_i < \bar{\omega}_i - \underline{\omega}_i$ is tunable, forcing $\omega_i(\tau)$ approach the interval $[\underline{\omega}_i + \delta_i, \bar{\omega}_i - \delta]$, and hence enter $[\underline{\omega}_i, \bar{\omega}_i]$ in finite time; constraint (5.2i) is the asymptotic stability condition established in Lemma 5.2.1, where

$$\Phi_{cont} \triangleq \left\{ (\omega, u) \;\middle|\; (5.1) \text{ holds } \forall t \in [\tau_0.\tau_0 + \tilde{t}],\ \forall i \in \mathscr{I}^u \right\}.$$

Finally, $c_i, d_i \in \mathbb{R}_>$ and $e_i \in \mathbb{R}_\geqslant$ refer to the weight coefficient on control effort, control magnitude penalty, and frequency invariance penalty, resp.

We refer to (5.2) as $Q_{cont}(\mathscr{G}, \mathscr{I}^u, \mathscr{I}^\omega, p_t^{fcst}, \lambda_0, \omega_0, \tau_0)$ to emphasize its dependence on the graph topology, controlled node indexes, transient-frequency-constrained node indexes, forecasted power injection, initial state, and initial time. If the context is clear, we use Q_{cont}. We use the same notational logic for other optimization problems in the rest of the chapter.

In practice, a convenient way to approximate the functional solution for Q_{cont} is by discretization. Specially, here we discretize the system periodically with time length $T \in \mathbb{R}_>$, and denote $N \triangleq \lceil \tilde{t}/T \rceil$ as the total number of steps. For every $k \in [0, N]_\mathbb{N}$, denote $\hat{\lambda}(k), \hat{\omega}(k)$, $\hat{u}(k)$, $\hat{p}^{fcst}(k)$ as the approximation of $\lambda(\tau_0 + kT), \omega(\tau_0 + kT)$, $u(\tau_0 + kT)$ and $p_t^{fcst}(\tau_0 + kT)$, resp., and let

$$\hat{\Lambda} \triangleq [\hat{\lambda}(0), \hat{\lambda}(1), \cdots, \lambda(N)], \tag{5.4a}$$

$$\hat{\Omega} \triangleq [\hat{\omega}(0), \hat{\omega}(1), \cdots, \hat{\omega}(N)], \tag{5.4b}$$

$$\hat{P}^{fcst} \triangleq [\hat{p}^{fcst}(0), \hat{p}^{fcst}(1), \cdots, \hat{p}^{fcst}(N-1)], \tag{5.4c}$$

$$\hat{U} \triangleq [\hat{u}(0), \hat{u}(1), \cdots, \hat{u}(N-1)], \tag{5.4d}$$

$$\hat{B} \triangleq [\hat{\beta}(0), \hat{\beta}(1), \cdots, \hat{\beta}(N-1)], \tag{5.4e}$$

$$\hat{\Gamma} \triangleq [\hat{\gamma}(0), \hat{\gamma}(1), \cdots, \hat{\gamma}(N)], \tag{5.4f}$$

be the collection of voltage angle difference, frequency, predicted power injection, and control

input discrete trajectories, resp. We formulate the discrete version of Q_{cont} in (5.6), where

$$\Phi_{disc} \triangleq \Big\{ (\hat{\Omega}, \hat{U}) \;\Big|\; \forall i \in \mathscr{I}^u,\ \forall k \in [0, N-1]_{\mathbb{N}},\ \text{it holds that}$$
$$\hat{\omega}_i(k)\hat{u}_i(k) \leqslant 0,\ \text{if } \hat{\omega}_i(k) \notin (\underline{\omega}_i^{\text{thr}}, \bar{\omega}_i^{\text{thr}})\hat{u}_i(k) = 0,\ \text{if } \hat{\omega}_i(k) \in (\underline{\omega}_i^{\text{thr}}, \bar{\omega}_i^{\text{thr}}) \Big\}. \tag{5.5}$$

Note that this set is nonlinear and non-smooth.

$$(Q_{disc}) \qquad \min_{\hat{\Lambda}, \hat{\Omega}, \hat{U}, \hat{B}, \hat{\Gamma}} \quad g(\hat{U}, \hat{B}, \hat{\Gamma}) \triangleq \sum_{i \in \mathscr{I}^u} \sum_{k=0}^{N-1} \big(c_i \hat{u}_i^2(k) + d_i \beta_i^2(k) \big) + \sum_{i \in \mathscr{I}^\omega} \sum_{k=1}^{N} e_i \gamma_i(k)$$

$$\text{s.t.} \quad \hat{\lambda}(k+1) = \hat{\lambda}(k) + TD\hat{\omega}(k),$$
$$M\hat{\omega}(k+1) = M\hat{\omega}(k) - T\big\{ E\hat{\omega}(k) + D^T Y_b \hat{\lambda}(k) - \hat{p}^{fcst}(k) - \hat{u}(k) \big\}, \quad \forall k \in [0, N-1]_{\mathbb{N}}, \tag{5.6a}$$

$$\hat{\lambda}(0) = \sin \lambda_0,\ \hat{\omega}(0) = \omega_0, \tag{5.6b}$$

$$\hat{u}(k) \in \mathbb{U}, \qquad \forall k \in [0, N-1]_{\mathbb{N}}, \tag{5.6c}$$

$$u_i^{\min} - \xi_i \beta_i(k) \leqslant \hat{u}_i(k) \leqslant u_i^{\max} + \xi_i \beta_i(k), \qquad \forall i \in \mathscr{I}^u,\ \forall k \in [0, N-1]_{\mathbb{N}}, \tag{5.6d}$$

$$\beta_i(k) \geqslant 0, \qquad \forall i \in \mathscr{I}^u, \forall k \in [0, N-1]_{\mathbb{N}}, \tag{5.6e}$$

$$\underline{\omega}_i - \lambda_i(\omega_0, \xi_i)(\gamma_i(k) - \delta) \leqslant \hat{\omega}_i(k) \leqslant \bar{\omega}_i + \lambda_i(\omega_0, \xi_i)(\gamma_i(k) - \delta), \quad \forall i \in \mathscr{I}^\omega,\ \forall k \in [1, N]_{\mathbb{N}}, \tag{5.6f}$$

$$\gamma_i(k) \geqslant 0, \qquad \forall i \in \mathscr{I}^\omega, \forall k \in [1, N]_{\mathbb{N}}, \tag{5.6g}$$

$$(\hat{\Omega}, \hat{U}) \in \Phi_{disc}, \tag{5.6h}$$

5.2.2 Constraint convexification

The major obstacle to solve Q_{disc} is dealing with the set Φ_{disc} in constraint (5.6h). To this end, we propose a convexification method that seeks to identify a subset of Φ_{disc} consisting of only linear constraints. This method relies on the notion of *reference trajectory*, which is a trajectory $(\hat{\Lambda}, \hat{\Omega}, \hat{U})$ of the system state and input for which there exist $\hat{B}$ and $\hat{\Gamma}$ such that (5.6)

are satisfied. The next result details this.

Lemma 5.2.3. *(Convexification of non-convex constraints): For any reference trajectory* $(\hat{F}^{ref}, \hat{\Omega}^{ref}, \hat{U}^{ref})$*, let*

$$\begin{aligned}\Phi_{cvx} \triangleq \Big\{ (\hat{\Omega}, \hat{U}) \;\Big|\; \forall i \in \mathscr{I}^u,\ \forall k \in [0, N-1]_{\mathbb{N}},\ \textit{it holds that} \\ \hat{\omega}_i(k) \geqslant \bar{\omega}_i^{thr},\ \hat{u}_i(k) \leqslant 0,\ \textit{if}\ \hat{\omega}_i^{ref}(k) \geqslant \bar{\omega}_i^{thr}; \\ \hat{\omega}_i(k) \leqslant \underline{\omega}_i^{thr},\ \hat{u}_i(k) \geqslant 0,\ \textit{if}\ \hat{\omega}_i^{ref}(k) \leqslant \underline{\omega}_i^{thr}; \\ \hat{u}_i(k) = 0,\ \textit{if}\ \underline{\omega}_i^{thr} < \hat{\omega}_i^{ref}(k) < \bar{\omega}_i^{thr} \Big\}. \end{aligned} \tag{5.7}$$

Then, $\emptyset \neq \Phi_{cvx} \subseteq \Phi_{disc}$ *is convex.*

Proof. The non-emptiness holds by simply noticing that $(\hat{\Omega}^{\text{ref}}, \hat{U}^{\text{ref}}) \in \Phi_{cvx}$. We show the inclusion by classifying each $k \in [0, N-1]_{\mathbb{N}}$ into three types regarding the value of $\hat{\omega}_i^{\text{ref}}(k)$. If $\hat{\omega}_i^{\text{ref}}(k) \geqslant \bar{\omega}_i^{\text{thr}}$, then at step k, only the first constraint in Φ_{cvx} is active, which satisfies the first constraint in Φ_{disc}, as well as the second one trivially, since in this case $\hat{\omega}_i(k) \notin (\underline{\omega}_i^{\text{thr}}, \bar{\omega}_i^{\text{thr}})$. Similar analysis holds if $\hat{\omega}_i^{\text{ref}}(k) \leqslant \underline{\omega}_i^{\text{thr}}$. Finally, if $\underline{\omega}_i^{\text{thr}} < \hat{\omega}_i^{\text{ref}}(k) < \bar{\omega}_i^{\text{thr}}$, then only the last constraint in Φ_{cvx} is active, which satisfies both two constraints in Φ_{disc}. Finally, the convexity of Φ_{cvx} follows by noting that it corresponds to the intersection of finitely many linear constraints over all $i \in \mathscr{I}^u$ and $k \in [0, N-1]_{\mathbb{N}}$. To see this, notice that for each i and k, as the value of $\hat{\omega}_i^{\text{ref}}(k)$ is given a priori by the reference trajectory, one and only one of the three constraints in Φ_{cvx} is active, leading to linearity. □

In light of Lemma 5.2.3, given a reference trajectory, we solve a convexified version of Q_{disc}, replacing Φ_{disc} by Φ_{cvx},

$$\begin{aligned}(Q_{cvx}) \qquad \min_{\hat{F}, \hat{\Omega}, \hat{U}} \quad & g(\hat{U}, \hat{B}, \hat{\Gamma}) \\ \text{s.t.} \quad & \text{(5.6a)} - \text{(5.6g) hold}, \end{aligned} \tag{5.8a}$$

$$(\hat{\Omega}, \hat{U}) \in \Phi_{cvx}. \tag{5.8b}$$

Since the convexification reduces the set Φ_{disc} to Φ_{cvx}, the optimal value of Q_{disc} is less than or equal to that of Q_{cvx}. For consistency, if the reference trajectory is the optimal solution of Q_{disc}, then both problems have the same optimal value.

5.2.3 Generation of reference trajectory

Here we introduce a method to generate the reference trajectory required by the convexification process of Φ_{disc} based on our previous work [ZC19c].

Proposition 5.2.4. *(Generation of reference trajectory): For every $i \in \mathscr{I}^u$ and every $k \in [0, N-1]_{\mathbb{N}}$, suppose $\underline{\omega}_i < \underline{\omega}_i^{thr} < \omega^{\infty} < \bar{\omega}_i^{thr} < \bar{\omega}_i$, and $\bar{\gamma}_i,\ \underline{\gamma}_i \in \mathbb{R}_{>}$. For every $k \in [0, N-1]_{\mathbb{N}}$, define,*

$$\hat{u}_i^a(k) \triangleq \begin{cases} \min\{0, \frac{\bar{\gamma}_i(\bar{\omega}_i - \hat{\omega}_i^{ref}(k))}{\hat{\omega}_i^{ref}(k) - \bar{\omega}_i^{thr}} - v_i(k)\} & \text{if } \hat{\omega}_i^{ref}(k) \geqslant \bar{\omega}_i^{thr}, \\ 0 & \text{if } \underline{\omega}_i^{thr} < \hat{\omega}_i^{ref}(k) < \bar{\omega}_i^{thr}, \quad \forall i \in \mathscr{I}^{\omega}, \\ \max\{0, \frac{\underline{\gamma}_i(\underline{\omega}_i - \hat{\omega}_i^{ref}(k))}{\underline{\omega}_i^{thr} - \hat{\omega}_i^{ref}(k)} - v_i(k)\} & \text{if } \hat{\omega}_i^{ref}(k) \leqslant \underline{\omega}_i^{thr}, \end{cases} \tag{5.9}$$

$$\hat{u}_i^{ref}(k) \triangleq \mathrm{sat}(\hat{u}_i^a(k); \xi_i, u_i^{\min}, u_i^{\max}), \qquad \forall i \in \mathscr{I}^{\omega},$$

$$\hat{u}_i^{ref}(k) \triangleq 0, \qquad \forall i \in \mathscr{I} \backslash \mathscr{I}^{\omega},$$

$$v_i(k) \triangleq \sum_{j:j\to i} b_{ji} \hat{\lambda}_{ji}^{ref}(k) - \sum_{l:i\to l} b_{il} \hat{\lambda}_{il}^{ref}(k) + \hat{p}_i^{fcst}(k) - E_i \hat{\omega}_i^{ref}(k), \qquad \forall i \in \mathscr{I}^{\omega}, .$$

Furthermore, set $\hat{U}^{ref} \triangleq [\hat{u}^{ref}(0), \hat{u}^{ref}(1), \cdots, \hat{u}^{ref}(N-1)]$ and let $(\hat{\Lambda}^{ref}, \hat{\Omega}^{ref})$ be the sate trajectory uniquely determined by (5.6a) *and* (5.6b) *using $\hat{u}^{ref}$ as input. Then there exists $\bar{T} \in \mathbb{R}_{>}$ such that for any $0 < T \leqslant \bar{T}$, $(\hat{\Lambda}^{ref}, \hat{\Omega}^{ref}, \hat{U}^{ref})$ is a reference trajectory.*

Proof. From the definition of $(\hat{\Lambda}^{\mathrm{ref}}, \hat{\Omega}^{\mathrm{ref}}, \hat{U}^{\mathrm{ref}})$ one can easily see that it naturally satisfies constraints (5.6a)-(5.6c) and (5.6h). We next show that the other constraints hold with each possible $\xi \in \{0,1\}^{|\mathscr{I}^u|}$ by pointing out a specific $\hat{B}$ and $\hat{\Gamma}$ associated with $(\hat{\Lambda}^{\mathrm{ref}}, \hat{\Omega}^{\mathrm{ref}}, \hat{U}^{\mathrm{ref}})$. For any

$i \in \mathscr{I}^u$, if $\xi_i = 0$, one can easily check that (5.6d)-(5.6e) holds by the definition of $\hat{u}_i^{\text{ref}}$ with a trivial choice of $\beta_i(k) \equiv 0$. Notice that since we assume that λ_i is always 1 if $\xi_i = 0$, there always exists $\gamma_i(k)$ sufficiently large such that (5.6f)-(5.6g) hold.

If $\xi_i = 1$ for some $i \in \mathscr{I}^u$ instead, then one can have $\beta_i(k)$ sufficiently large to meet (5.6d)-(5.6e). Further if $\omega_{i,0} \notin [\underline{\omega}_i, \bar{\omega}_i]$, resulting in $\lambda_i(\omega_0, \xi_i) = 1$, then one can still choose $\gamma_i(k)$ sufficiently large so that (5.6f)-(5.6g) hold. Finally, if $\omega_{i,0} \in [\underline{\omega}_i, \bar{\omega}_i]$, then we show that (5.6f)-(5.6g) also hold with a trivial choice of $\gamma_i(k) = 0$ for every $k \in [1, N]_{\mathbb{N}}$. We first claim that there exists $c \in \mathbb{R}_>$ such that, for every $k \in [0, N-1]_{\mathbb{N}}$ and $i \in \mathscr{I}$,

$$|\hat{\omega}_i^{\text{ref}}(k+1) - \hat{\omega}_i^{\text{ref}}(k)| \leqslant cT. \tag{5.10}$$

Note that $\hat{x}^{\text{ref}}(k) \triangleq (\hat{\lambda}^{\text{ref}}(k), \hat{\omega}^{\text{ref}}(k)) \in \mathbb{R}^{m+n}$, obtained by substituting $\hat{u}^{\text{ref}}$ into (5.6a)-(5.6b), satisfies $\hat{x}^{\text{ref}}(k+1) = \hat{x}^{\text{ref}}(k) + Th(\hat{x}^{\text{ref}}(k), \hat{p}^{fcst}(k))$, which correspond to the Euler approximation of the continuous-time dynamics $\dot{x}^{\text{ref}}(t) = h(x^{\text{ref}}(t), p_t^{fcst}(t))$. Here, for simplicity, we omit the explicit expression of h, but one can see [ZC19c] that it is Lipschitz in its first component, and hence the solution of the continuous-time dynamics exists and is unique for any $t \geqslant 0$, and $\|x^{\text{ref}}(t)\| \leqslant r_1$ for sufficiently large $r_1 \in \mathbb{R}_>$. By [But08, Theorem 212A], there exists $c_1 \in \mathbb{R}_>$ such that

$$\|x^{\text{ref}}(\tau_0 + kT) - \hat{x}^{\text{ref}}(k)\| \leqslant c_1 T, \ \forall k \in [0, N-1]_{\mathbb{N}.}$$

Further, the Lipschitz property of h and the uniform boundedness of $x^{\text{ref}}(t)$ imply that there exists $r_2 \in \mathbb{R}_>$ such that $\|\dot{x}^{\text{ref}}(t)\| \leqslant r_2$ for any $t \geqslant \tau_0$. Therefore, it holds for all $k \in [0, N-1]_{\mathbb{N}}$ and all $i \in \mathscr{I}$ that

$$\begin{aligned} |\hat{\omega}_i^{\text{ref}}(k+1) - \hat{\omega}_i^{\text{ref}}(k)| &\leqslant \|\hat{x}^{\text{ref}}(k+1) - \hat{x}^{\text{ref}}(k)\| \\ &\leqslant \|\hat{x}^{\text{ref}}(k+1) - x^{\text{ref}}(\tau_0 + (k+1)T)\| + \|\hat{x}^{\text{ref}}(k) - x^{\text{ref}}(\tau_0 + kT)\| \end{aligned}$$

$$
\begin{aligned}
&\quad + \|x^{\mathrm{ref}}(\tau_0+(k+1)T) - x^{\mathrm{ref}}(\tau_0+kT)\| \\
&\leqslant 2c_1T + \|\int_{kT}^{(k+1)T} \dot{x}^{\mathrm{ref}}(\tau)\mathrm{d}\tau\| \\
&\leqslant 2c_1T + \sqrt{m+n}\int_{kT}^{(k+1)T} \|\dot{x}^{\mathrm{ref}}(\tau)\|\mathrm{d}\tau = (2c_1 + r_2\sqrt{m+n})T.
\end{aligned}
$$

Hence, (5.10) follows by letting $c \triangleq 2c_1 + r_2\sqrt{m+n}$.

Next, we prove (5.6f) holds by induction, i.e., for any $i \in \mathscr{I}^{\omega}$, if $\hat{\omega}_i^{\mathrm{ref}}(k) \in [\underline{\omega}_i, \bar{\omega}_i]$ for some $k \in [0, N-2]_{\mathbb{N}}$, then it also holds by replacing k by $k+1$. Note that by (5.10), if $\hat{\omega}_i^{\mathrm{ref}}(k) \in [\underline{\omega}_i + cT, \bar{\omega}_i - cT]$, then $\hat{\omega}_i^{\mathrm{ref}}(k+1) \in [\underline{\omega}_i, \bar{\omega}_i]$. Therefore, we only need to consider the case when $\hat{\omega}_i^{\mathrm{ref}}(k) \in (\bar{\omega}_i - cT, \bar{\omega}_i]$ and $\hat{\omega}_i^{\mathrm{ref}}(k) \in (\underline{\omega}_i, \underline{\omega}_i + cT]$. For simplicity, we only prove the first case (the other holds similarly). Without loss of generality, we choose T small enough so that $cT < \bar{\omega}_i - \bar{\omega}_i^{\mathrm{thr}}$ for every $i \in \mathscr{I}^{\omega}$, ensuring $\hat{\omega}_i^{\mathrm{ref}}(k) > \bar{\omega}_i^{\mathrm{thr}}$. From the system dynamics, one has $M_i\hat{\omega}_i^{\mathrm{ref}}(k+1) = M_i\hat{\omega}_i^{\mathrm{ref}}(k) + T\left(v_i(k) + \hat{u}_i^{\mathrm{ref}}(k)\right)$. Substituting (5.9), one has

$$
M_i\hat{\omega}_i^{\mathrm{ref}}(k+1) \leqslant M_i\hat{\omega}_i^{\mathrm{ref}}(k) + T\frac{\bar{\gamma}_i(\bar{\omega}_i - \hat{\omega}_i^{\mathrm{ref}}(k))}{\hat{\omega}_i^{\mathrm{ref}}(k) - \bar{\omega}_i^{\mathrm{thr}}} \leqslant M_i\hat{\omega}_i^{\mathrm{ref}}(k) + T\frac{\bar{\gamma}_i(\bar{\omega}_i - \hat{\omega}_i^{\mathrm{ref}}(k))}{\bar{\omega}_i - cT - \bar{\omega}_i^{\mathrm{thr}}}.
$$

By substituting $b(j) \triangleq \hat{\omega}_i^{\mathrm{ref}}(j) - \bar{\omega}_i$ for $j = k$ and $k+1$ into the above inequality, it holds

$$
M_i b(k+1) \leqslant \left(M_i - \frac{T\bar{\gamma}_i}{\bar{\omega}_i - cT - \bar{\omega}_i^{\mathrm{thr}}}\right) b(k).
$$

Since $b(k) \leqslant 0$, let $\bar{T}$ be such that $M_i - \frac{\bar{T}\bar{\gamma}_i}{\bar{\omega}_i - c\bar{T} - \bar{\omega}_i^{\mathrm{thr}}} > 0$. Then, $b(j+1) \leqslant 0$ for $0 < T \leqslant \bar{T}$, i.e., if $\hat{\omega}_i^{\mathrm{ref}}(k) \leqslant \bar{\omega}_i$, then $\hat{\omega}_i^{\mathrm{ref}}(k+1) \leqslant \bar{\omega}_i$, and the induction holds. □

Notice that a small sampling length T reduces the discretization gap between Q_{cont} and Q_{disc}, as well as guarantees the qualification of $(\hat{F}^{\mathrm{ref}}, \hat{\Omega}^{\mathrm{ref}}, \hat{U}^{\mathrm{ref}})$ in Proposition 5.2.4 as a reference trajectory. On the other hand, the number of constraints appearing in Q_{cvx} grows linearly with respect to $1/T$. Hence, there is a trade-off among discretization accuracy, reference trajectory qualification, and computational complexity.

5.3 From centralized to distributed closed-loop receding horizon feedback

In this section we design a feedback controller in a receding horizon fashion by having the input at a given state $(\lambda(t), \omega(t))$ at time t with a forecasted power injection p_t^{fcst} be the first step of the optimal control input trajectory of $Q_{cvx}(\mathscr{G}, \mathscr{I}^u, \mathscr{I}^\omega, \hat{P}^{fcst}, \lambda(t), \omega(t), t)$. We first consider a centralized implementation, where a single operator gathers global state information, computes the control law, and broadcasts it. Building on it, we propose a distributed strategy, where several independent operators are responsible for computing control signals within its own region using only regional information.

5.3.1 Centralized control with stability and frequency invariance

Formally, at time t, the centralized controller measures the current output $(f(t), \omega(t))$ and forecasts a power injection profile $p_t^{fcst}(\tau)$ with $\tau \in [t, t+\tilde{t}]$ as well as its corresponding discretization $\hat{P}^{fcst}$, cf. (5.4c). Let $(\hat{\Lambda}^*_{cvx}, \hat{\Omega}^*_{cvx}, \hat{U}^*_{cvx})$ be the optimal solution of $Q_{cvx}(\mathscr{G}, \mathscr{I}^u, \mathscr{I}^\omega, \hat{P}^{fcst}, f(t), \omega(t), t)$. The centralized control law is then given by

$$u(x(t), p_t^{fcst}) \triangleq \hat{u}^*_{cvx}(0), \tag{5.11}$$

where $u^*_{cvx}(0)$ is the first column of $\hat{U}^*_{cvx}$. The next result states that the controller is able to stabilize the system without changing its open-loop equilibrium point, and, at the same time, guarantees safe frequency region invariance and attractivity.

Theorem 5.3.1. *(Centralized control with stability and frequency constraints): Under Assumption 5.2.2 and for any initial state* $(\lambda(0), \omega(0))$*, the closed-loop system* (2.8) *with controller* (5.11) *and sufficiently small sampling length T satisfies:*

(i) For any $i \in \mathscr{I}^u$ *with any* $\xi_i \in \{0,1\}$ *and any* $t \in \mathbb{R}_{\geqslant}$, $u_i(x(t), p_t^{fcst}) = 0$ *if* $\omega_i(t) \in (\underline{\omega}_i^{thr}, \bar{\omega}_i^{thr})$*;*

(ii) For any $i \in \mathscr{I}^{\omega}$ with $\xi_i = 1$, if $\omega_i(0) \in [\underline{\omega}_i, \bar{\omega}_i]$, then $\omega_i(t) \in [\underline{\omega}_i, \bar{\omega}_i]$ for any $t \geqslant 0$.

Furthermore, if in addition condition (2.9) *hold, and $(\lambda(0), \omega(0)) \in \mathscr{T}(r)$ with some $0 \leqslant r < \bar{r}$, then:*

(iii) For any $\xi \in \{0,1\}^{|\mathscr{I}^u|}$, $(\lambda^{\infty}, \omega^{\infty}\mathbf{1}_n)$ is locally asymptotically stable, $(\lambda(t), \omega(t)) \in \mathscr{T}(r)$ for every $t \geqslant 0$, and $(\lambda(t), \omega(t)) \to (\lambda^{\infty}, \omega^{\infty}\mathbf{1}_n)$;

(iv) For any $i \in \mathscr{I}^u$ with any $\xi_i \in \{0,1\}$, $u_i(x(t), p_t^{fcst})$ converges to 0 in finite time;

(v) For any $i \in \mathscr{I}^{\omega}$ with $\xi_i = 1$, if $\omega_i(0) \notin [\underline{\omega}_i, \bar{\omega}_i]$, then there exists a finite t_1 such that $\omega_i(t) \in [\underline{\omega}_i, \bar{\omega}_i]$ for any $t \geqslant t_1$.

Proof. We first show that u is well-defined by proving that $\hat{u}^*_{cvx}(0)$ exists and is unique. Notice that $(\hat{\Lambda}^{\text{ref}}, \hat{\Omega}^{\text{ref}}, \hat{U}^{\text{ref}})$ defined in Proposition 5.2.4 always qualifies as a reference trajectory for sufficiently small T. Hence the feasible set of Q_{cvx} is non-empty, and thus there exists at least one optimal solution. Uniqueness follows from the strict convexity of the objective function. For (i), note that in $Q_{cvx}(\mathscr{G}, \mathscr{I}^u, \mathscr{I}^{\omega}, \hat{P}^{fcst}, \lambda(t), \omega(t), t)$, if $\omega_i(t) \in (\underline{\omega}_i^{\text{thr}}, \bar{\omega}_i^{\text{thr}})$ for some $i \in \mathscr{I}^u$, then by (5.8b) and the fact that $\hat{\omega}_i^{\text{ref}}(0) = \omega_i(t)$, one has $\hat{u}^*_{i,cvx}(0) = 0$, and hence the statement follows by (5.11).

As we have shown in Lemma 4.2.3, the statement in (ii) is equivalent to

$$\dot{\omega}_i(t) \leqslant 0, \text{ if } \omega_i(t) = \bar{\omega}_i, \tag{5.12a}$$

$$\dot{\omega}_i(t) \geqslant 0, \text{ if } \omega_i(t) = \underline{\omega}_i. \tag{5.12b}$$

For simplicity, here we only prove (4.7a). Since $(\hat{\Lambda}^*_{cvx}, \hat{\Omega}^*_{cvx}, \hat{U}^*_{cvx})$ is feasible for $Q_{cvx}(\mathscr{G}$, $\mathscr{I}^u, \mathscr{I}^{\omega}, \hat{P}^{fcst}$, $\lambda(t), \omega(t), t)$, it satisfies constraint (5.6). Extracting the ith equation with $k = 1$ from (5.6a), it holds

$$M_i \hat{\omega}^*_{i,cvx}(1) = M_i \hat{\omega}^*_{i,cvx}(0) + T\big\{ -E_i \hat{\omega}^*_{i,cvx}(0) - [D^T Y_b]_i \hat{\lambda}^*_{cvx}(0) + \hat{p}_i^{fcst}(0) + \hat{u}^*_{i,cvx}(0) \big\}. \tag{5.13}$$

Note first, by (5.6b), $\hat{\lambda}^*_{cvx}(0) = \sin\lambda(t)$ and $\hat{\omega}^*_{i,cvx}(0) = \omega_i(t)$; secondly, $u_i(x(t), p_t^{fcst}) = \hat{u}^*_{i,cvx}(0)$; thirdly, $\hat{p}_i^{fcst}(0) \triangleq p_{i,t}^{fcst}(t)$, which by assumption equals $p_i(t)$; fourthly, by (5.6f), $\hat{\omega}^*_{i,cvx}(1) \leqslant \bar{\omega}_i$. These four facts imply that, when $\omega_i(t) = \bar{\omega}_i$,

$$-E_i\bar{\omega}_i(t) - [D^T]_i Y_b \sin\lambda(t) + p_i(t) + u_i(x(t), p_t^{fcst}) \leqslant 0. \tag{5.14}$$

From (2.8b), one sees that (5.14) is exactly (4.7a), concluding our reasoning.

To prove statement (iii), since $(\hat{\Lambda}^*_{cvx}, \hat{\Omega}^*_{cvx}, \hat{U}^*_{cvx}) \in \Phi_{cvx}$, by Lemma 5.2.3, one has $(\hat{\Lambda}^*_{cvx}, \hat{\Omega}^*_{cvx}, \hat{U}^*_{cvx}) \in \Phi_{disc}$, which further implies that for every $i \in \mathscr{I}^u$,

$$\begin{aligned} \hat{\omega}^*_{i,cvx}(0)\hat{u}^*_{i,cvx}(0) \leqslant 0, \text{ if } \hat{\omega}^*_{i,cvx}(0) \notin (\underline{\omega}_i^{\text{thr}}, \bar{\omega}_i^{\text{thr}}), \\ \hat{u}^*_{i,cvx}(0) = 0, \text{ if } \hat{\omega}^*_{i,cvx}(0) \in (\underline{\omega}_i^{\text{thr}}, \bar{\omega}_i^{\text{thr}}). \end{aligned}$$

Since $\hat{\omega}^*_{i,cvx}(0) = \omega_i(t)$, together with the definition of controller (5.11) and Lemma 5.2.1, it holds that the closed-loop system is asymptotically stable.

To prove statement (iv), since we have already shown the converge of $(\lambda(t), \omega(t))$, it holds that for arbitrarily small $\delta \in \mathbb{R}_>$, there exists $\tilde{t} \in \mathbb{R}_\geqslant$ such that $|\omega_i(t) - \omega^\infty| < \delta$ for any $i \in \mathscr{I}^u$ at any $t \geqslant \tilde{t}$. Let $\delta \triangleq \min_{i\in\mathscr{I}^u}\{\min(\bar{\omega}_i^{\text{thr}} - \omega^\infty, \omega^\infty - \underline{\omega}_i^{\text{thr}})\} > 0$. Now consider any $t \geqslant \tilde{t}$, one has $\omega_i(t) \in (\underline{\omega}_i^{\text{thr}}, \bar{\omega}_i^{\text{thr}})$, which, by statement (i), implies $u_i(x(t), p_t^{fcst}) = 0$.

Finally, to prove statement (v), by (iii), since every ω_i ultimately converges to ω^∞, it must first enter $[\underline{\omega}_i, \bar{\omega}_i]$, which, by (ii), cannot leave the safe region afterwards. □

Note that to compute the centralized control signal in (5.11), the operator should complete the following steps at every time: a) collect state information and forecast power injection of the entire network, b) determine the optimal trajectory $\hat{U}^*_{cvx}$ by solving Q_{cvx}, and c) broadcast the control signals to the corresponding controllers. The time to complete any of these three steps grows with the size of the network. This motivates the developments of our next section.

5.3.2 Distributed control using regional information

Here we describe our approach to design a distributed control strategy that takes advantage of cooperation to optimize control effort while ensuring stability and frequency invariance. The idea is to divide the power network into regions, and have each controller make decisions based on the state and power injection prediction information within its region. The network partition relies on the following assumption.

Assumption 5.3.2. *(Controlled nodes in induced subgraphs): Let $\mathscr{G}_\beta = (\mathscr{I}_\beta, \mathscr{E}_\beta),\ \beta \in [1,d]_{\mathbb{N}}$ be induced subgraphs of $\mathscr{G}$ (i.e., $\mathscr{I}_\beta \subseteq \mathscr{I}$, $\mathscr{E}_\beta \subseteq \mathscr{E}$, and $(i,j) \in \mathscr{E}_\beta$ if $(i,j) \in \mathscr{E}$ with $i,j \in \mathscr{I}_\beta$). We assume that each controlled node is contained in one and only one region, i.e.,*

$$\mathscr{I}^u \subseteq \bigcup_{\beta=1}^{d} \mathscr{I}_\beta, \tag{5.15a}$$

$$\mathscr{I}_\alpha \bigcap \mathscr{I}_\beta \bigcap \mathscr{I}^u = \emptyset,\ \forall \alpha,\beta \in [1,d]_{\mathbb{N}} \text{ with } \alpha \neq \beta. \tag{5.15b}$$

The induced subgraphs represent the regions of the network. Our distributed control strategy consists of implementing the centralized control for every induced subgraph $\mathscr{G}_\beta$, where for every line $(i,j) \in \mathscr{E}'_\beta \subseteq \mathscr{I}_\beta \times (\mathscr{I} \setminus \mathscr{I}_\beta)$ connecting $\mathscr{G}_\beta$ and the rest of the network, we treat its power flow $f_{ij}(\tau)$ as an external power injection whose forecasted value is a constant equaling its current value $f_{ij}(t)$ for $\tau \in [t, t+\tilde{t}]$. Formally,

$$p^{fcst,f}_{t,\beta,i}(\tau) \triangleq \sum_{\substack{j \to i \\ (i,j) \in \mathscr{E}'}} f_{ij}(t) - \sum_{\substack{i \to j \\ (i,j) \in \mathscr{E}'}} f_{ij}(t),\ \forall \tau \in [t, t+\tilde{t}], \tag{5.16}$$

as the forecasted (starting from the current time t) power flow from transmission lines in $\mathscr{E}'_\beta$ injecting into node $i \in \mathscr{I}_\beta$. Let $p^{fcst,f}_{t,\beta} : [t, t+\tilde{t}] \to \mathbb{R}^{|\mathscr{I}_\beta|}$ be the collection of all such $p^{f}_{t,\beta,i}$'s with $i \in \mathscr{I}_\beta$. Also, let $p^{fcst}_{t,\beta} : [t, t+\tilde{t}] \to \mathbb{R}^{|\mathscr{I}_\beta|}$ be the collection of all $p^{fcst}_{t,i}$'s with $i \in \mathscr{I}_\beta$, and denote $p^{fcst,o}_{t,\beta} \triangleq p^{fcst,f}_{t,\beta} + p^{fcst}_{t,\beta}$ as the overall forecasted power injection for $\mathscr{G}_\beta$. Denote $\hat{P}^{fcst,o}_{\beta}$ as its

discretization. Define $\mathscr{I}_\beta^u \triangleq \mathscr{I}^u \bigcap \mathscr{I}_\beta$ (resp. $\mathscr{I}_\beta^\omega \triangleq \mathscr{I}^\omega \bigcap \mathscr{I}_\beta$) as the collection of nodes within $\mathscr{G}_\beta$ with available controllers (resp. with frequency constraints). Let $(f_\beta, \omega_\beta) \in \mathbb{R}^{|\mathscr{I}_\beta|+|\mathscr{E}_\beta|}$ be the collection of states within $\mathscr{G}_\beta$. Similarly to (5.11), let $(\hat{F}^*_{cvx,\beta}, \hat{\Omega}^*_{cvx,\beta}, \hat{U}^*_{cvx,\beta})$ be the optimal solution of $Q_{cvx}(\mathscr{G}_\beta, \mathscr{I}_\beta^u, \mathfrak{G}_\beta, \hat{P}_\beta^{fcst,o}, f_\beta(t), \omega_\beta(t), t)$. The control law is given by

$$u_i(x(t), p_t^{fcst}) \triangleq \hat{u}^*_{i,cvx,\beta}(0),\ \forall i \in \mathscr{I}^u, \tag{5.17}$$

where $u^*_{i,cvx,\beta}(0)$ is the ith entry of $u^*_{cvx,\beta}(0)$ (the first column of $\hat{U}^*_{cvx,\beta}$). The next result details the properties of this strategy.

Proposition 5.3.3. *(Distributed control with stability and frequency constraints): Given power injection p and under Assumptions 5.2.2 and 5.3.2 with sufficiently small sampling length T, the following statements hold for the closed-loop system* (2.8) *under controller* (5.17)*:*

(i) For any $i \in \mathscr{I}^u$ with any $\xi_i \in \{0,1\}$ and any $t \in \mathbb{R}_{\geqslant}$, $u_i(x(t), p_t^{fcst}) = 0$ if $\omega_i(t) \in (\underline{\omega}_i^{thr}, \bar{\omega}_i^{thr})$;

(ii) For any $i \in \mathscr{I}^\omega$ with $\xi_i = 1$, if $\omega_i(0) \in [\underline{\omega}_i, \bar{\omega}_i]$, then $\omega_i(t) \in [\underline{\omega}_i, \bar{\omega}_i]$ for any $t \geqslant 0$.

Furthermore, if in addition condition (2.9) *hold, and $(\lambda(0), \omega(0)) \in \mathscr{T}(r)$ with some $0 \leqslant r < \bar{r}$, then:*

(iii) $(\lambda^\infty, \omega^\infty \mathbf{1}_n)$ is locally asymptotically stable, $(\lambda(t), \omega(t)) \in \mathscr{T}(r)$ for every $t \geqslant 0$, and $(\lambda(t), \omega(t)) \to (\lambda^\infty, \omega^\infty \mathbf{1}_n)$;

(iv) For any $i \in \mathscr{I}^u$ with any $\xi_i \in \{0,1\}$, $u_i(x(t), p_t^{fcst})$ converges to 0 within a finite time;

(v) For any $i \in \mathscr{I}^\omega$ with $\xi_i = 1$, if $\omega_i(0) \notin [\underline{\omega}_i, \bar{\omega}_i]$, then there exists a finite t_1 such that $\omega_i(t) \in [\underline{\omega}_i, \bar{\omega}_i]$ for any $t \geqslant t_1$.

Proof. First notice that each u_i is well-defined, as by Assumption 5.3.2, for every $i \in \mathscr{I}^u$, u_i is assigned to one and only one subgraph, and hence $\hat{u}^*_{i,cvx,\beta}(0)$ is determined uniquely by a single

$Q_{cvx}(\mathscr{G}_\beta, \mathscr{I}_\beta^u, \mathfrak{G}_\beta, \hat{P}_\beta^{fcst}, \lambda_\beta(t), \omega_\beta(t), t)$. The proofs of all statements follow similar arguments as the ones in Theorem 5.3.1. For statement (ii), similar to the way we have (5.14), it holds that when $\omega_i(t) = \bar{\omega}_i$, $-E_i\bar{\omega}_i(t) - [D_\beta^T]_i f_\beta(t) + p_{t,\beta,i}^{fcst,f}(t) + p_i(t) + u_i(x(t), p_t^{fcst}) \leqslant 0$, where D_β is the incidence matrix for $\mathscr{G}_\beta$. Notice that this inequality is equivalent to (5.14) as $[D_\beta^T]_i f_\beta(t) + p_{t,\beta,i}^{fcst,f}(t) = -[D^T]_i f(t)$ by (5.16), implying frequency invariance. □

5.4 Simulations

We first illustrate the performance of the distributed controller in the IEEE 39-bus power network displayed in Fig. 5.1. Network parameters are the same with what we chose in Sec-

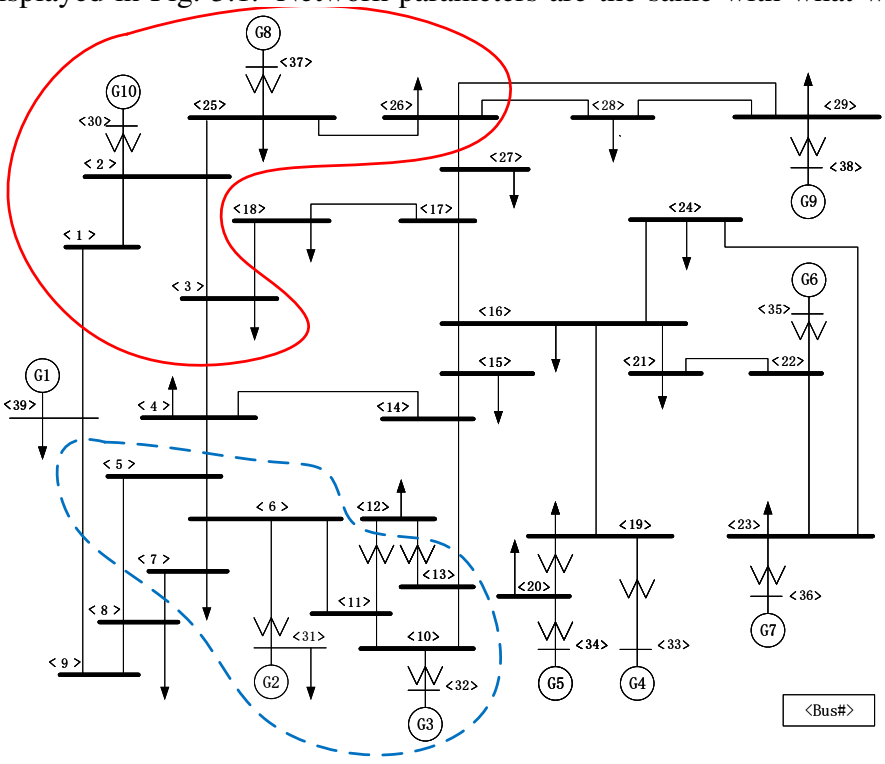

Figure 5.1: IEEE 39-bus power network.

tion 3.5 and 4.5. The initial state $(\lambda(0), \omega(0))$ is chosen to be the equilibrium with respect to the initial power injections. Let $\mathscr{I}^\omega = \{30, 31\}$ be the two generators with transient frequency requirements. As shown in Fig. 3.3, we assign each of them a region containing its 2-hop neigh-

bors. Let $\mathscr{I}^u = \{3,7,25,30,31\}$ be the collection of nodal indexes with controllers. Notice that Assumption 5.3.2 holds in this scenario. To set up the optimization problem Q_{cvx} so as to define our controller (5.17), for every $i \in \mathscr{I}^u$, we set $\bar{\gamma}_i = \underline{\gamma}_i = 1$ required in (5.9), $c_i = 2$ if $i \in \mathscr{I}^\omega$ and $c_i = 1$ if $i \in \mathscr{I}^u \backslash \mathscr{I}^\omega$, $T = 0.001s$, $N = 150$ so that the predicted time horizon is $\tilde{t} = 0.15$s. For simplicity, for every $i \in \mathscr{I}^u$, let $\xi_i = 1$ and $d_i = 0$, i.e., we impose neither hard nor soft constraints on the control signal amplitude, and therefore, there is no need to specify $u_i^{\min}$ and $u_i^{\max}$. For every $i \in \mathscr{I}^\omega$, let $e_i = 500$, $\bar{\omega}_i = -\underline{\omega}_i = 0.2$Hz and $\bar{\omega}_i^{\text{thr}} = -\underline{\omega}_i^{\text{thr}} = 0.1$Hz. The nominal frequency is 60Hz, and hence the safe frequency region is $[59.8\text{Hz},\ 60.2\text{Hz}]$. We take $p_t^{fcst}(\tau) = (1+\tau-t)p(\tau)$ for every $\tau \in [t, t+\tilde{t}]$, that is, the forecasted power injection error $p_t^{fcst}(\tau) - p(\tau)$ satisfies Assumption 5.2.2, and grows linearly in time. Note here we allow p to be time-varying.

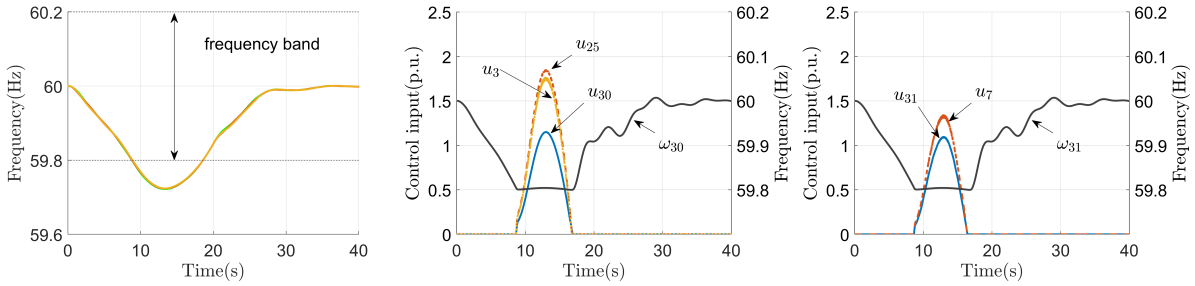

(a) (b) (c)

Figure 5.2: Plot (a) shows the frequency trajectories of generators 30 and 31 without the controller, going beyond the lower safe frequency bound. With the centralized controller, plot (b) and (c) show the trajectories of the control inputs and frequency within each region.

We show that the proposed controller is able to maintain the targeted generator frequencies within the safe region, provided that these frequencies are initially in the safe region. We perturb all non-generator nodes by a sinusoidal power injection whose magnitude is proportional to the corresponding node's initial power injection. Specifically, for every $i \in \{1,2,\cdots,29\}$, let $p_i(t) = (1+\delta(t))p_i(0)$, where $\delta(t) = 0.25\sin(\pi t/20)$ for $t < 20$, and $\delta(t) = 0$ for $t \geqslant 20$. For $i \in \{30,31,\cdots,39\}$, let $p_i(t) \equiv p_i(0)$. Fig. 5.2(a) shows the open-loop frequency responses of the two generators without the controller. One can see that both trajectories exceed the lower

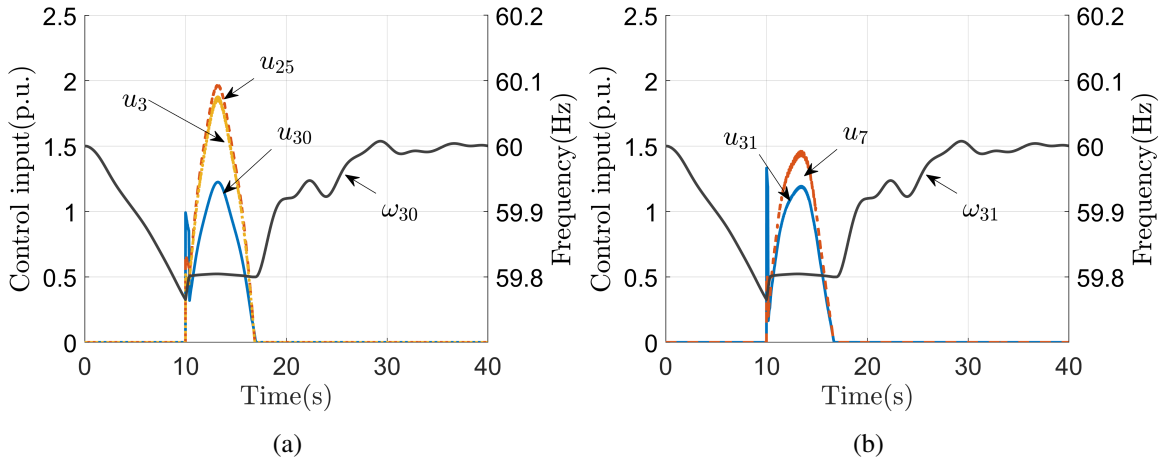

Figure 5.3: Frequency and control input trajectories with centralized controller available only after $t = 10s$, plot (a) for the region with generator 30, and plot (b) for the region with generator 31.

bound around 8s. With the distributed control, Fig. 5.2(b) and (c) show the frequency and control input responses in the left-top region and left-bottom region, resp. Both frequency responses stay within the safe bound all the time and converge to 60Hz. Also, all control signals vanish to 0 within 20s. In Fig. 5.2(b), since we assign a higher cost weight on u_{30}, and the same weight on u_{25} and u_3, the latter two have a similar trajectory with magnitude higher than the first one. On the other hand, notice that for every $i \in \mathscr{I}^{\omega}$, u_i is always 0, while ω_i is above the lower frequency threshold denoted by the dashed line. All these observations are in agreement with the result of Proposition 5.3.3(i)-(iv) (even though here we assume the power injection is time-varying).

Next, we simulate the case where generator frequencies are initially outside the safe frequency region to show how the controller brings the frequencies back to the safe region. We apply the same setup used in Fig. 5.2, but only enable the controller after $t = 10s$. The plots in Fig.5.3 shows the frequency trajectories and control trajectories of each region. Note that both two frequency trajectories are lower than 59.8Hz at $t = 10s$. However, as the controller becomes active after $t = 10s$, they come back to the safe region and never leave, in accordance with Proposition 5.3.3(v).

Next, we compare the performance of the centralized controller (5.11), the distributed

controller (5.17), and the controller we proposed in Chapter 4 in the IEEE 9-bus network with the regional partition shown in Fig. 5.4. Since the control framework in Chapter 4 requires that controllers are available only for nodes with transient frequency constraints, for fairness, we let $\mathscr{I}^{\omega} = \mathscr{I}^{u} = \{1,2,3\}$ for controllers (5.11) and (5.17) (adding nodes with controllers to $\mathscr{I}^{u}$/ $\mathscr{I}^{\omega}$ would further enhance their performance). We employ a similar set-up as in the previous simulation, here with $T = 0.01s$; $p_i(t) \equiv p_i(0)$ for $i = 1,2,3$, and $p_i(t) = (1+\delta(t))p_i(0)$ for $i = 4,5,\cdots,9$, with the coefficient 0.25 replaced by 1.5 in $\delta(t)$ so that the open-loop frequency responses exceed the safe frequency bounds.

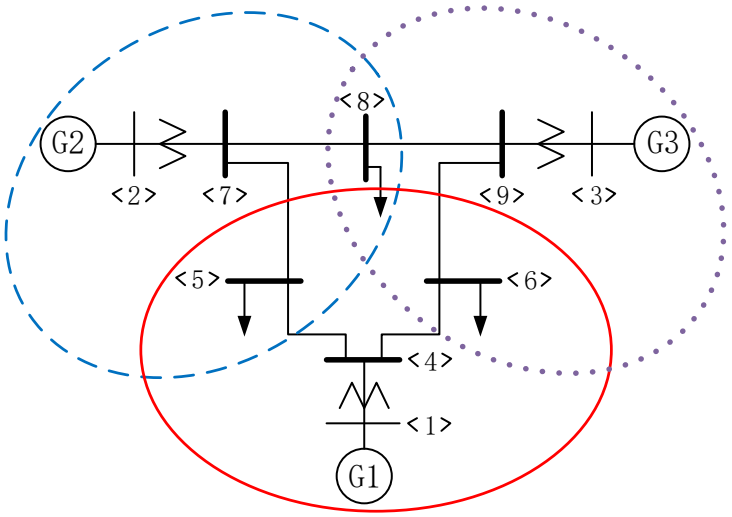

Figure 5.4: IEEE 9-bus power network with network partition.

Fig. 5.5 shows the input trajectories of the generators indexed from 1 to 3 for each of the three controllers. Since all of them achieve frequency invariance and stabilization, we do not show the state trajectories. In terms of the overall control cost, the centralized controller performs the best, due to its capability of accessing the entire network parameters, state, and power injection information, and hence all three generators cooperatively reduce the total cost. This capability is, however, weakened in the distributed controller, as the controller in each region only considers its regional optimality, losing inter-region cooperation. The controller from Chapter 4, which is not designed by optimizing control effort, tends to have the largest cost. On the hand, in

terms of implementation, the centralized controller requires global network information as well as solving a large-scale optimization problem. In comparison, the distributed controller only accesses network information within its region, and solves a small-scale optimization problem. The controller in Chapter 4 can be computed the fastest and only needs information of 1-hop neighbors.

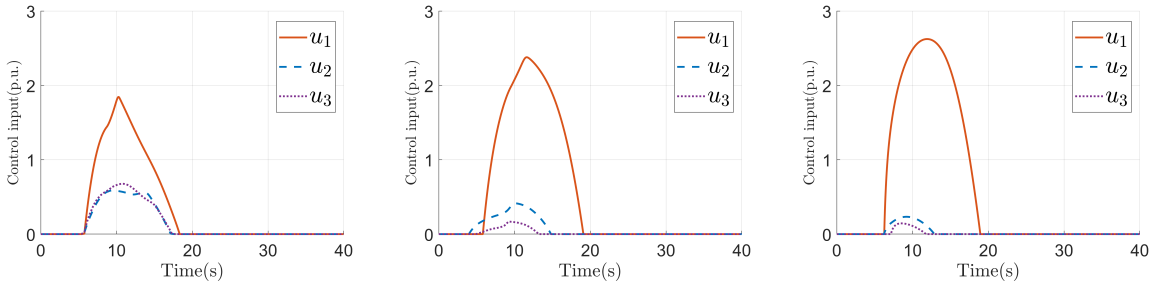

(a) (b) (c)

Figure 5.5: Input trajectories of controlled generators in IEEE 9-bus example under (a) centralized controller, (b) distributed controller, and (c) controller proposed in [ZC19c]. All of them guarantee stability and frequency invariance.

Acknowledgements

Chapter 5, in part, is a reprint of the material [ZC19e] submitted as 'Model predictive control for transient frequency regulation of power networks.' by Y. Zhang and J. Cortés, to the IEEE Transactions on Automatic Control, as well as [ZC18b] where it appears as 'Transient frequency control with regional cooperation for power networks' by Y. Zhang and J. Cortés in the proceedings of the 2018 IEEE Conference on Decision and Control. The dissertation author was the primary investigator and author of these papers. This research was supported by AFOSR Award FA9550-15-1-0108.

Chapter 6

Distributed bilayered control for transient frequency safety and system stability

In addition to the baseline requirements of frequency safety and asymptotic stability, we proposed a MPC-based controller in Chapter 5 that enables regional nodal cooperations. However, the prediction horizon used is limited by trade-offs between the discretization accuracy and the computational complexity, limiting its performance. Moreover, the implementation of the MPC-based controller is only partially distributed: given a set of regions in the network, a centralized controller aggregates information and determines the control actions within each region, independently of the others. Finally, we are not able to prove its Lipschitz continuity in system state, leading to potential jumps in control signals.

In this chapter we propose a bilayer controller without any issue mentioned above. The bottom layer is a model predictive controller that, based on periodically sampled system information, optimizes control resources to have transient frequency evolve close to a safe desired interval. The top layer is a real-time controller assisting the bottom-layer controller to guarantee transient frequency safety is actually achieved. We show that control signals at both layers are Lipschitz in the state and do not jeopardize stability of the network. Furthermore, we carefully

characterize the information requirements at each bus necessary to implement the controller and employ saddle-point dynamics to introduce a distributed implementation that only requires information exchange with up to 2-hop neighbors in the power network. Simulations on the IEEE 39-bus power network illustrate our results.

6.1 Problem statement

In this chapter, we still consider the same power network dynamics (2.8) used in Chapter 4 and 5. We further assume that the power injection p designed by the tertiary layer and secondary layer is balanced, i.e., $\mathbf{1}_n^T p = 0$. This assumption is reasonable, given that our focus here is on the system transient frequency behavior, which instead lies within the scope of primary control.

The control requirements are similar to those mentioned in Section 4.1 and 5.1. For clarity and narrative integrity, we re-state them as follows and replace the control signal u in (2.8) by α,

(i) *Frequency safety:* For each $i \in \mathscr{I}^{\omega} \subseteq \mathscr{I}^{u}$, let $\underline{\omega}_i \in \mathbb{R}$ and $\bar{\omega}_i \in \mathbb{R}$ be lower and upper safe frequency bounds, with $\underline{\omega}_i < \bar{\omega}_i$. If ω_i is initially safe, i.e., $\omega_i(0) \in [\underline{\omega}_i, \bar{\omega}_i]$, then we require that the entire trajectory stay within $[\underline{\omega}_i, \bar{\omega}_i]$. On the other hand, if ω_i is initially unsafe, then we require that there exists a finite time t_0 such that $\omega_i(t) \in [\underline{\omega}_i, \bar{\omega}_i]$ for every $t \geqslant t_0$. This requirement is equivalent to asking the set $[\underline{\omega}_i, \bar{\omega}_i]$ to be both invariant and attractive for each $i \in \mathscr{I}^{\omega}$.

(ii) *Local asymptotic stability:* The closed-loop system should preserve the asymptotic stability properties of the open-loop system (2.8) with $\alpha \equiv \mathbf{0}_n$.

(iii) *Lipschitz continuity:* The controller should be a Lipschitz function in the state argument. This ensures the existence and uniqueness of solution for the closed-loop system and rules out discontinuities in the control signal.

(iv) *Economic cooperation:* Each bus in $\mathscr{I}^u$ should cooperate with the others to reduce the overall cost of the control input.

(v) *Distributed nature:* The controller α should be implementable in distributed way, i.e., node i should be able to compute α_i by only exchanging information with its neighboring nodes and edges.

In Section 6.2, we introduce a centralized controller architecture that meets the requirements (i)-(iv). We later build on this architecture in Section 6.3 to provide a distributed controller that satisfies all requirements (i)-(v).

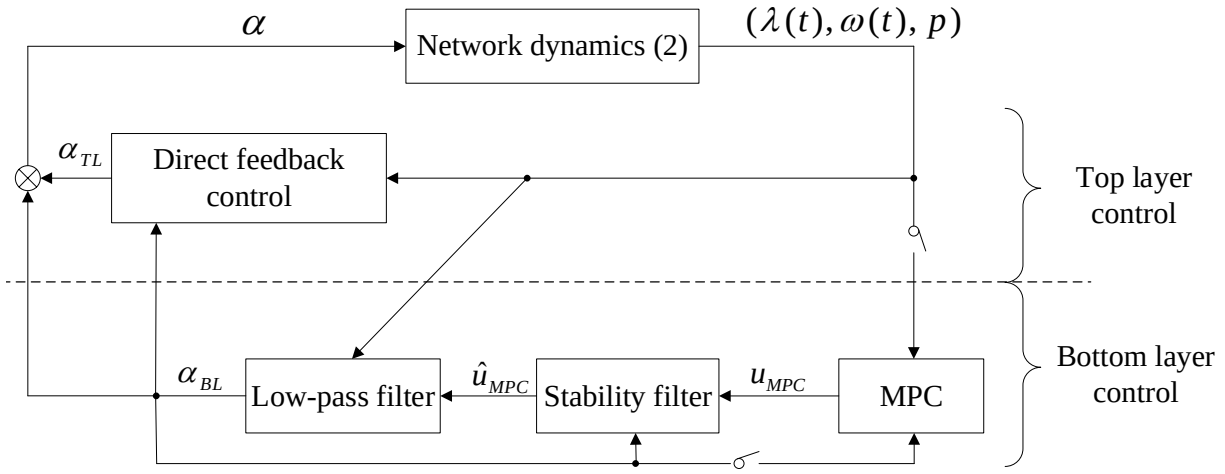

Figure 6.1: Block diagram of the closed-loop system with the proposed controller architecture.

6.2 Centralized bilayered controller

Here, we propose a centralized controller to address the requirements posed in Section 6.1. Our idea for design starts from considering MPC to account for the economic cooperation requirement; however, MPC cannot be run continuously due to the computational burden of its online optimization. We therefore compute MPC solutions periodically. Given the reliance

of the MPC implementation on sampled system states that are potentially outdated, we include additional components that employ real-time state information to tune the output of the MPC implementation and ensure stability and frequency safety. Figure 6.1 shows the overall structure of the closed-loop system. The control signal α is defined by

$$\alpha = \alpha_{TL} + \alpha_{BL}. \tag{6.1}$$

Roughly speaking, the bottom-layer controller α_{BL} periodically and optimally allocates control effort, while respecting an stability constraint and steering the frequency trajectories as a first step to achieve frequency invariance and attractivity. The top-layer controller α_{TL}, implemented in real time, slightly tunes the control trajectory generated by the bottom layer, ensuring frequency invariance and attractivity. In the following, we provide detailed definitions of each of the design elements.

6.2.1 Bottom-layer controller design

We introduce here the bottom-layer control signal α_{BL}, which results from the combination of three components. The MPC component periodically samples the system state, solves an optimization problem online, and updates its output signal u_{MPC}. The purpose of having this MPC component is to efficiently allocate control resources to achieve the frequency safety requirement. Given the discrete-time nature of this component, the stability filter is designed to produce an output $\hat{u}_{MPC}$ that filters out the unstable part in u_{MPC}. Since $\hat{u}_{MPC}$ is merely a piecewise continuous signal, to avoid discontinuity in the control signal, the low-pass filter further smooths it to generate an input α_{BL} that is continuous in time. The bottom-layer controller by itself stabilizes the system (without the need of the top layer) but does not guarantee frequency safety. This is precisely the role of the top-layer design, which based on real-time system state information, slightly tunes the control signal generated by the bottom layer in order to achieve

frequency safety while maintaining system stability. Note that, except for the MPC component, all other components can access real-time information.

Next, we introduce each component in the bottom layer and characterize their properties.

MPC component

Based on the most recent sampled system information, the MPC component updates its output after solving an optimization problem online. Formally, denote $\{\Delta^w\}_{w\in\mathbb{N}}$ as the collection of sampling time instants, where $\Delta^{w+1} > \Delta^w \geqslant 0$ holds for every $w \in \mathbb{N}$. At each sampling time $t = \Delta^w$, define a piece-wise continuous signal $p_t^{fcst} : [t, t+\tilde{t}] \to \mathbb{R}^n$ as the predicted value of the true power injection p for the $\tilde{t}$ seconds immediately following t. Note that here we particularly allow the predicted power injection to be time-varying, although its true value is time-invariant. For convenience of exposition, we define

$$x \triangleq (\lambda, \omega, \alpha_{BL})$$

as the augmented collection of system states (the last state comes from the low-pass filter component). Let $x(\Delta^w) = (\lambda(\Delta^w), \omega(\Delta^w), \alpha_{BL}(\Delta^w))$ be the augmented system state value at the sampling time Δ^w.

In the predicted model, we discretize the system dynamics with time step $T > 0$, and denote $N \triangleq \lceil \tilde{t}/T \rceil$ as the predicted step length. At every $t = \Delta^w$, the MPC component solves the following optimization problem,

$$\min_{\hat{X},\hat{u},\mathscr{B}} \quad g(\hat{X},\hat{u},\mathscr{B}) \triangleq \sum_{k=1}^{N} \Big(\sum_{i\in\mathscr{I}^u} c_i \hat{\alpha}_{BL,i}^2(k) + \sum_{i\in\mathscr{I}^\omega} d_i \beta_i^2(k) \Big)$$

$$\text{s.t.} \quad F\hat{x}(k+1) = A\hat{x}(k) + B_1 \hat{p}^{fcst}(k) + B_2 \hat{u} \tag{6.2a}$$

$$\hat{u} \in \mathbb{A}, \tag{6.2b}$$

$$\hat{x}(1) = x(\Delta^w), \tag{6.2c}$$

$$\underline{\omega}_i - \beta_i(k) \leqslant \hat{\omega}_i(k) \leqslant \bar{\omega}_i + \beta_i(k),\ \forall i \in \mathscr{I}^{\omega}, \forall k \in [1,N]_{\mathbb{N}}, \tag{6.2d}$$

$$|\hat{u}_i| \leqslant \varepsilon_i |\alpha_{BL,i}(\Delta^w)|, \quad \forall i \in \mathscr{I}^{u}. \tag{6.2e}$$

In this optimization, (6.2a) combines the linearized, discretized dynamics corresponding to (2.8) as well as the low-pass filter introduce later, and $\hat{x} \triangleq (\hat{\lambda}, \hat{\omega}, \hat{\alpha}_{BL}) \in \mathbb{R}^{m+2n}$ corresponds to the predicted system state. Depending on the specific discretization method, one can choose different matrices F, $A \in \mathbb{R}^{(m+2n)\times(m+2n)}$ and $B_1, B_2 \in \mathbb{R}^{(m+2n)\times n}$ (Section 6.2.2 below contains a detailed discussion on discretization); $\hat{p}^{fcst}(k) \triangleq p^{fcst}_{\Delta^w}(\Delta^w + (k-1)T)$ for every $k \in [1,N]_{\mathbb{N}}$; (6.2b) specifics the control availability for each bus; (6.2c) is the initial condition; (6.2d) represents a soft version of the frequency safety constraint, where we penalize in the cost function the deviation of predicted frequency from its desired bounds; (6.2e) restricts the value of the control input $\hat{u}_i \in \mathbb{R}$ with respect to the state of the low-pass filter via a tunable parameter $\varepsilon_i > 0$; finally, the objective function g combines the overall cost of control effort and the penalty on the violation of the frequency safety requirement, where $c_i > 0$ for each $i \in \mathscr{I}^{u}$ and $d_i > 0$ for each $i \in \mathscr{I}^{\omega}$ are design parameters. For compactness, we define

$$\hat{X} \triangleq [\hat{x}(1), \hat{x}(2), \cdots, x(N)], \tag{6.3a}$$

$$\mathscr{B} \triangleq [\beta(1), \beta(2), \cdots, \beta(N)], \tag{6.3b}$$

$$\hat{P}^{fcst} \triangleq [\hat{p}^{fcst}(1), \hat{p}^{fcst}(2), \cdots, \hat{p}^{fcst}(N)], \tag{6.3c}$$

where for every $k \in [1,N]_{\mathbb{N}}$, $\beta(k)$ is the collection of $\beta_i(k)$'s over $i \in \mathscr{I}^{\omega}$.

We denote by $\mathbf{R}(\mathscr{G}, \mathscr{I}^{u}, \mathscr{I}^{\omega}, p^{fcst}_{\Delta^w}, x(\Delta^w))$ as the optimization problem (6.2) to emphasize its dependence on network topology, nodal indexes with exogenous control signals, nodal indexes with transient frequency requirement, forecasted power injection, and state values at the sampling time. We may simply use $\mathbf{R}$ if the context is clear. Also, we denote $(\hat{X}^*, \hat{u}^*, \mathscr{B}^*)$ as its optimal solution.

Remark 6.2.1. *(Selection of frequency violation penalty coefficient):* The parameter $d = \{d_i\}_{i\in\mathscr{I}^\omega}$ in the objective function plays a fundamental rule in determining how the predicted frequency can exceed the safe bounds. In the extreme case $d = \mathbf{0}_{|\mathscr{I}^\omega|}$ (i.e., no penalty for frequency violation), the MPC controller loses its functionality of adjusting frequency. As d grows, the controller ensures that the violation of the frequency safety requirement become smaller. The top-layer control introduced later adds additional input to the resulting bottom-layer controller to ensure the frequency requirement is strictly satisfied. •

Given the open-loop optimization problem (6.2), the function u_{MPC} corresponding to the MPC component in Figure 6.1 is defined as follows: for $w \in \mathbb{N}$ and $t \in [\Delta^w, \Delta^{w+1})$, let

$$u_{MPC}(t) = \hat{u}^*(\mathscr{G}, \mathscr{I}^u, \mathscr{I}^\omega, p^{fcst}_{\Delta^w}, x(\Delta^w)). \tag{6.4}$$

Note the last two arguments that $\hat{u}^*$ depends on: forecasted power injection value and state value of the entire network at a sampling time. To implement (6.4), a straightforward idea is to have one operator globally gather the above two values, obtain $\hat{u}^*$ by solving $\mathbf{R}$, and finally broadcast $\hat{u}^*_i$ to the ith node. Later in Section 6.3, we propose an alternative distributed computation algorithm to reduce the computational burden. The next result characterizes the dependence of the controller on the sampled state values and predicted power injection.

Proposition 6.2.2. *(Piece-wise affine and continuous dependence of optimal solution on sampling state and predicted power injection): Suppose F is invertible, then the optimization problem $\mathbf{R}(\mathscr{G}, \mathscr{I}^u, \mathscr{I}^\omega, p^{fcst}_{\Delta^w}, x(\Delta^w))$ in* (6.2) *has a unique optimal solution $(\hat{X}^*, \hat{u}^*, \mathscr{B}^*)$. Furthermore, given $\mathscr{G}$, $\mathscr{I}^u$, and $\mathscr{I}^\omega$, $\hat{u}^*$ is continuous and piece-wise affine in $(\hat{P}^{fcst}, x(\Delta^w))$, that is, there exist $l \in \mathbb{N}, \{H_\xi\}^l_{\xi=1}$, $\{S_\xi\}^l_{\xi=1}$, $\{h\}^l_{\xi=1}$, and $\{s_\xi\}^l_{\xi=1}$ with suitable dimensions such that*

$$\hat{u}^* = S_\xi z + s_\xi, \text{ if } z \in \left\{y \mid H_\xi y \leqslant h_\xi\right\} \text{ for } \xi \in [1,l]_{\mathbb{N}} \tag{6.5}$$

holds for every $z \in \mathbb{R}^{(N+2)n+m}$, where z is the collection of $(\hat{P}^{fcst}, x(\Delta^w))$ in column-vector form.

Proof. We start by noting that **R** is feasible (hence at least one optimal solution exists) for any given z. This is because, given a state trajectory $\hat{X}$ of (6.2a) with input $\hat{u} = \mathbf{0}_n$ and initial condition (6.2c), choosing a sufficiently large $\beta(k)$ for each $k \in [1,N]_{\mathbb{N}}$ makes it satisfy constraint (6.2d). The uniqueness follows from the facts that I) g is strongly convex in $(\hat{u}, \mathscr{B})$; II) $\hat{X}$ is uniquely and linearly determined by $\hat{u}$; III) all constraints are linear in $(\hat{X}, \hat{u}, \mathscr{B})$. To show continuity and piece-wise affinity, we separately consider $2^{|\mathscr{I}^u|}$ cases, depending on the sign of each $\{\alpha_{BL,i}(\Delta^w)\}_{i\in\mathscr{I}^u}$. Specifically, let $\eta \triangleq \{\eta_i\}_{i\in\mathscr{I}^u} \in \{1,-1\}^{|\mathscr{I}^u|}$ and define $\mathfrak{B}^\eta \triangleq \left\{z \middle| (-1)^{\eta_i}\alpha_{BL,i}(\Delta^w) \geqslant 0,\ \forall i \in \mathscr{I}^u\right\}$. Note that every z lies in at least one of these sets and that, in any $\mathfrak{B}^\eta$, the sign of each $\alpha_{BL,i}(\Delta^w)$ with $i \in \mathscr{I}^u$ is fixed. Hence all the $|\mathscr{I}^u|$ constraints in (6.2e) can be transformed into one of the following forms

$$-\varepsilon_i\alpha_{BL,i}(\Delta^w) \leqslant \hat{u}_i \leqslant \varepsilon_i\alpha_{BL,i}(\Delta^w) \quad \text{if } \alpha_{BL,i}(\Delta^w) \geqslant 0, \tag{6.6a}$$

$$\varepsilon_i\alpha_{BL,i}(\Delta^w) \leqslant \hat{u}_i \leqslant -\varepsilon_i\alpha_{BL,i}(\Delta^w) \text{ if } \alpha_{BL,i}(\Delta^w) \leqslant 0. \tag{6.6b}$$

Note that if $\alpha_{BL,i}(\Delta^w) = 0$, then $\hat{u}_i = 0$. Therefore, in every $\mathfrak{B}^\eta$, z appears in **R** in a linear fashion; hence, it is easy to re-write **R** into the following form:

$$\begin{aligned} \min_{s} \quad & s^T K s \\ \text{s.t.} \quad & Gs \leqslant W + J^\eta z, \end{aligned} \tag{6.7}$$

where s is the collection of $(\hat{X}, \hat{u}, \mathscr{B})$ in vector form and $K \succeq 0$, G, W and J^η are matrices with suitable dimensions. Note that only J^η depends on η. By [Bor03, Theorem 1.12], for every $\eta \in \{-1,1\}^{|\mathscr{I}^u|}$, s^* is a continuous and piece-wise affine function of z whenever $z \in \mathfrak{B}^\eta$. Since each $\mathfrak{B}^\eta$ consists of only linear constraints and the union of all $\mathfrak{B}^\eta$'s with $\eta \in \{1,-1\}^{|\mathscr{I}^u|}$ is $\mathbb{R}^{(N+2)n+m}$, one has that s^* is piece-wise affine in z on $\mathbb{R}^{(N+2)n+m}$. Lastly, to show the continuous

dependence of s^* on z on $\mathbb{R}^{(N+2)n+m}$, note that since such a dependence holds on every closed set $\mathfrak{B}^\eta$, we only need to prove that s^* is unique for every z lying on the boundary shared by different $\mathfrak{B}^\eta$'s. This holds trivially as s^* is unique for every $z \in \mathbb{R}^{(N+2)n+m}$, which we have proven above. □

Notice that the continuity and piece-wise affinity established in Proposition 6.2.2 together suffice to ensure that $\hat{u}^*$ is globally Lipschitz in z, and hence in the sampled system state. To see this point, one can easily check that $\max_{\xi \in [1,l]_\mathbb{N}} \|S_\xi\|$ qualifies as a global Lipschitz constant.

In addition, Proposition 6.2.2 also suggests an alternative to directly solve **R** without treating it as an optimization problem. Specifically, we can first compute and store $\{H_\xi\}_{\xi=1}^l$, $\{S_\xi\}_{\xi=1}^l$, $\{h\}_{\xi=1}^l$, and $\{s_\xi\}_{\xi=1}^l$, and then compute $\hat{u}^*$ online via (6.5). However, such an approach, usually called explicit MPC [AA09], suffers from the curse of dimensionality, in that the number of regions l grows exponentially fast in $m+n$, input size $|\mathscr{I}^u|$, and horizon length N.

Stability and low-pass filters

Here we introduce the stability and low-pass filters, explain the motivation behind their definitions and characterize their properties. Note that the sampling mechanism used for the MPC component inevitably introduces delays in the bottom layer. Specifically, for any time $t \in (\Delta^w, \Delta^{w+1})$, i.e., between two adjacent sampling times, $u_{MPC}(t)$ is fully determined by the old sampled system information at time Δ^w, as opposed to the current information. To eliminate the potential negative effect of delay on system stability, we introduce a stability filter that filters out the unstable part in the signal u_{MPC}. The low-pass filter after the stability filter simply smooths the output of the stability filter to ensure that the output of the bottom layer is continuous in time. Formally, for every $i \in \mathscr{I}^u$ at any $t \geqslant 0$, define the stability filter as

$$\hat{u}_{MPC,i}(\alpha_{BL}(t), u_{MPC}(t)) = \text{sat}(u_{MPC,i}(t); \varepsilon_i|\alpha_{BL,i}(t)|, -\varepsilon_i|\alpha_{BL,i}(t)|), \tag{6.8}$$

and define the low-pass filter as

$$\dot{\alpha}_{BL,i}(t) = -\frac{1}{T_i}\alpha_{BL,i}(t) - \omega_i(t) + \hat{u}_{MPC,i}(t), \quad \forall i \in \mathscr{I}^u,$$
$$\alpha_{BL,i} \equiv 0, \quad \forall i \in \mathscr{I} \setminus \mathscr{I}^u, \tag{6.9}$$

where the tunable parameter $T_i \in \mathbb{R}_>$ determines the bandwidth of the low-pass filter.

Note that both the stability and the low-pass filters possess a natural distributed structure: for each $i \in \mathscr{I}^u$, $\alpha_{BL,i}$ only depends ω_i and $\hat{u}_{MPC,i}$, where the latter one only depends on $u_{MPC,i}$ and $\alpha_{BL,i}$. This implies that to implement $\hat{u}_{MPC,i}$ and $\alpha_{BL,i}$, it only requires local information at node i. Throughout the rest of the chapter, we interchangeably use $\hat{u}_{MPC,i}(\alpha_{BL}(t), u_{MPC}(t))$ and $\hat{u}_{MPC,i}(t)$ for simplicity.

The next result establishes that $\hat{u}_{MPC}$ is Lipschitz continuous in the system state and an important property of the bottom-layer controller α_{BL} that we use later to establish system stability.

Lemma 6.2.3. *(Lipschitz continuity and stability condition): For the signal $\hat{u}_{MPC}$ defined in* (6.8)*, $\hat{u}_{MPC}$ is Lipschitz in system state at every sampling time $t = \Delta^w$ with $j \in \mathbb{N}$. Furthermore, if α_{TL} is Lipschitz in system state, then both α_{TL} and α_{BL} are continuous in time. Additionally,*

$$\alpha_{BL,i}(t)\hat{u}_{MPC,i}(t) \leqslant \varepsilon_i \alpha_{BL,i}^2(t), \quad \forall t \geqslant 0, \ \forall i \in \mathscr{I}. \tag{6.10}$$

Proof. If $t = \Delta^w$, then since $|\hat{u}_i^*| \leqslant \varepsilon_i |\alpha_{BL,i}(\Delta^w)|$ by (6.2e) and $u_{MPC,i}(\Delta^w) = \hat{u}_i^*$ for every $i \in \mathscr{I}^u$, using (6.8) we deduce that $\hat{u}_{MPC,i}(\alpha_{BL}(t), u_{MPC}(t))|_{t=\Delta^w} = \hat{u}_i^*$. The Lipschitz continuity follows by Proposition 6.2.2. To show the time-domain continuity, since $\hat{u}_{MPC}$ is Lipschitz at every sampling point and the top-layer controller is also Lipschitz by hypothesis (we demonstrate this point later in Section 6.2.3), one has that the solutions of both α_{TL} and the closed-loop system (2.8) exist and are unique and continuous in time. Note that u_{MPC} in (6.4) is defined to

be a piece-wise constant signal. One has, by (6.8), that $\hat{u}_{MPC}$ is piece-wise continuous, which further makes α_{BL} a continuous signal in time due to the low-pass filter. Condition (6.10) simply follows from the definition of saturation function. □

Remark 6.2.4. *(Link between designs of the MPC component and stability filter):* Note that, regardless of the MPC component output u_{MPC}, the output of the stability filter $\hat{u}_{MPC}$ defined in (6.8) always meets condition (6.10). This implies that any inaccuracy in the MPC component (e.g., errors in sampled state measurement, forecasted power injection, or system parameters) cannot cause instability. However, to ensure the Lipschitz continuity in Lemma 6.2.3, we formulate constraint (6.2e) employing the same coefficient ε_i in the stability filter (6.8). It is in this sense that both are linked. •

Remark 6.2.5. *(Continuous versus periodic sampling in the MPC component):* Given the reliance of the MPC component on periodically sampled information, the role of the stability filter is to filter out the unstable parts in u_{MPC}. If the MPC component were to sample the system state in a continuous fashion instead, then the constraint (6.2e) would ensure that the output of the MPC component already satisfies the stability condition (6.10), and hence there would be no need for the stability filter. •

6.2.2 Discretization with sparsity preservation

As we have introduced the dynamics of the low-pass and stability filters, we are now able to explicitly explain the computation of matrices F, A, B_1 and B_2 in the prediction model (6.2a). To obtain the prediction model used in the MPC component, we first construct a continuous-time linear model by neglecting the top-layer controller and the stability filter ($\alpha \approx \alpha_{BL}$ and $\hat{u}_{MPC} \approx u_{MPC}$), and then linearizing the nonlinear dynamics in Figure 6.1. Our second step consists of appropriately discretizing this linear model.

Notice that the transformation from a nonlinear continuous-time nonlinear model to a

discrete one does not affect closed-loop system stability due to the presence of the stability filter. In fact, any prediction model in the MPC component cannot jeopardize stability (cf. Remark 6.2.4). On the other hand, such a model simplification is reasonable since α_{BL} is designed to only slightly tune the control signal, and we have described in Remark 6.2.5 how the stability filter barely changes its input.

We obtain the linear model by assuming $\alpha \approx \alpha_{BL}$ and $\hat{u}_{MPC} \approx u_{MPC}$, and approximating the systems dynamics in Figure 6.1 by

$$\begin{aligned}
\dot{\lambda}(t) &= D\omega(t), \\
M\dot{\omega}(t) &= -E\omega(t) - D^T Y_b \lambda(t) + p + \alpha_{BL}(t), \\
\dot{\alpha}_{BL,i}(t) &= -\frac{1}{T_i}\alpha_{BL,i}(t) - \omega_i(t) + u_{MPC,i}(t), \quad \forall i \in \mathscr{I}^u, \\
\alpha_{BL,i} &\equiv 0, \quad \forall i \in \mathscr{I} \setminus \mathscr{I}^u,
\end{aligned} \tag{6.11}$$

where the first two equations come from (2.8) by linearizing the nonlinear sinusoid function via $\sin(Y_b\lambda(t)) \approx Y_b\lambda(t)$. Now we re-write the above linear dynamics into the following compact form,

$$\dot{x}(t) = \tilde{A}x(t) + \tilde{B}_1 p + \tilde{B}_2 u_{MPC}(t), \tag{6.12}$$

for certain matrices $\tilde{A}$, $\tilde{B}_1$, and $\tilde{B}_2$, with $\tilde{A}$ stable [Pai89]. Additionally, one can easily check that the linearized dynamics (6.11) and (6.12) preserve the locality of (2.8b) and (6.9).

We consider the following three discretization methods with stepsize $\mathbb{T} > 0$ to construct F, A, B_1, and B_2 matrices in (6.2a) approximating the continuous dynamics (6.12).

a) Impulse invariant discretization:

$$F \triangleq I_{m+2n},\ A \triangleq e^{\tilde{A}\mathbb{T}},\ B_s \triangleq \int_0^{\mathbb{T}} e^{\tilde{A}\tau}\mathrm{d}\tau\tilde{B}_s,\ s = 1,2, \tag{6.13}$$

b) Forward Euler discretization:

$$F \triangleq I_{m+2n},\ A \triangleq \mathbb{T}\tilde{A} + I_{m+2n},\ B_s \triangleq \mathbb{T}\tilde{B}_s,\ s = 1,2, \tag{6.14}$$

c) Backward Euler discretization:

$$F \triangleq I_{m+2n} - \mathbb{T}\tilde{A},\ A \triangleq I_{m+2n},\ B_s \triangleq \mathbb{T}\tilde{B}_s,\ s = 1,2, \tag{6.15}$$

where F should be invertible for uniqueness of solution of the discretized dynamics.

Note that with a fixed $\mathbb{T}$, the impulse invariant and backward Euler methods usually have better approximation accuracy than the forward Euler method. In fact, since all eigenvalues of $\tilde{A}$ have non-positive real part, a basic discretization requirement is that all eigenvalues of $F^{-1}A$ are in the unit circle to maintain stability. One can easily prove that the impulse invariant and backward Euler discretization always meet this requirement for any $\mathbb{T} > 0$, but the forward Euler method requires a sufficiently small $\mathbb{T}$ to preserve stability; therefore, with a same predicted time horizon $\tilde{t}$, the forward Euler method has the largest predicted step length N and hence makes the optimization problem **R** harder to solve. On the other hand, the backward Euler method might require a small enough $\mathbb{T}$ to guarantee the invertibility of F, but numerically we have found this to be easily satisfiable. Therefore, we set aside the forward Euler method from our considerations of discretization. On the other hand, the impulse invariant method fails to preserve the sparsity of $\tilde{A}$, $\tilde{B}_1$, and $\tilde{B}_2$, which are essential for the design of distributed solvers of **R**. Instead, the matrices F, A, B_1 and B_2 resulting from the backward Euler discretization are all sparse. This justifies our choice, throughout the rest of the chapter, of the backward Euler method for discretization.

6.2.3 Top-layer controller design

In this section we describe the top-layer controller. By design, cf. (6.2), the bottom-layer controller makes a trade-off between the control cost and the violation of frequency safety, and hence does not strictly guarantee the latter. This is precisely the objective of the top-layer controller: ensuring frequency safety at all times by slightly adjusting, if necessary, the effect of the bottom-layer controller. Formally, for every $i \in \mathscr{I}^{\omega}$, let $\bar{\gamma}_i, \underline{\gamma}_i > 0$, and $\underline{\omega}_i^{\text{thr}}, \bar{\omega}_i^{\text{thr}} \in \mathbb{R}$ with $\underline{\omega}_i < \underline{\omega}_i^{\text{thr}} < 0 < \bar{\omega}_i^{\text{thr}} < \bar{\omega}_i$. We use the design from [ZC19c] for the top layer. For $i \in \mathscr{I}^{\omega}$, $\alpha_{DF,i}(x(t), p)$ takes the form

$$\begin{cases} \min\{0, \frac{\bar{\gamma}_i(\bar{\omega}_i - \omega_i(t))}{\omega_i(t) - \bar{\omega}_i^{\text{thr}}} + v_i(x(t), p)\} & \omega_i(t) > \bar{\omega}_i^{\text{thr}}, \\ 0 & \underline{\omega}_i^{\text{thr}} \leqslant \omega_i(t) \leqslant \bar{\omega}_i^{\text{thr}}, \\ \max\{0, \frac{\underline{\gamma}_i(\underline{\omega}_i - \omega_i(t))}{\underline{\omega}_i^{\text{thr}} - \omega_i(t)} + v_i(x(t), p)\} & \omega_i(t) < \underline{\omega}_i^{\text{thr}}, \end{cases} \tag{6.16}$$

where

$$v_i(x(t), p) \triangleq E_i \omega_i(t) + [D^T]_i \sin(Y_b \lambda(t)) - p_i - \alpha_{BL,i}(t),$$

and for $i \in \mathscr{I} \setminus \mathscr{I}^{\omega}$, simply $\alpha_{DF,i} \equiv 0$. Note that this almost the same controller we proposed in Chapter 4, where the only difference is the addition of α_{BL}, and the class-$\mathscr{K}$ being linear for simplicity. Also, Based on our results in Chapter 4, one can easily shown that the top-layer controller can be implemented in a decentralized fashion, and is locally Lipschitz in x. For brevity, we may use $\alpha_{DF,i}(x(t), p)$ (respectively, $v_i(x(t), p)$) and $\alpha_{DF,i}(t)$ (respectively $v_i(t)$) interchangeably.

Each $\alpha_{DF,i}$, with $i \in \mathscr{I}^{\omega}$, behaves as a passive and myopic transient frequency regulator without prediction capabilities. We offer the following observations about its definition: first, $\alpha_{DF,i}$ only depends on local system information and does not incorporate any global knowledge;

second, $\alpha_{DF,i}$ vanishes as long as the current frequency is within $[\underline{\omega}_i^{\text{thr}}, \bar{\omega}_i^{\text{thr}}]$, a subset of the safe frequency interval, with no consideration for the possibility of future large disturbances; third, $\alpha_{DF,i}$ can be non-zero when the current frequency is out of $[\underline{\omega}_i^{\text{thr}}, \bar{\omega}_i^{\text{thr}}]$ and hence close to the safe frequency boundaries. However, this could also lead to over-reaction, especially when $\bar{\gamma}_i$ and $\underline{\gamma}_i$ are small, as the disturbance may disappear suddenly, in which case even without the top-layer controller, the frequency would remain safe afterwards. As pointed out above, the top-layer controller only steps in if the input from the bottom-layer controller is not sufficient to ensure frequency safety.

6.2.4 Frequency safety and local asymptotic stability

Having introduced the elements of both layers in Figure 6.1, we are now ready to show that the proposed centralized control strategy meets requirements (i)-(iv) in Section 6.1. We focus on the first two requirements, since we have already established the Lipschitz continuity of each individual component, and the MPC component by design takes care of the economic cooperation among the controlled buses.

With regard to stability, we here consider the following energy function for the closed-loop system,

$$\bar{V}(x) = V(x) + \frac{1}{2} \sum_{i \in \mathscr{J}^u} \alpha_{MPC,i}^2, \tag{6.17}$$

with V defined in (4.1).

Furthermore, define the level set

$$\mathscr{T}_\rho \triangleq \left\{ x \,\middle|\, \lambda \in \mathscr{R}_{\text{cl}},\, \bar{V}(x) \leqslant \rho c \right\}, \tag{6.18}$$

where $\rho \geqslant 0$ and $c \triangleq \min_{\tilde{\lambda} \in \partial \mathscr{R}} \bar{V}(\tilde{\lambda}, \mathbf{0}_n, \mathbf{0}_n)$. Now we are ready to prove that system (2.8) with

the proposed controller guarantees frequency safety and local asymptotic stability at the same time.

Theorem 6.2.6. *(Bilayered control with stability and frequency guarantees): Under condition* (2.9)*, assume that* $\varepsilon_i T_i < 1$ *for every* $i \in \mathscr{I}^u$*, then the system* (2.8) *with the bilayered controller defined by* (6.1)*,* (6.4)*,* (6.8)*,* (6.9)*, and* (6.16) *satisfies*

(i) for any $i \in \mathscr{I}^\omega$*, if* $\omega_i(0) \in [\underline{\omega}_i, \bar{\omega}_i]$*, then* $\omega_i(t) \in [\underline{\omega}_i, \bar{\omega}_i]$ *for every* $t \geqslant 0$*;*

(ii) for any $i \in \mathscr{I}^\omega$*, if* $\omega_i(0) \notin [\underline{\omega}_i, \bar{\omega}_i]$*, then there exists* t_0 *such that* $\omega_i(t) \in [\underline{\omega}_i, \bar{\omega}_i]$ *for every* $t \geqslant t_0$*. Furthermore,* $\omega_i(t)$ *monotonically approaches* $[\underline{\omega}_i, \bar{\omega}_i]$ *before entering it;*

(iii) if the initial state $(\lambda(0), \omega(0), \alpha_{BL}(0))$ *is in* $\mathscr{T}_\rho$ *for some* $0 < \rho < 1$*, then* $(\lambda(t), \omega(t), \alpha_{BL}(t))$ *stays in* $\mathscr{T}_\rho$ *for all* $t > 0$*, and converges to* $(\lambda_\infty, \mathbf{0}_n, \mathbf{0}_n)$*. Furthermore,* $\alpha(t)$*,* $\alpha_{BL}(t)$*, and* $\alpha_{TL}(t)$ *all converge to* $\mathbf{0}_n$ *as* $t \to \infty$*.*

Proof. by Lemma 4.2.3, it is easy to see that statement (i) is equivalent to asking that, for any $i \in \mathscr{I}^\omega$ at any $t \geqslant 0$,

$$\dot{\omega}_i(t) \leqslant 0 \text{ if } \omega_i(t) = \bar{\omega}_i, \tag{6.19a}$$

$$\dot{\omega}_i(t) \geqslant 0 \text{ if } \omega_i(t) = \underline{\omega}_i. \tag{6.19b}$$

For simplicity, we only prove (6.19a), and (6.19b) follows similarly. Note that by (2.8b), (6.1), and (6.16), one has

$$\begin{aligned}
\dot{\omega}_i(t) &= -E_i\omega_i(t) - [D^T]_i \sin(Y_b\lambda(t)) + p_i + \alpha_i(t) \\
&= -E_i\omega_i(t) - [D^T]_i \sin(Y_b\lambda(t)) + p_i + \alpha_{BL,i}(t) + \alpha_{DF,i}(t) \\
&= -v_i(t) + \alpha_{DF,i}(t).
\end{aligned}$$

Now if $\omega_i(t) = \bar{\omega}_i$, then $-v_i(t) + \alpha_{DF,i}(t) = -v_i(t) + \min\{0, v_i(t)\} \leqslant 0$; hence condition (6.19a) holds.

Note that (ii) follows from (i) and (iii). This is because, for any $i \in \mathscr{I}$, if ω_i converges to $0 \in (\underline{\omega}_i, \bar{\omega}_i)$, there must exist a finite time t_0 such that $\omega_i(t_0) \in [\underline{\omega}_i, \bar{\omega}_i]$, which, by (i), implies that $\omega_i(t) \in [\underline{\omega}_i, \bar{\omega}_i]$ at any $t \geqslant t_0$. We then prove statement (iii), To show the invariance of $\mathscr{T}_\rho$, first, it is easy to see that $c > 0$ by noticing that $\lambda_\infty \notin \partial\mathscr{R}$, and $V(\tilde{\lambda}, \mathbf{0}_n, \mathbf{0}_n)$ is non-negative, equaling 0 if and only if $\tilde{\lambda} = \lambda_\infty$. Next, we show that $\dot{\bar{V}} \leqslant 0$ for every $x \in \mathscr{T}_\rho$. We obtain after some computations that

$$\dot{\bar{V}} = -\omega^T(t) E \omega(t) + \sum_{i \in \mathscr{I}^\omega} \omega_i(t) \alpha_{DF,i}(t) - \sum_{i \in \mathscr{I}^u} \left(\frac{1}{T_i} \alpha_{BL,i}^2(t) - \alpha_{BL,i}(t) \hat{u}_{MPC,i}(t) \right).$$

Note that by the definition of α_{TL} in (6.16), $\omega_i(t)\alpha_{DF,i}(t) \leqslant 0$ holds for every $i \in \mathscr{I}^\omega$ at every $t \geqslant 0$, in that $\alpha_{DF,i}(t) = 0$ whenever $\underline{\omega}_i^{\text{thr}} \leqslant \omega_i(t) \leqslant \bar{\omega}_i^{\text{thr}}$, and $\alpha_{DF,i}(t) \geqslant 0$ (reps. $\leqslant 0$) if $\omega_i(t) \geqslant \bar{\omega}_i^{\text{thr}} > 0$ (respectively, $\omega_i(t) \leqslant \underline{\omega}_i^{\text{thr}} < 0$). Therefore, together with condition (6.10) in Lemma 6.2.3, we have

$$\dot{\bar{V}} \leqslant -\omega^T(t) E \omega(t) - \sum_{i \in \mathscr{I}^u} (\frac{1}{T_i} - \varepsilon_i) \alpha_{BL,i}^2(t) \leqslant 0,$$

and hence $\bar{V}(x(t)) \leqslant \rho c$ for all $t \geqslant 0$. Finally, by the definition of c, one can check that λ stays in $\mathscr{R}_{\text{cl}}$ all the time, otherwise there exists some $t \geqslant 0$ such that $\lambda(t) \in \partial\mathscr{R}$, resulting in $\bar{V}(x(t)) \geqslant c > \rho c$. Therefore, the set $\mathscr{T}_\rho$ is invariant.

The convergence of state follows by LaSalle Invariance Principle [Kha02, Theorem 4.4]. Specifically, $\omega(t)$ and $\alpha_{BL}(t)$ converge to $\mathbf{0}_n$ (notice that $\alpha_{BL,i} \equiv 0$ for each $i \in \mathscr{I} \backslash \mathscr{I}^u$). Next we show that $\lim_{t\to\infty} \alpha_{DF,i}(t) = 0$ for every $i \in \mathscr{I}^\omega$, which implies that $\lim_{t\to\infty} \alpha_{TL}(t) = \mathbf{0}_n$ as $\alpha_{DF,i} \equiv 0$ for each $i \in \mathscr{I} \backslash \mathscr{I}^\omega$. This simply follows from (6.16) since $\alpha_{DF,i}(t) = 0$ whenever $\underline{\omega}_i^{\text{thr}} \leqslant \omega_i(t) \leqslant \bar{\omega}_i^{\text{thr}}$, where $0 \in (\underline{\omega}_i^{\text{thr}}, \bar{\omega}_i^{\text{thr}})$, and we have shown that $\lim_{t\to\infty} \omega(t) = \mathbf{0}_n$. The convergence of $\alpha(t)$ follows by its definition (6.1). □

Remark 6.2.7. *(Independence of controller on equilibrium point):* It should be pointed out that in Theorem 6.2.6, the proposed controller is able to locally stabilize the system without a priori knowledge on the steady-state voltage angle λ_∞. Specifically, both α_{BL} and α_{TL} are not functions of λ_∞. •

Remark 6.2.8. *(Control framework without bottom layer):* We have shown in Chapter 4 that the top-layer controller by itself makes the closed-loop system meet all requirements except for the economic cooperation. Such a lack of cooperation can be observed in two aspects. First, since α_{TL} is only defined for nodes in $\mathscr{I}^\omega$, those in $\mathscr{I}^u \backslash \mathscr{I}^\omega$ do not get involved in controlling frequency transients. Second, the top-layer control is a non-optimization-based state feedback, where each $\alpha_{DF,i}$ with $i \in \mathscr{I}^\omega$ is merely in charge of controlling the transient frequency for its own node i. •

6.3 Controller decentralization

The centralized bilayered controller meets the requirements (i)-(iv) stated in Section 6.1. In this section, we focus on the requirement (v) on the distributed implementation of the controller. While introducing each controller component in Figure 6.1, our discussion has shown that only the MPC component requires access to global system information, whereas all other components can be implemented in a distributed fashion. In this section, we show that by having each node and edge communicate within its 2-hop neighbors, one can solve the optimization problem **R** in (6.2) online and hence exactly recover the MPC component $\hat{u}^*$ in (6.4). The key idea is to properly assign the decision variables in the optimization problem to each node so that the cost function can be represented as sum of local costs and the constraints can be written locally. Once this is in place, we report to saddle-point dynamics to find the solution of **R** in a distributed way.

6.3.1 Strong convexification of the objective function

We start here by transforming the optimization problem **R** into an equivalent form whose objective function is strongly convex in all its arguments. Such property is useful later when characterizing the convergence properties of distributed algorithm to the optimizer. Formally, let

$$g^{\text{aug}}(\hat{X},\hat{u},\mathscr{B}) \triangleq \sum_{k=1}^{N-1} \|F\hat{x}(k+1) - A\hat{x}(k) - B_1\hat{p}^{fcst}(k) - B_2\hat{u}\|_2^2 + \sum_{k=1}^{N}\left(\sum_{i\in\mathscr{I}} c_i\hat{\alpha}_{BL,i}^2(k) + \sum_{i\in\mathscr{I}^\omega} d_i\beta_i^2(k)\right) + \|\hat{x}(0) - x(\Delta^w)\|_2^2. \tag{6.20}$$

We denote by $\mathbf{R}^{\text{aug}}$ the optimization problem with objective function g^{aug} and constraints given by (6.2a)-(6.2e). Letting $Y \triangleq (\hat{X},\hat{u},\mathscr{B}) \in \mathbb{R}^{(m+2n+|\mathscr{I}^\omega|)N+n}$, we can re-write $\mathbf{R}^{\text{aug}}$ into the following compact form

$$\begin{aligned} &\min_Y \frac{1}{2}Y^THY + f^TY + a \\ \text{s.t.}\quad & S_1Y \leqslant s_1, && (6.21a)\\ & S_2Y = s_2, && (6.21b)\end{aligned}$$

for suitable

$$\begin{aligned} &H \in \mathbb{R}^{((m+2n+|\mathscr{I}^\omega|)N+n)\times((m+2n+|\mathscr{I}^\omega|)N+n)}, \quad f \in \mathbb{R}^{(m+2n+|\mathscr{I}^\omega|)N+n}, \qquad a \in \mathbb{R},\\ &S_1 \in \mathbb{R}^{(2|\mathscr{I}^\omega|N+2|\mathscr{I}^u|)\times((m+2n+|\mathscr{I}^\omega|)N+n)}, \quad S_2 \in \mathbb{R}^{((m+2n)N+n-|\mathscr{I}^u|)\times((m+2n+|\mathscr{I}^\omega|)N+n)},\\ &s_1 \in \mathbb{R}^{2|\mathscr{I}^\omega|N+2|\mathscr{I}^u|}, \qquad s_2 \in \mathbb{R}^{(m+2n)N+n-|\mathscr{I}^u|}.\end{aligned}$$

The next result shows the equivalence between **R** and $\mathbf{R}^{\text{aug}}$.

Lemma 6.3.1. *(Equivalent transformation to strong convexity): The optimization problem* **R** *and* $\mathbf{R}^{aug}$ *posses exactly the same optimal solution. Furthermore, if F is invertible, then* g^{aug} *is*

strongly convex in $(\hat{X}, \hat{u}, \mathscr{B})$.

Proof. The equivalence between $\mathbf{R}$ and $\mathbf{R}^{\text{aug}}$ follows by noting that g^{aug} corresponds to augmenting g with equality constraints. For notational simplicity, we assume that $c_i = 1$ for all $i \in \mathscr{I}$ and $d_i = 1$ for all $i \in \mathscr{I}^{\omega}$ (the proof holds for general positive values with minor modifications). To show strong convexity, one can write H as an upper-triangular block matrix, whose diagonal matrices are $F^T F + J^T J$, $F^T F + A^T A + J^T J$, $A^T A + J^T J$, $B_2^T B_2$, and $I_{|\mathscr{I}^{\omega}|N}$, where $J \in \mathbb{R}^{(m+2n)\times n}$ is a matrix mapping the whole state $\hat{x}$ to the partial state $\hat{\alpha}_{BL}$, i.e., $\hat{\alpha}_{BL} = J\hat{x}$. It is easy to see that both J and B_2 are full-column-rank matrices, which, together with the invertibility assumption on F, implies that all five matrices are positive definite. Hence, all eigenvalues of H are real and strictly positive, leading to strong convexity of g^{aug}, as claimed. □

6.3.2 Separable objective with locally expressible constraints

Next, we explain how the problem data defining the optimization $\mathbf{R}^{\text{aug}}$ has a structure that makes it amenable to distributed algorithmic solutions. We start by assigning the decision variables $Y = (\hat{X}, \hat{u}, \mathscr{B})$ in $\mathbf{R}^{\text{aug}}$ to the nodes and edges in the network. We partition the states into voltage angle difference, frequency, and low-pass filter state, i.e., $\hat{x} = (\hat{\lambda}, \hat{\omega}, \hat{\alpha}_{BL})$. For every $k \in [0, N]_{\mathbb{N}}$, $i \in [1, n]_{\mathbb{N}}$, and $j \in [1, m]_{\mathbb{N}}$, we assign $\omega_i(k)$, $\hat{u}_i$, and $\hat{\alpha}_{BL,i}(k)$ to the ith node, and $\hat{\lambda}_j(k)$ to the jth edge. For every $i \in \mathscr{I}^{\omega}$, we assign $\beta_i(k)$ to the ith node. In the subsequent discussion, we say a constraint or function is *local* for the power network $\mathscr{G}$ if its decision variables are all from either of the following two cases: a) a node $i \in \mathscr{I}$ and its neighboring edges $(i, j) \in \mathscr{E}$, and b) an edge $(i, j) \in \mathscr{E}$ and its neighboring nodes i and j. We claim that

(i) if F, A, B_1 and B_2 are determined by (6.15), then every constraint in (6.2) is local.

(ii) the objective function g^{aug} can be written as a sum of local objective functions.

To see (i), note that (6.2b)-(6.2e) are a collection of constraints, each depending only on variables owned by a single node. Constraint (6.2a) is also local by noticing the following

two points. First, the dynamics of each state in (6.11) is uniquely determined by the states of its neighbors. Second, we have shown in Section 6.2.2 that the backward Euler discretization (6.15) preserves locality. To see (ii), first note that the sum of $\alpha^2_{BL,i}(k)$ (respectively, $\beta^2_i(k)$) over i is naturally the sum of local variables. Second, the two-norm square of $F\hat{x}(k+1) - A\hat{x}(k) - B_1\hat{p}^{fcst}(k) - B_2\hat{u}$ for every $k \in [1, N-1]_{\mathbb{N}}$ is the sum of square of all its $m+2n$ entries, where each entry is local due to the locality of discretized dynamics. Similarly, $\|\hat{x}(0) - x(\Delta^w)\|_2^2$ is also the sum of local variables.

6.3.3 Distributed implementation via saddle-point dynamics

Here we introduce a saddle-point dynamics to recover the unique optimal solution Y^* of $\mathbf{R}^{\text{aug}}$ in a distributed fashion. We start from the Lagrangian of $\mathbf{R}^{\text{aug}}$

$$\mathfrak{L}(Y, \eta, \mu) = g^{\text{aug}}(Y) + \eta^T(S_1 Y - s_1) + \mu^T(S_2 Y - s_2), \tag{6.22}$$

where $\eta \in \mathbb{R}_{\geqslant 0}^{2|\mathscr{I}^\omega|N+2|\mathscr{I}^u|}$ and $\mu \in \mathbb{R}^{(m+2n)N+n-|\mathscr{I}^u|}$ are the Lagrangian multiplier corresponding to constraints (6.21a) and (6.21b), respectively. Note that we have shown that a) $\mathbf{R}$ is feasible (cf. Proposition 6.2.2), b) $\mathbf{R}$ and $\mathbf{R}^{\text{aug}}$ are equivalent (cf. Lemma 6.3.1), and c) all constraints in $\mathbf{R}^{\text{aug}}$ are linear. These three points together imply that the refined Slater condition and strong duality hold, [BV04, Section 5.2.3], which further implies that at least one primal-dual solution (Y^*, η^*, μ^*) of $\mathbf{R}^{\text{aug}}$ exists, and the set of primal-dual solutions is exactly the set of saddle points of $\mathfrak{L}$ on the set $\mathbb{R}^{(m+2n+|\mathscr{I}^\omega|)N+n} \times (\mathbb{R}_{\geqslant 0}^{2|\mathscr{I}^\omega|N+2|\mathscr{I}^u|} \times \mathbb{R}^{(m+2n)N+n-|\mathscr{I}^u|})$ [BV04, Section 5.4.2]. Therefore, one can apply the saddle-point dynamics [CMLC18] to recover one solution (Y^*, η^*, μ^*), where $\hat{u}^*$ is the MPC output signal we need. Formally, the saddle-point dynamics of $\mathbf{R}^{\text{aug}}$ is

$$\varepsilon_Z \frac{dZ}{d\tau} = -\nabla_Z \mathfrak{L}(Z, \eta, \mu) = -(HZ + f + S_1^T \eta + S_2^T \mu), \tag{6.23a}$$

$$\varepsilon_\eta \frac{d\eta}{d\tau} = [\nabla_\eta \mathfrak{L}(Z,\eta,\mu)]_\eta^+ = [S_1 Z - s_1]_\eta^+, \tag{6.23b}$$

$$\varepsilon_\mu \frac{d\mu}{d\tau} = \nabla_\mu \mathfrak{L}(Z,\eta,\mu) = S_2 Z - s_2, \tag{6.23c}$$

where ε_Z, ε_η, and ε_μ are tunable positive scalars.

Given the strong convexity of g^{aug}, the following result states the global convergence of the dynamics (6.23), and its proof directly follows from [CMLC18, Theorem 4.2].

Theorem 6.3.2. *(Global asymptotic convergence of saddle-point dynamics): Starting from any initial condition $(Z(0),\eta(0)\mu(0))$, it holds that $Z(\tau)$ globally asymptotically converges to the unique optimal solution Y^* of $\mathbf{R}^{aug}$.*

To conclude, we justify how the saddle-point dynamics (6.23) can be implemented in a distributed fashion to recover Y^*. We first assign (Z,η,μ) to different nodes and edges. In (6.23), the primal variable Z corresponds to Y, and its assignment is exactly the same, as discussed at the beginning of Section 6.3.2. Since all constraints are local with respect to a node or an edge, we assign each entry of (η,μ) to the corresponding node or edge. With this assignment, and due to locality, the dual variables dynamics (6.23b) and (6.23c) are distributed, i.e., for each entry of η or μ, if it belongs to a node (respectively, edge), then its time derivative only depends on primal and dual variables of its own and of neighboring edges (respectively, nodes). On the other hand, the primal dynamics (6.23a) requires 2-hop communication, i.e., for each entry of Z, if it belongs to a node (respectively, edge), then its time derivative depends on primal and dual variables of its neighboring nodes (respectively, edges).

Remark 6.3.3. *(Time scale in saddle-point dynamics):* Since the MPC component updates its output at time instants $\{\Delta^w\}_{w\in\mathbb{N}}$ according to (6.4), a requirement on the saddle-point dynamics (6.23) solving $\mathbf{R}$ (or equivalently $\mathbf{R}^{\text{aug}}$) is that it returns the optimal solution within $\Delta^{w+1}-\Delta^w$ seconds starting from Δ^w for every $w\in\mathbb{N}$. To achieve this, one may tune ε_Y, ε_η, and ε_μ to accelerate the convergence of the saddle-point dynamics. In practice, this corresponds to run-

ning (6.23) on a faster time scale, which puts requirements on the hardware regarding communication bandwidth and computation time. •

Remark 6.3.4. *(Comparison with controller with regional coordination based on network decomposition):* The proposed distributed algorithm treats each bus and transmission line as an agent, and recovers the optimal solution by allowing each agent to exchange information only with its neighbors.In Chapter 5 and our previous work [ZC19d], we have proposed an alternative algorithm that does not rely on participation of every agent at the expense of not recovering the global optimal solution. The basic idea of this alternative implementation is to consider a set of regions in the network. Each region, independently of the rest, possesses its own centralized controller in charge of gathering regional information and broadcasting control signals to controllers within the region. To account for the couplings in the dynamics, flows that connect a region and the rest of the network are assumed constant when computing the controller in each region. Although there can be nodes and edges shared by multiple regions, the control signal regulated on a shared node belongs to only one region. This implementation does not recover the exact optimal solution and only ensures partial cooperation among the control inputs. •

6.4 Simulations

We verify our results on the IEEE 39-bus power network shown in Figure 3.3. All parameters in the power network dynamics (2.8) still come from the Power System Toolbox [CCR09] used in the Chapter 4 and 5. Let $\mathscr{I}^{\omega} = \{30, 31, 32, 37\}$ be four generator buses with transient frequency requirements. The safe frequency region is $[\underline{\omega}_i, \bar{\omega}_i] = [-0.2Hz,\ 0.2Hz]$ for every $i \in \mathscr{I}^{\omega}$ (as ω corresponds to the shifted frequency, the safe frequency region without shifting is thus $[59.8Hz,\ 60.2Hz]$). Let $\{3, 7, 25\}$ be another three non-generator buses that can provide control signals, so that $\mathscr{I}^{u} = \{3, 7, 25, 30, 31, 32, 37\}$. To set up the optimization problem (6.2) used in the MPC component (6.4), we use (6.15) for the discretization. The controller parameters are

Table 6.1: Controller parameters.

parameter	value	parameter	value
$\tilde{t}$	$10s$	$p_t^{fcst}(\tau),\ \forall \tau \in [t, t+\tilde{t}]$	$p(\tau)$
$\mathbb{T}$	$0.2s$	$c_i,\ \forall i \in \mathscr{I}^{\omega}$	4
N	50	$c_i,\ \forall i \in \mathscr{I}^{u} \backslash \mathscr{I}^{\omega}$	1
d	100	$\Delta^w,\ \forall w \in \mathbb{N}$	w
$\varepsilon_i,\ \forall i \in \mathscr{I}^{u}$	1.9	$\bar{\gamma}_i$ and $\underline{\gamma}_i,\ \forall i \in \mathscr{I}^{\omega}$	1
$T_i,\ \forall i \in \mathscr{I}^{u}$	$0.5s$	$\bar{\omega}_i^{\text{thr}}$ and $-\underline{\omega}_i^{\text{thr}}$	$0.1Hz$

summarized in Table 6.1. In addition, we apply the saddle-points dynamics (6.23) to generate the output of the MPC component in a distributed fashion.

We first show that the bilayered controller defined by (6.1), (6.4), (6.8), (6.9), (6.16) is able to maintain the transient frequency of selected nodes within the safe region without changing the equilibrium point (cf. Theorem 6.2.6(i) and (iii)). Although in the dynamics (2.8) we assume that the power injection is constant, in simulations we perturb all non-generator nodes by a time-varying power injection. Specifically, for every $i \in [1,29]_{\mathbb{N}}$, let $p_i(t) = (1+\delta(t))p_i(0)$ where

$$\delta(t) = \begin{cases} 0.2\sin(\pi t/50) & \text{if } 0 \leqslant t \leqslant 25, \\ 0.2 & \text{if } 25 < t \leqslant 125, \\ 0.2\sin(\pi(t-100)/50) & \text{if } 125 < t \leqslant 150, \\ 0 & \text{if } 150 < t. \end{cases}$$

The deviation $\delta(t)p_i(0)$ has both fast ramp-up and ramp-down periods and a long intermediate constant period. We have chosen it this way to test the capability of the controller against both slow-varying and fast-varying disturbances. Figure 6.2(a) shows the open-loop frequency responses of nodes 30, 31, 32, and 37 (i.e., nodes with the frequency safety requirement). All four frequency trajectories, which almost overlap with each other, exceed the lower safe fre-

quency bound $59.8Hz$. However, with the controller enabled, in Figure 6.2(b), their frequencies all evolve within the safe region, and they all return to $60Hz$ as the disturbance disappears. Figure 6.2(c) shows the corresponding control signals. Note that, due to our specific choice of c_i's, the controller tends to use more non-generator control signals (i.e., α_3, α_7, and α_{25}) than generator ones (i.e., α_{31}, α_{32}, α_{33}, and α_{37}). Also, note that they split into two groups and the control signals within each group possess almost the same trajectories.

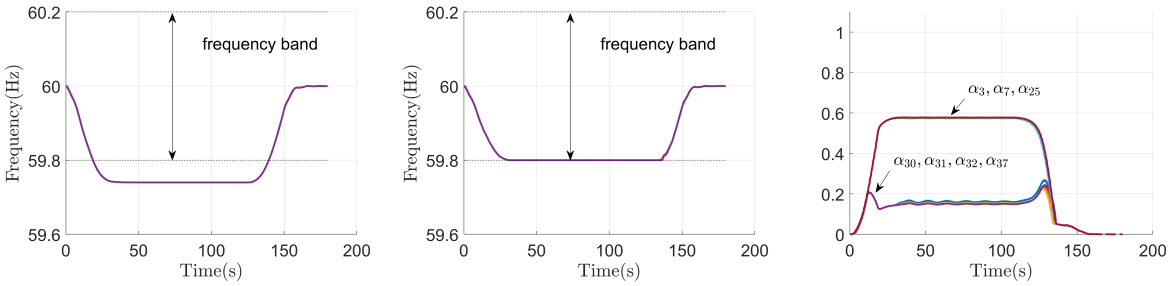

Figure 6.2: Frequency and control input trajectories with and without transient frequency control.

Next we compare the performance of the proposed controller with other approaches. Figures 6.3(a) and (b) show the frequency trajectories and control signals using the controller with regional coordination based on network decomposition proposed in Chapter 5. As mentioned in Remark 6.3.4, although this controller achieves frequency safety, it only allows control cooperation within a limited region, instead of the entire network. This can be seen from Figure 6.3(b), where, with the same control cost coefficients (cf. Table 6.1), the two groups of control trajectories are not as uniform as those in Figure 6.2(c) and have a larger magnitude. Figures 6.3(c) and (d) are the frequency and control trajectories with only the top-layer controller, as proposed in Chapter 4, cf. Remark 6.2.8. Since it is a non-optimization-based control strategy, each control signal does not cooperate with others. In this specific scenario, the top-layer controller leads to fluctuations even during the time interval [25,125]s, when the disturbance is constant. This is because the top-layer controller is myopic, without further consideration for the effects of the

rest of the network. The economic advantage of the proposed bilayered control can be also seen by computing the overall control cost over [0,180]s of the proposed controller, the controller in [ZC19d], and the controller in Chapter 4, which are 163.60, 231.13 and 656.68, respectively.

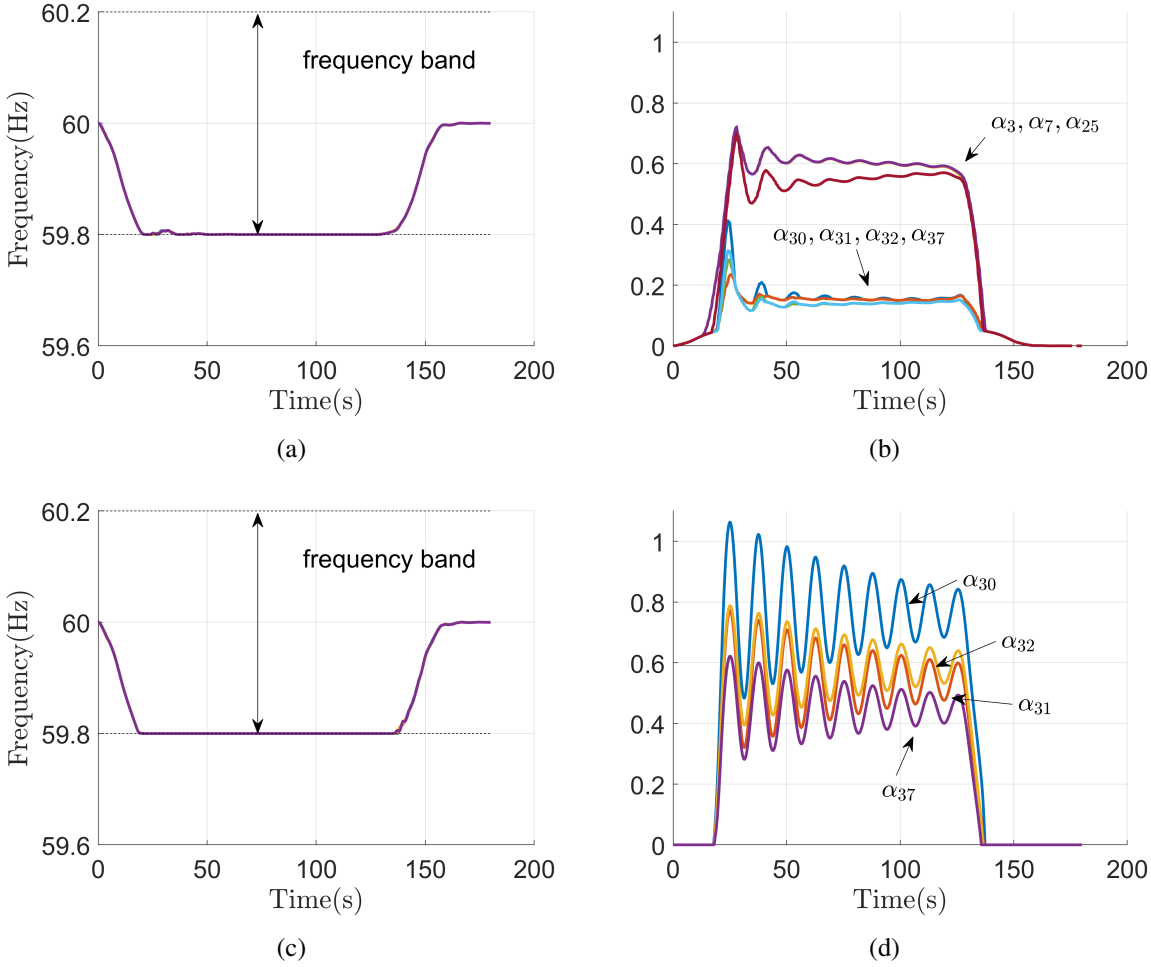

Figure 6.3: Comparison of frequency and control input trajectories with other approaches.

Next, we examine the role of the bottom and top layers in determining the value of the input signal of our distributed controller. For node 30, Figure 6.4(a) shows that $\alpha_{BL,30}$ is responsible for the larger share in the overall control signal α_{30}, whereas $\alpha_{TL,30}$ provides a slightly tuning during most of the time. If we reduce the penalty d_{30} from 100 to 10, in Figure 6.4(b), the dominance of $\alpha_{BL,30}$ decreases, in accordance with our discussion in Remark 6.2.1. On the

contrary, if we raise d_{30} to 1000, the contribution of the top layer becomes much smaller, as shown in Figure 6.4(c). Figure 6.4(d) shows how the saddle-point dynamics (6.23) converges to the value of $u_{MPC,30}(50)$ starting from an initial guess. Here we have used $\varepsilon_Z = 5 \cdot 10^{-4}$ and $\varepsilon_\eta = \varepsilon_\mu = 2.5 \cdot 10^{-4}$ to ensure convergence is attained within $1s$, cf. Table 6.1.

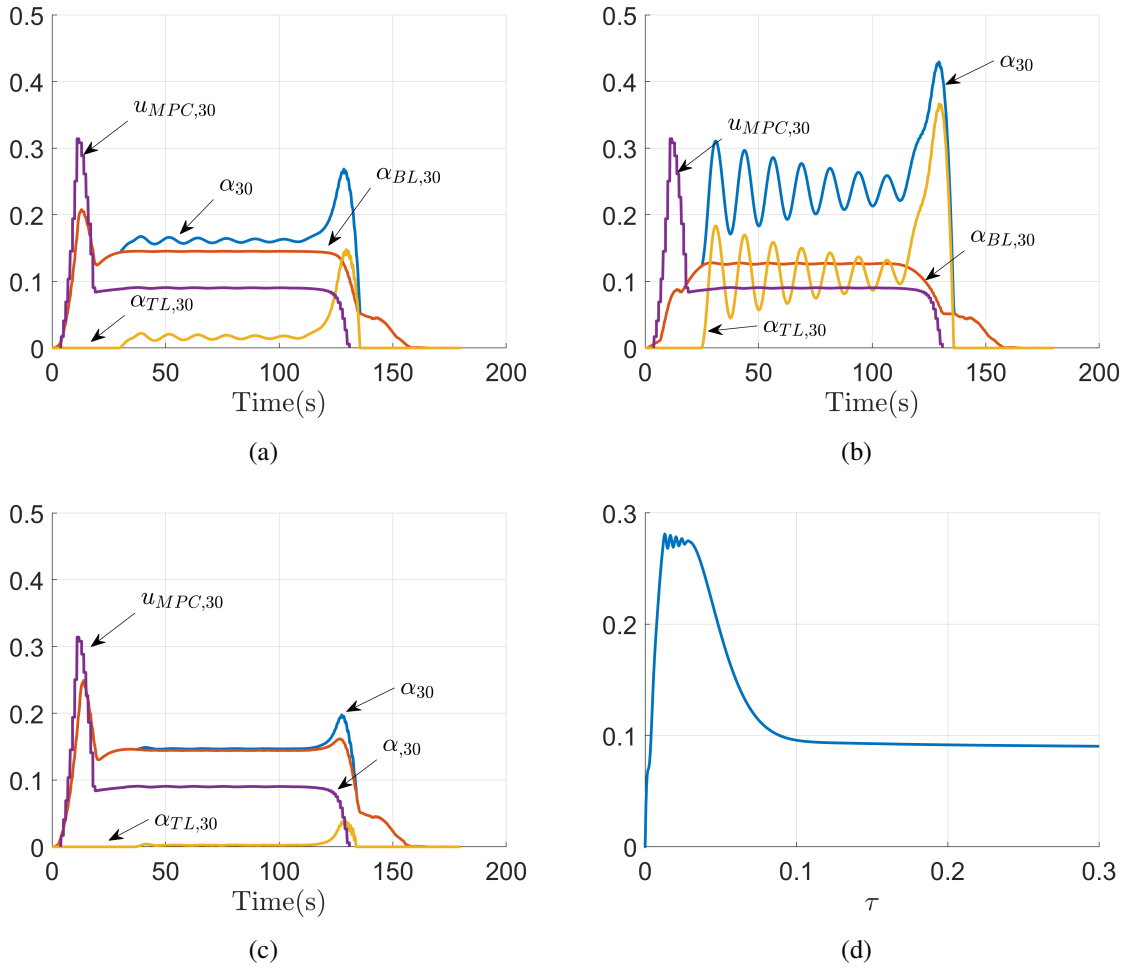

Figure 6.4: Decomposition of the control signal at node 30.

Lastly, we show that the distributed controller is able to steer the frequency to the safe region from unsafe initial conditions. To do this, we consider the set-up of Figure 3.6 but intentionally disable the controller for the first 30 seconds. For clarity, we only show the frequency and control trajectories at node 30 in Figure 6.5(a). Note that the frequency quickly moves

above the safe lower bound after the controller becomes active at $t = 30$s. Figure 6.5(b) shows the control signal, where after some brief transient, $\alpha_{BL,30}$ still dominates the overall control signal.

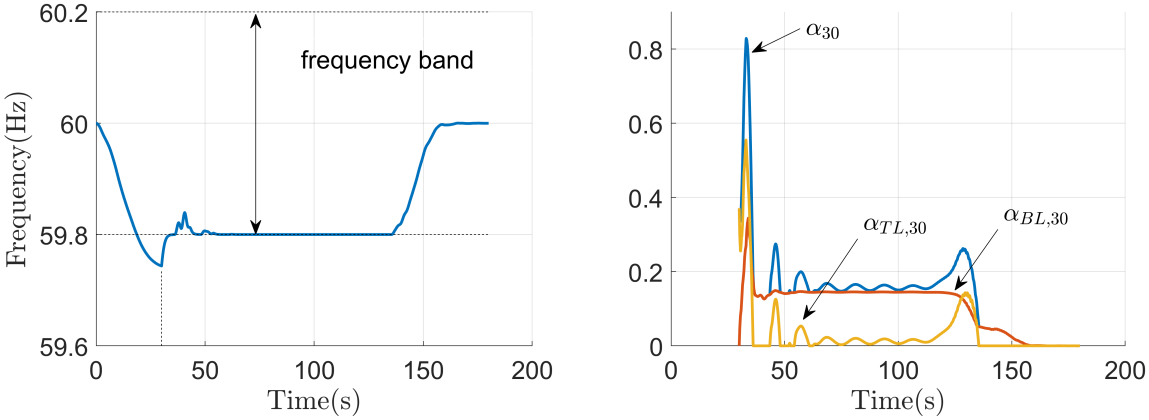

(a) (b)

Figure 6.5: Frequency and control input trajectories at node 30 when the controller is only turned on after 30s. In plot (a), the frequency gradually comes back to the safe region once the controller kicks in. Plot (b) shows the control signals.

Chapter 7

Closing remarks

The work of this thesis is motivated by the emerging issues in transient-state estimation and control raised by the integration of low-inertia renewables into the power grid. This thesis has started from analyzing transient-state safety subject to disturbances, and then proposed three transient frequency controllers, followed by discussions and extensions from robustness, control cost, and distributed implementation.

7.1 Conclusions

In Chapter 3, we have considered the problem of efficiently describing the set of disturbances to a power network that do not affect its transient-state safety in terms of frequency and power flow. Under the assumption that a bound on the amplitude of the disturbance is available, we have devised a sampling method to provide inner and outer approximations of the transient-state tolerableness set. These approximations can be computed with arbitrary accuracy, at the cost of increasing the computational complexity. We have also introduced a metric to measure the approximation gap and designed an algorithm to optimize it for a given fixed number of sampling points.

Going beyond transient-state analysis and further controlling transient frequency, from

Chapter 4 to Chapter 6, we have proposed three different distributed controllers. By establishing and enforcingconditions on set invariance and set attractivity, we have shown that all three controllers are able to maintain the nodal frequency of actuated buses within a desired safe region and to recover from undesired initial conditions. Meanwhile, they preserve network asymptotic stability without shifting the open-loop equilibrium point. In detail, we have shown that the controller proposed in Chapter 4 is Lipschitz continuous, robust against measurement uncertainty, and simple for implementation, as it requires no communication among control signals regulating on different buses; however, this controller turns out to be myopic, possessing no prediction capability, and this may lead to over-reaction and overuse of the control resources. To this aspect, we proposed the MPC-based controller in Chapter 5 that takes control cost into account. Through network partition and a careful treatment on transmission lines connecting different regions, we showed that the controller can be implemented in a partially distributed fashion—each region, independently of the rest, possesses its own centralized controller in charge of gathering regional information and broadcasting control signals to controllers within the region. Finally, we propose a bilayer controller in Chapter 6. Adopting a receding horizon approach, the bottom-layer controller periodically updates its output, enabling global cooperation among buses to reduce the overall control effort while respecting stability and soft frequency constraints. The top-layer controller, as a continuous state feedback controller, tunes the output of the bottom-layer control signal as required to rigorously enforces frequency safety and attractivity. We have shown that the entire control structure can be implemented in a distributed fashion, where the control signal can be computed by having nodes interact with up to 2-hop neighbors in the power network. The bilayer controllers inherit most of the advantages from the previous two controllers without having their disadvantages: unlike the short-sighted controller in Chapter 4, the bilayer controller is cable of predicting future disturbance and hence optimally and globally schedules control resources; unlike the MPC-based controller in Chapter 5, the bilayer controller is provably Lipschitz in system state, fully distributed, and computationally easy to implement.

7.2 Future work

Although this thesis is all about transient-state analysis and transient frequency control, it still leaves (and creates more!) research directions. Here we list a few possible topics.

For the transient-state analysis, due to the need of finding the explicit solution of power network dynamics, our current result is established on a linearized dynamical model. To this aspect, it would be interesting to quantify the difference between the tolerableness sets of the nonlinear swing dynamics and its linearized version. In addition, we assume that the disturbance can be modeled as the multiplication of a trajectory form and its independent time-invariant amplitude. Future work may relax the assumption by allowing trajectory-coupled and time-varying amplitude.

The three transient frequency controllers proposed in this thesis have their own work worthy investigation. In Chapter 4, it would be interesting to further explore the analysis of the effect of actuator dynamics of the generators on the guarantees on transient frequency and performance of our controller, and the understanding of the connection between actuation effort and network connectivity. For the controller in Chapter 5, we may quantify the optimality loss during the process of convexification in the open-loop optimization problem, and study the trade-offs between discretization accuracy, reference trajectory qualification, and computational complexity. Future work for Chapter 6 will explore the optimization of the sampling sequences employed in the bottom layer to improve performance, the quantitative evaluation of the contributions of the top- and bottom-layer control signals, and the acceleration of saddle-point dynamics to reduce the communication burden. Interestingly, since the choice of prediction model in the bottom layer cannot affect system closed-loop stability or frequency safety, this presents opportunities for incorporating system identification and machine learning techniques to progressively improve the prediction model quality.

With regards to the controllers proposed in this thesis, there are common theoretical as-

pects requiring more analysis. Since the underlying power network model we considered ignores the dynamical influence of voltage and reactive power on voltage angle and frequency, it would be interesting to extend the current results to more realistic models. Future work will also extend transient frequency control to the control of transient states consisting of frequency, power flow, and voltage. In a broader context, we may extend the proposed control methodologies to other safety-critical systems to improve transient behavior during stabilization.

Bibliography

[AA09] A. Alessio and B. Alberto. A survey on explicit model predictive control. In *Nonlinear Model Predictive Control*, pages 345–369. Springer, 2009.

[ACE+19] A. D. Ames, S Coogan, M. Egerstedt, G. Notomista, K. Sreenath, and P. Tabuada. Control barrier functions: Theory and applications. *arXiv preprint arXiv:1503.01160*, 2019.

[Alt14] M. Althoff. Formal and compositional analysis of power systems using reachable sets. *IEEE Transactions on Power Systems*, 29(5):2270–2280, 2014.

[AM06] A. Alam and E.B. Makram. Transient stability constrained optimal power flow. In *IEEE Power and Energy Society General Meeting*, Montreal, Canada, June 2006. Electronic proceedings.

[AMA13] M. Anghel, F. Milano, and P. Antonis. Algorithmic construction of Lyapunov functions for power system stability analysis. *IEEE Transactions on Circuits and Systems I: Regular Papers*, 60(9):2533–2546, 2013.

[AMDM01] F. L. Alvarado, J. Meng, C. L. DeMarco, and W. S. Mota. Stability analysis of interconnected power systems coupled with market dynamics. *IEEE Transactions on Power Systems*, 10(4):695–701, 2001.

[ÅströmK14] K. J. Åström and P. R. Kunmar. Control: a perspective. *Automatica*, 50(1):3–42, 2014.

[AXGT17] A. D. Ames, X. Xu, J. W. Grizzle, and P. Tabuada. Control barrier function based quadratic programs for safety critical systems. *IEEE Transactions on Automatic Control*, 62(8):3861–3876, 2017.

[BCM09] F. Bullo, J. Cortés, and S. Martinez. *Distributed Control of Robotic Networks*. Applied Mathematics Series. Princeton University Press, 2009. Electronically available at `http://coordinationbook.info`.

[BDS98] R. F. Baumeister, K. Dale, and K. L. Sommer. Freudian defense mechanisms and empirical findings in modern social psychology: reaction formation, projection, displacement, undoing, isolation, sublimation, and denial. *American Journal of*

Psychiatry, 66(6):1081–1124, 1998.

[BH81] A. R. Bergen and D. J. Hill. A structure preserving model for power system stability analysis. *IEEE Transactions on Power Apparatus and Systems*, 100(1):25–35, 1981.

[Big94] N. Biggs. *Algebraic Graph Theory*. Cambridge University Press, 2 edition, 1994.

[BLH15] T. S. Borsche, T. Liu, and D. J. Hill. Effects of rotational inertia on power system damping and frequency transients. In *IEEE Conf. on Decision and Control*, pages 5940–5946, Osaka, Japan, 2015.

[BLR+10] A. Brooks, E. Lu, D. Reicher, C. Spirakis, and B. Weihl. Demand dispatch. *IEEE Power and Energy Magazine*, 8(3):20–29, 2010.

[BM08] F. Blancini and S. Miani. *Set-theoretic Methods in Control*. Birkhäuser, Boston, MA, 2008.

[Bor03] F. Borrelli. *Constrained Optimal Control of Linear and Hybrid Systems*. Springer, New York, 2003.

[BS93] J. Bowen and V. Stavridou. Safety-critical systems, formal methods and standards. *Software Engineering Journal*, 8(4):189 – 209, 1993.

[BS16] Q. Ba and K. Savla. On distributed computational approaches for optimal control of traffic flow over networks. In *Allerton Conf. on Communications, Control and Computing*, pages 1102–1109, Monticello, IL, 2016.

[But08] J. C. Butcher. *Numerical Methods for Ordinary Differential Equations*. Wiley, New York, 2nd edition, 2008.

[BV04] S. Boyd and L. Vandenberghe. *Convex Optimization*. Cambridge University Press, 2004.

[CCR09] K. W. Cheung, J. Chow, and G. Rogers. *Power System Toolbox, v 3.0*. Rensselaer Polytechnic Institute and Cherry Tree Scientific Software, 2009.

[CDG12] Y. C. Chen and A. D. Domínguez-García. A method to study the effect of renewable resource variability on power system dynamics. *IEEE Transactions on Power Systems*, 27(4):1978–1989, 2012.

[CH08] C. Cao and N. Hovakimyan. Design and analysis of a novel L1 adaptive control architecture with guaranteed transient performance. *IEEE Transactions on Automatic Control*, 53(2):586–591, 2008.

[CJKT02] E. Camponogara, D. Jia, B.H. Krogh, and S. Talukdar. Distributed model predictive control. *IEEE Control Systems*, 22(1):44–52, 2002.

[CMLC18] A. Cherukuri, E. Mallada, S. H. Low, and J. Cortés. The role of convexity in saddle-point dynamics: Lyapunov function and robustness. *IEEE Transactions on Automatic Control*, 63(8):2449–2464, 2018.

[CSD16] H. Choi, P. J. Seiler, and S. V. Dhople. Propagating uncertainty in power-system DAE models with semidefinite programming. *IEEE Transactions on Power Systems*, 32(4):3146–3156, 2016.

[CWV94] H.-D. Chiang, F. F. Wu, and P. P. Varaiya. A BCU method for direct analysis of power system transient stability. *IEEE Transactions on Power Systems*, 9(3):1194–1208, 1994.

[Dan06] T. Dang. Approximate reachability computation for polynomial systems. In J. P. Hespanha and A. Tiwari, editors, *Hybrid Systems: Computation and Control*, volume 3927 of *Lecture Notes in Computer Science*, pages 138–152. Springer, Santa Barbara, CA, 2006.

[Dar05] F. Darema. Grid computing and beyond: The context of dynamic data driven applications systems. *Proceedings of the IEEE*, pages 692–697, 2005.

[DB12] F. Dörfler and F. Bullo. Synchronization and transient stability in power networks and nonuniform Kuramoto oscillators. *SIAM Journal on Control*, 50(3):1616–1642, 2012.

[DCB13] F. Dörfler, M. Chertkov, and F. Bullo. Synchronization in complex oscillator networks and smart grids. *Proceedings of the National Academy of Sciences*, 110(6):2005–2010, 2013.

[DK08] J. Driesen and F. Katiraei. *Design for distributed energy resources*, 6(3):30–40, 2008.

[DN11] A. S. Deese and C. O. Nwankpa. Utilization of FPAA technology for emulation of multiscale power system dynamics in smart grids. *IEEE Transactions on Smart Grid*, 2(4):606–614, 2011.

[DSSPG19] F. Dörfler, S.Bolognani, J. W. Simpson-Porco, and S. Grammatico. Distributed control and optimization for autonomous power grids. In *European Control Conference*, Naples, Italy, June 2019.

[DZG13] E. Dall'Anese, H. Zhu, and G. B. Giannakis. Distributed optimal power flow for smart microgrids. *IEEE Transactions on Smart Grid*, 4(3):1464–1475, 2013.

[EGHA16] A. El-Guindy, D. Han, and M. Althoff. Formal analysis of drum-boiler units to maximize the load-following capabilities of power plants. *IEEE Transactions on Power Systems*, 31(6):4691–4702, January 2016.

[EGSS+18] A. El-Guindy, K. Schaab, B. Schürmann, O. Stursberg, and M. Althoff. Formal LPV control for transient stability of power systems. In *Power and Energy Society General Meeting (PESGM)*, pages 1–5, 2018.

[Ers14] T. Erseghe. Distributed optimal power flow using ADMM. *IEEE Transactions on Power Systems*, 29(5):2370–2380, 2014.

[FCE+99] R. Fried, R. S. Cherkaoui, C. C. Enz, A. Germond, and E. A. Vittoz. Approaches for analog VLSI simulation of the transient stability of large power networks. *IEEE Transactions on Circuits and Systems I: Fundamental Theory and Applications*, 46(10):1249–1263, 1999.

[FIDM14] A. Fuchs, M. Imhof, T. Demiray, and M. Morari. Stabilization of large power systems using VSC-HVDC and model predictive control. *IEEE Transactions on Power Delivery*, 29(1):480 – 488, 2014.

[GM16] T. Guo and J. V. Milanovićs. Online identification of power system dynamic signature using PMU measurements and data mining. *IEEE Transactions on Power Systems*, 31(3):1760–1768, May 2016.

[GP01] R. Grunbaum and J. Pernot. Thyristor-controlled series compensation: A state of the art approach for optimization of transmission over power links. Technical report, ABB, 2001.

[GTK14] A. Gajduk, M. Todorovski, and L. Kocarev. Stability of power grids: an overview. *The European Physical Journal Special Topics*, (223):2387–2409, 2014.

[GVM+11] J. M. Guerrero, J. C. Vasquez, J. Matas, L. G. Vicuna, and M. Castilla. Hierarchical control of droop-controlled AC and DC microgrids–A general approach toward standardization. *IEEE Transactions on Industrial Electronics*, 58(1):158–172, 2011.

[HG05] O. Harkegard and S.T. Glad. Resolving actuator redundancy—optimal control vs. control allocation. *Automatica*, 41(1):137–144, 2005.

[HGKX17] A. Halder, X. Geng, P. R. Kumar, and L. Xie. Architecture and algorithms for privacy preserving thermal inertial load management by a load serving entity. *IEEE Transactions on Power Systems*, 32(4):3275–3286, July 2017.

[HJX08] J. Huang, C. Jiang, and R. Xu. A review on distributed energy resources and microgrid. *Renewable and Sustainable Energy Reviews*, 12:2472–2483, 2008.

[Ili07] M. D. Ilic. From hierarchical to open access electric power systems. *Proceedings of the IEEE*, pages 1060–1084, 2007.

[JK02] D. Jia and B. Krogh. Min-max feedback model predictive control for distributed

control with communication. In *American Control Conference*, Anchorage, AK, 2002.

[JLSH15] H. Jiang, J. Lin, Y. Song, and D. J. Hill. MPC-based frequency control with demand-side participation: A case study in an isolated wind-aluminum power system. *IEEE Transactions on Power Systems*, 30(6):3327–3337, 2015.

[JMLJ13] J. J. Justo, F. Mwasilu, J. Lee, and J. W. Jung. AC-microgrids versus DC-microgrids with distributed energy resources: A review. *Renewable and Sustainable Energy Reviews*, 24:387–405, 2013.

[KB06a] M. Kloetzer and C. Belta. Reachability analysis of multi-affine systems. In J. P. Hespanha and A. Tiwari, editors, *Hybrid Systems: Computation and Control*, volume 3927 of *Lecture Notes in Computer Science*, pages 348–362. Springer, Santa Barbara, CA, 2006.

[KB06b] M. Krstic and M. Bement. Nonovershooting control of strict-feedback nonlinear systems. *IEEE Transactions on Automatic Control*, 51(12):1938–1943, 2006.

[Kha02] H. K. Khalil. *Nonlinear Systems*. Prentice Hall, 3 edition, 2002.

[Kni02] J. C. Knight. Safety critical systems: challenges and directions. In *Proceedings of the 24th International Conference on Software Engineering*, Orlando, Florida, 2002.

[KPA+04] P. Kundur, J. Paserba, V. Ajjarapu, G. Andersson, A. Bose, C. Canizares, N. Hatziargyriou, D. Hill, A. Stankovic, C. Taylor, T. V. Cutsem, and V. Vittal. Definition and classification of power system stability. *IEEE Transactions on Power Systems*, 19(2):1387–1401, 2004.

[Kro17] B. D. Kroposki. Basic research needs for autonomous energy grids: Summary report of the workshop on autonomous energy grids. Technical report, National Renewable Energy Laboratory, 2017.

[Kub71] L. S. Kubie. The destructive potential of humor in psychotherapy. *American Journal of Psychiatry*, 127(7):861–866, 1971.

[Kun94] P. Kundur. *Power System Stability and Control*. McGraw-Hill, 1994.

[LAVT18] D. Lee, L. Aolaritei, T. L. Vu, and K. Turitsyn. Robustness against disturbances in power systems under frequency constraints. *arXiv preprint arXiv:1803.00817*, 2018.

[LZT12] A. Y. S. Lam, B. Zhang, and D. Tse. Distributed algorithms for optimal power flow problem. In *IEEE Conf. on Decision and Control*, pages 430–437, Maui, HI, 2012.

[MBB08] J. Machowski, J. W. Bialek, and J. R. Bumby. *Power System Dynamics: Stability and Control*. Wiley, Chichester, England, 2008.

[MCS11] N. W. Miller, K. Clark, and M. Shao. Frequency responsive wind plant controls: Impacts on grid performance. In *IEEE Power and Energy Society General Meeting*, Detroit, MI, October 2011. Electronic proceedings.

[MDH+18] F. Milano, F. Dörfler, G. Hug, D. J. Hill, and G. Verbič. Foundations and challenges of low-inertia systems. In *Power Systems Computation Conference*, Dublin, Ireland, June 2018. Electronic proceedings.

[Mit07] I. M. Mitchell. Comparing forward and backward reachability as tools for safety analysis. In *Hybrid Systems: Computation and Control*, pages 428–443. Springer, 2007.

[MM09] P. McDaniel and S. McLaughlin. Security and privacy challenges in the smart grid. *IEEE Security & Privacy*, 7(3):75–77, 2009.

[MPAH14] M. A. Mahmud, H. R. Pota, M. Aldeen, and M. J. Hossain. Partial feedback linearizing excitation controller for multimachine power systems to improve transient stability. *IEEE Transactions on Power Systems*, 29:561–571, 2014.

[MRRS00] D. Q. Mayne, J. B. Rawlings, C. V. Rao, and P. O. M. Scokaert. Constrained model predictive control: Stability and optimality. *Automatica*, 36:789–814, 2000.

[MSV11] N. W. Miller, M. Shao, and S. Venkataraman. California ISO (CAISO) frequency response study. Technical report, General Electric International, Inc, 2011.

[MZL14] E. Mallada, C. Zhao, and S. H. Low. Optimal load-side control for frequency regulation in smart grids. In *Allerton Conf. on Communications, Control and Computing*, pages 731–738, Monticello, IL, October 2014.

[NCF+14] M. H. Nazari, Z. Costello, M. J. Feizollahi, S. Grijalva, and M. Egerstedt. Distributed frequency control of prosumer-based electric energy systems. *IEEE Transactions on Power Systems*, 29:2934–2942, 2014.

[NFP+13] I. Nagel, L. Fabre, M. Pastre, F. Krummenacher, R. Cherkaoui, and M. Kayal. High-speed power system transient stability simulation using highly dedicated hardware. *IEEE Transactions on Power Systems*, 28(4):4218–4227, 2013.

[NNK11] T. T. Nguyen, V. L. Nguyen, and A. Karimishad. Transient stability-constrained optimal power flow for online dispatch and nodal price evaluation in power systems with flexible ac transmission system devices. *IET Generation, Transmission & Distribution*, 5:332–346, 2011.

[NRZ+15] C. Newcombe, T. Rath, F. Zhang, B. Munteanu, M. Brooker, and M. Deardeuff. How Amazon web services uses formal methods. *Communications of the ACM*, 58(4):66–73, 2015.

[Pai89] A. Pai. *Energy Function Analysis for Power System Stability*. Springer, New York, 1989.

[PBD17] B. K. Poolla, S. Bolognani, and F. Dorfler. Optimal placement of virtual inertia in power grids. *IEEE Transactions on Automatic Control*, 62(12):6209–6220, 2017.

[PERV12] M. Pavella, D. Ernst, and D. Ruiz-Vega. *Transient Stability of Power Systems: A Unified Approach to Assessment and Control*. Kluwer Academic Publishers, 2012.

[PKT06] P. Pouyan, P. S. Kundur, and C. W. Taylor. The anatomy of a power grid blackout-root causes and dynamics of recent major blackouts. *IEEE Power and Energy Magazine*, 4(5):22–29, 2006.

[PM97] M. H. Protter and C. B. Jr. Morrey. *A First Course in Real Analysis*. Undergraduate Texts in Mathematics. Springer, New York, 2nd edition, 1997.

[Pra06] S. Prajna. Barrier certificates for nonlinear model validation. *Automatica*, 42(1):117–126, 2006.

[Res98] S. I. Resnick. *A Probability Path*. Birkhäuser Boston, 1998.

[SIF16] J. A. Short, D. G. Infield, and L. L. Freris. Stabilization of grid frequency through dynamic demand control. *IEEE Transactions on Power Systems*, 22(3):1284–1293, August 2016.

[SLJ15] B. L. Stevens, F. L. Lewis, and E. N. Johnson. *Aircraft Control and Simulation: Dynamics, Controls Design, and Autonomous Systems*. Wiley, 2015.

[SMZ17] S. Soltan, D. Mazauric, and G. Zussman. Analysis of failures in power grids. *IEEE Transactions on Control of Network Systems*, 4(2):288–300, 2017.

[SPZG14] W. Sun, H. Pan, Y. Zhang, and H. Gao. Multi-objective control for uncertain nonlinear active suspension systems. *Mechatronics*, 24(4):32–40, 2014.

[SZH+16] W. Sun, Y. Zhang, Y. Huang, H. Gao, and O. Kaynak. Transient-performance-guaranteed robust adaptive control and its application to precision motion control systems. *IEEE Transactions on Industrial Electronics*, 63(10):6510 – 6518, 2016.

[TJ13] W. Tang and R. Jain. Game-theoretic analysis of the nodal pricing mechanism for electricity markets. In *IEEE Conf. on Decision and Control*, pages 562–567, Florence, Italy, December 2013.

[VAMT16] T. L. Vu, S. M. A. Araifi, M. S. E. Moursi, and K. Turitsyn. Toward simulation-free estimation of critical clearing time. *IEEE Transactions on Power Systems*, 31(6):4722–4731, 2016.

[VHRW08] A. N. Venkat, Ian A. Hiskens, J. B. Rawlings, and S. J. Wright. Distributed MPC strategies with application to power system automatic generation control. *IEEE Transactions on Control Systems Technology*, 16(6):1192–1206, 2008.

[VNM+18] T. L. Vu, H. D. Nguyen, A. Megretski, J. Slotine, and K. Turitsyn. Inverse stability problem and applications to renewables integration. *IEEE Control Systems Letters*, 2(1):133–138, 2018.

[VPA14] H. N. Villegas-Pico and D. C. Aliprantis. Voltage ride-through capability verification of wind turbines with fully-rated converters using reachability analysis. *IEEE Transactions on Energy Conversion*, 29(2):392–405, 2014.

[WA04] J. T. Wen and M. Arcak. A unifying passivity framework for network flow control. *IEEE Transactions on Automatic Control*, 49(2):162–174, 2004.

[WLL+18] Z. Wang, F. Liu, S. H. Low, C. Zhao, and S. Mei. Distributed frequency control with operational constraints, part I: Per-node power balance. *IEEE Transactions on Smart Grid*, 9(4):1798–1811, 2018.

[WZQG15] T. Wang, Y. Zhang, J. Qiu, and H. Gao. Adaptive fuzzy backstepping control for a class of nonlinear systems with sampled and delayed measurements. *IEEE Transaction on Fuzzy Systems*, 23(2):302 – 312, 2015.

[XTGA15] X. Xu, P. Tabuada, J. W. Grizzle, and A. D. Ames. Robustness of control barrier functions for safety critical control. *IFAC-PapersOnLine*, 48(27):54 – 61, 2015.

[YNM17] Y. Yang, T. Nishikawa, and A. E. Motter. Small vulnerable sets determine large network cascades in power grids. *Science*, 358(6365), 2017.

[YT94] B. Yao and M. Tomizuka. Smooth robust adaptive sliding mode control of manipulators with guaranteed transient performance. In *American Control Conference*, pages 1176–1180, Baltimore, MD, USA, 1994.

[ZC16] Y. Zhang and J. Cortés. Quantifying the robustness of power networks against initial failure. In *European Control Conference*, pages 2072–2077, Aalborg, Denmark, July 2016.

[ZC17] Y. Zhang and J. Cortés. Transient-state feasibility set approximation of power networks against disturbances of unknown amplitude. In *American Control Conference*, pages 2767–2772, Seattle, WA, May 2017.

[ZC18a] Y. Zhang and J. Cortés. Distributed transient frequency control in power net-

works. In *IEEE Conf. on Decision and Control*, pages 4595–4600, Miami Beach, FL, December 2018.

[ZC18b] Y. Zhang and J. Cortés. Transient frequency control with regional cooperation for power networks. In *IEEE Conf. on Decision and Control*, pages 2587–2592, Miami Beach, FL, December 2018.

[ZC19a] Y. Zhang and J. Cortés. Characterizing tolerable disturbances for transient-state safety in power networks. *IEEE Transactions on Network Science and Engineering*, 2019. To appear.

[ZC19b] Y. Zhang and J. Cortés. Distributed bilayered control for transient frequency safety and system stability in power grids. *IEEE Transactions on Control of Network Systems*, 2019. Submitted.

[ZC19c] Y. Zhang and J. Cortés. Distributed transient frequency control for power networks with stability and performance guarantees. *Automatica*, 105:274–285, 2019.

[ZC19d] Y. Zhang and J. Cortés. Double-layered distributed transient frequency control with regional coordination. In *American Control Conference*, Philadelphia, PA, July 2019. To appear.

[ZC19e] Y. Zhang and J. Cortés. Model predictive control for transient frequency regulation of power networks. *IEEE Transactions on Automatic Control*, 2019. Submitted.

[ZTLL14] C. Zhao, U. Topcu, N. Li, and S. H. Low. Design and stability of load-side primary frequency control in power systems. *IEEE Transactions on Automatic Control*, 59(5):1177–1189, 2014.